The Biosorption of Chromium and Copper from AMD Contaminated Water Using Banana Peels as a Biomass Adsorbent

This dissertation is submitted in the fulfilment of the requirements for the degree of Master of Engineering: Chemical Engineering in the Faculty of Engineering and the Built Environment at Durban University of Technology

S'THEMBILE MZIMELA

Supervisor: Prof P. Musonge

Co-Supervisor: Prof B. F. Bakare

June 2022

DECLARATION

I, ***S'thembile Mzimela***, hereby declare that the content presented in this thesis entitled **"*The Biosorption of Chromium and Copper from AMD Contaminated Water using Banana Peels as a Biomass Adsorbent*"** is a record of my research work conducted to obtain the Masters in Engineering in Chemical Engineering degree at Durban University of Technology (DUT). The content of this research work has not been previously published or written by another person for the award of any other degree at DUT or any other educational institution. Moreover, I declare that the content presented in the thesis does not violate any copyrights as all the work of others has been indicated accordingly through in-text referencing as well as a comprehensive list of references listed at the end of the thesis.

Author **Sthembile Mzimela**

19 June 2022

Signature Date

Supervisor **Prof P. Musonge**

June 21, 2022

Signature Date

Co-supervisor **Prof B. F. Bakare**

21 June 2022

Signature Date

ACKNOWLEDGEMENTS

I would like to firstly acknowledge and thank my supervisors Prof B. F. Bakare and Prof P. Musonge for giving me the opportunity and guidance to do this project. I thank the Durban University of Technology for the opportunity it has given me to obtain my Master's degree. I thank the National Research Funding institute for funding my dissertation work. I thank the Mangosuthu University of Technology for allowing me the facilities and the resources to conduct my project until completion. I thank my colleagues for their encouragement and support throughout the project. Finally, I thank God, through Jesus Christ, for giving me the strength and wisdom to successfully finish my dissertation.

DEDICATION

I dedicate this work in honour of my parents, Patricia Sibusisiwe Leonorah Mzimela and Sabelo Archibald Mzimela.

LIST OF CONFERENCE PRESENTATIONS

1.1 Conference Papers

Mzimela, S.; Musonge, P.; Bakare, B.F. 2018. The characterization of banana peels as a biomass adsorbent for removing heavy metals from wastewater. Paper presented at the *Advances in Composites, Biocomposites and Nanocomposites*. Nelson Mandela Bay Stadium, Port Elizabeth, South Africa, 2018/11/07 - 2018/11/09. Durban University of Technology, 481-491.

Mzimela, S.; Musonge, P.; Bakare, B.F. 2022. Evaluation of Musa Acuminata (Banana Peels) as a Biomass Adsorbent in Treating Water Contaminated with Chromium (Cr^{6+}). Paper presented at the *33rd JOHANNESBURG International Conference on "Chemical, Biological and Environmental Engineering" (JCBEE-22)*. Johannesburg, March 17-18, 2022. Pilares D'Elegância, Lda,

ABSTRACT

The presence of heavy metals in water from industrial activities negatively affects human health. Metal accumulation in human bodies is toxic and can lead to carcinogenic effects when consumed for prolonged periods. There is no acceptable method for permanently removing heavy metals in water. As a result, water for human consumption and domestic use from various water sites contains harmful heavy metals. This study investigates the removal of hexavalent chromium (Cr^{6+}) and copper (Cu^{2+}) from drinking water through the adsorption process using banana peels as biomass material. Banana peels were evaluated for their ability to remove heavy metals from water as a cheaper alternative resource to conventional adsorbents such as activated carbon. Cr^{6+} and Cu^{2+} are some of the most common heavy metals found in potable (drinking) water and they were chosen for this study amongst other heavy metals.

Batch studies were conducted using water that was synthesized with the chosen metals. Parameters such as pH, agitation speed, biosorbent dose, initial metal concentration, and contact time were varied to determine their effect on biosorption. pH was varied between 2 and 7, agitation speed was varied between 100 and 200 rpm, dosage was varied between 1 and 6 grams, initial concentration was between 5 and 100 mg/L and contact time was also varied between 5 and 140 minutes. Each variable was done one factor at a time while keeping other values constant. The height of the column for column studies was studied between 5 and 30 cm at constant pH "4", 5mg/L initial metal concentration and volumetric flowrate of 4mL/min.

Results from the study showed that pH for both Cr^{6+} and Cu^{2+} was highest at pH "4" with % removal of 65% and 94%, respectively. Agitation speed had a high % removal at 180 rpm for Cr^{6+} (67%) and 160 and 180 rpm for Cu^{2+} (95%). Increase in biosorbent dose also increased biosorption efficiency from 17% to 95% for Cu^{2+} across the range, and from 58% to 65% for removing Cr^{6+}. In the study of initial metal concentration, banana peels performed better at lower metal concentrations for both metals. Highest % removal efficiency for Cr^{6+} was found at 5 mg/L at 64% and for Cu^{2+} at 10, 15 and 20 mg/L at 95%. Contact time between 5 and 140 minutes found that equilibrium was reached within 30 minutes for Cr^{6+} and within 50 minutes for Cu^{2+}.

Adsorption equilibrium isotherms and kinetics were studied for both metals and found that the biosorption of Cr^{6+} followed the Freundlich isotherm and Langmuir isotherm models with R^2 of 0.99 and 0.95 respectively, and the process kinetics followed the pseudo-second-order kinetic reaction with R^2 of ~ 1. The biosorption of Cu^{2+} followed the Langmuir isotherm model with R^2 of 0.96 and Langmuir q_m of 15.41 mg/g and the process kinetics followed the pseudo-first-order kinetic reaction as well as the intra-particle diffusion model with both R^2 of 0.98.

Banana peels were characterized for their properties and the Fourier transform infrared (FTIR) spectroscopy identified the functional groups in the peels which were hydroxyls, carboxylic acids, alkanes, and amines. Most of the groups were active in the removal of Cr^{6+} and Cu^{2+}. The scanning electron microscopy (SEM) identified the surface of the peels to be rough with uneven areas and the energy-dispersive x-ray spectroscopy (EDS) analysis identified the elements present in the peels which were carbon (C), oxygen (O), potassium (K), chloride (Cl) and silicon (Si). The x-ray diffraction (XRD) was used to identify the phase of the peels and it was found that the peels were amorphous with some crystallinity containing a crystal salt called sylvite. The Brunauer–Emmett–Teller (BET) analysis identified the pores of the banana peels to be mesoporous with a pore size of 2.9 nm, a surface area of 5.69 m^2/g, and a pore volume of 0.002605 cm^3/g.

Column experiments in a fixed-bed column were studied for the removal of Cr^{6+} and the breakthrough time t_b increased from 10 min at 5cm to 420 min at 30 cm. The mass transfer zone H_B also increased from 0.206 at 5 cm to 7.426 at 30 cm. Other column performance indicators such as the adsorbent exhaustion rate (AER) and the number of volumes processed (NBV) showed that biosorption was efficient and dependent on bed height for better performance. The process favoured the Adams-Bohart model with R^2 ranging between 0.94 to 0.98 and the Yoon-Nelson model with R^2 ranging between 0.93 and 0.97.

It can be concluded from this study that banana peels have the ability of removing Cu and Cr in potable water and has provided some insight for scaling-up of adsorption columns.

Keywords: Adsorption Column, Biosorption, Banana peels, Characterization, Kinetics

TABLE OF CONTENTS

LIST OF TABLES

LIST OF FIGURES

GLOSSARY

°C	degrees Celsius
µm	micrometre
Å	Angstrom
AAS	Atomic Absorption Spectroscope
AMD	Acid Mine Drainage
BET	Brunauer-Emmett-Teller
cm	centimetre
Cr^{6+}	hexavalent chromium
Cu^{2+}	divalent copper
d_s	particle size distribution
EDS/EDAX	Energy Dispersive X-ray Spectroscopy
FTIR	Fourier-Transform Infrared
ICP-MS	Induced Coupled Plasma-Mass Spectrometry
MW	molecular weight
N	molar
ppb	parts per billion
ppm	parts per million
rpm	revolutions per minute
SEM	Scanning Electron Microscope
XRD	X-ray Diffraction Spectrometry

CHAPTER 1: INTRODUCTION

Mining and industrial activities in South Africa continue to be a threat to the environment, particularly to water sources contaminated with heavy metals though there are stringent regulations and legislation put in place by the government to protect the environment (Fashola, Ngole-Jeme and Babalola 2016; Olalde 2016). Given the challenges facing the remediation of water from heavy metals caused by these activities, current water treatment methods also play a big role in the poor quality of water where inefficient and high cost of water treatment plants operation and maintenance, as well as high energy intensive operations, are a limitation. The study of agricultural waste for use as a biomass adsorbent in the adsorption process has been on the rise. It is one of the identified solutions to help increase the quality of drinking water at reduced costs and energy requirements for water treatment plant operation, as the process is dependent on the adsorbent used for effective removal (Ushakumary and Madhu 2013; Masukume, Onyango and Maree 2014; Schwantes *et al.* 2016). In this chapter, a detailed background is given on the challenges faced in drinking water treatment from dissolved heavy metals. A problem statement is included as well as the proposed method which will cover the main challenges faced in the treatment of potable water containing heavy metals. Lastly, the chapter also includes a detailed structural layout outline for the entire thesis.

1.1 Background of Study

1.1.1 Introduction

South Africa is a water-scarce country that has been greatly affected not only by poor rain conditions but also by the reduction of water availability due to water pollution by industrial activities and the capacity of water treatment plant facilities. One of the major factors contributing to water pollution is the high levels of heavy metal concentration caused by industrial waste tailings such as acid mine drainage (AMD). AMD is the flow of acidic water containing organic and inorganic pollutants to the

environment. This emanates mostly from abandoned and backfilled opencast mines that are no longer operational (Akcil and Koldas 2006). The process of AMD formation occurs when a sulfide-rich mineral is exposed to water and oxygen to produce sulfide-rich water where these sulfide-rich minerals are dissolvable. Iron sulfide is the most common sulfide mineral found in water (Akcil and Koldas 2006). Water from these mines drains into control reservoirs with limited capacities, causing overspills and seepages into nearby water systems (Geldenhuis and Bell 1998). Industries such as electroplating, leather tanning, water cooling, and pigment manufacturing are also negatively impacting the environment by discharging heavy metals from untreated or partially treated effluents to nearby water streams (Bhaumik *et al.* 2013).

1.1.2 Heavy Metal Contamination and its Effects to Humans and the Environment

In South Africa, regions affected by heavy metal contamination are groundwater systems and water streams that are close to mines such as those that are near the gold mines in Witwatersrand, Johannesburg, as well as coal mines in the Witbank Coalfields where informal settlements currently reside (Bell *et al.* 2001). Contaminated water is characterized by high sulphate content along with high metal concentrations, resulting in high toxicity and acidity content (Tutu, McCarthy and Cukrowska 2008). In South Africa, the most commonly found heavy metals in water are arsenic (sp. gravity 5.7), lead (11.34), cadmium (8.65), mercury (13.54), chromium (7.19), and copper (4.1-4.3) (Fu and Wang 2011; Ushakumary and Madhu 2013; Olujimi *et al.* 2015; Mahlangu, Simate and de Beer 2018).

Copper, a heavy metal found in ground and surface water, is a trace element essential for human health. Copper is found in all body tissues and mostly exists within the brain, liver, heart, kidneys and skeletal muscles (Wilson 2017). Copper is one of the important minerals responsible for making red blood cells as well as maintaining the nervous system and the immune system. However, too much copper in the body affects the functions of the brain (Wilson 2017). Copper concentrations generally found in drinking water are at very low concentrations of about 0.009mg/L (Manne *et al.*

2022). The high copper content in the bloodstream can cause reactive free oxygen species which can damage the proteins, lipids and DNA (Hossain *et al.* 2012). Excessive copper compounds in human bodies can also cause diseases such as schizophrenia, mental illness, and Alzheimer's disease (Wilson 2017). A study done by (Verlicchi and Grillini 2020) found that the concentration of copper in water was exceeded by 2% in a study of surface and groundwater between South Africa and Mozambique. Guideline limits for copper, Cu^{2+}, present in water for drinking were established in the World Health Organization (WHO) guidelines, as well as in the South African Water Guidelines from the Department of Water Affairs and Forestry (DWAF) for domestic use. Table 1.1.1 below demonstrates the guidelines from both institutions.

Table 1.1: Guidelines set by DWAF and WHO for Cu^{2+} in Domestic Water

References	Source/Organization	Guideline limits
(Affairs 2012)	South African Water Guidelines: Domestic Use: Cu^{2+}	0-1 mg/L
(Organization 1993)	World Health Organization: Cu^{2+}	<2 mg/L

Another heavy metal, chromium, exists in two oxidation states, hexavalent chromium, Cr^{6+}, and trivalent chromium, Cr^{3+} (Ali, Saeed and Mabood 2016). Cr^{6+} exists in several forms depending on the pH [i.e., chromate ($Cr_2O_4^{2-}$); hydrochromate ($HCrO^{4-}$); dichromate ($Cr_2O_7^{2-}$); etc]. Cr^{3+} is present in human blood for blood mechanism maintenance with a daily recommended dietary uptake of Cr^{3+} is 50 – 200 µg (Organization 1993; Ali, Saeed and Mabood 2016). However, Cr^{6+} is a poisonous form/state of chromium and its toxic effects when ingested into the bloodstream include rashes, nose bleeds, respiratory tract infections, a suppressed immune system, hepatic diseases and lung cancer, amongst other health complications (Ali, Saeed and Mabood 2016). The presence of Cr^{6+} in water has mainly come from the production of ferrochromium industries, where smelters are used in a pyro-metallurgical carbo-thermic reduction process for reducing chromite ore in the

production of the ferrochrome alloy (Loock, Beukes and Van Zyl 2014). These ferrochrome smelters are in the Bushveld Igneous Complex regions of the Limpopo Province and there are 13 sites in total. A study done by (Loock, Beukes and Van Zyl 2014) studied surface water around the region to determine the Cr^{6+} levels in the water as a the result of smelters nearby. The maximum amount of Cr^{6+} found near one of the sites was recorded at 219.6 µg/L, greater than the limit set by WHO and DWAF of <50µg/L. Another study was done (Edokpayi *et al.* 2018) where 8 water boreholes were tested around Muledane village, Limpopo Province, South Africa. Chromium concentrations ranging from 0.005 – 0.15 mg/L were detected which was well above the allowable concentration threshold of Cr^{6+} in water. A recent study on the quality of water on heavy metals between South Africa and Mozambique was performed by (Verlicchi and Grillini 2020), where it was found that the Cr^{6+} levels in surface and groundwater range between 0.001 and 0.40 mg/L.

Set guidelines have been put in place to limit the amount of Cr^{6+} present in water for domestic use. Table 1.2 below shows the guideline limits set by WHO and the DWAF.

Table 1.2: Guidelines set by DWAF and WHO for Cr^{6+} in Domestic Water

References	Source/Organization	Guideline limits
(Forestry 1996)	South African Water Guidelines: Domestic Use: Cr^{6+}	0-50 µg/L
(Organization 2020)	World Health Organization: Cr^{6+}	<50 mg/L

There is no specific treatment method employed to remove heavy metals, however, removal of heavy metals in water is mainly achieved in the tertiary stage of water treatment after filtration (Ahalya, Ramachandra and Kanamadi 2003). Common methods employed for removing heavy metals in water are chemical precipitation, reverse osmosis, ion exchange, ultrafiltration, coagulation and flocculation and/or adsorption amongst other treatment methods (Ahalya, Ramachandra and Kanamadi 2003).

1.1.3 Water Treatment Methods Employed for Removing Heavy Metals

Chemical precipitation: The most common method to treat heavy metals in water treatment is chemical precipitation which is followed by filtration in the secondary water treatment stage. Chemical precipitation is a process where chemicals react with heavy metals present in wastewater to form insoluble precipitates (Fu and Wang 2011). The pH of the water is increased through the aid of coagulants for removing metals by precipitation, therefore forming metal hydroxide solids (Ayres, Davis and Gietka 1994; BrbootI, AbiD and Al-ShuwaikI 2011). Heavy metals such as Cr^{6+} and Cu^{2+} are conventionally removed by using $Ca(OH)_2$ and NaOH as hydroxide precipitates in wastewater treatment, where Cr^{6+} is first converted to Cr^{3+} by using ferrous sulfate ($FeSO_4$) (Fu and Wang 2011). These insoluble precipitates are then separated through sedimentation or filtration from wastewater. Treated water is then decanted and discharged by appropriate means to the environment or to be reused elsewhere (Fu and Wang 2011). However, this process generates large quantities of relatively low-density sludge, which presents dewatering and disposable challenges (Ahalya, Ramachandra and Kanamadi 2003; Fu and Wang 2011; Mulopo 2015). Another challenge with this process is that some metal hydroxides are amphoteric and the combination creates a problem for the used hydroxide precipitates since the ideal pH for one metal to be removed may put another metal back into the solution. The third challenge faced is when complexing agents are in wastewater they may prevent metal hydroxide precipitation of some metals, causing inefficient removal of some of these metals in wastewater (Fu and Wang 2011). Lastly, the use of sulfide precipitation method can present potential danger of accumulating toxic H_2S fumes from the combination of heavy metals with sulfide precipitants in acid conditions. In most cases metal sulfides form colloidal precipitates, causing, in some cases, separation challenges in the settling and/or filtration process (Fu and Wang 2011).

Reverse Osmosis: Reverse osmosis (RO) is a pressure-driven process where a semi-permeable membrane is used for removing heavy metals from wastewater (Ahalya, Ramachandra and Kanamadi 2003; Gunatilake 2015). The membrane operates at a pressure greater than the osmotic

pressure where dissolved solids are also present in wastewater. RO can remove a wide range of metallic ions and it is increasingly becoming popular within the chemical and environmental engineering industry for its high removal efficiency. The technique also accounts for more than 20% of the world's desalination operations. The disadvantage of RO is its high-power consumption due to pumping pressures as well as the regeneration and restoration of its semi-permeable membranes (Ahalya, Ramachandra and Kanamadi 2003; Fu and Wang 2011).

Ion Exchange: This process has been used in a wide number of applications for removing heavy metals from wastewater. Ion exchange is a process where heavy metals from wastewater are exchanged with ions held by electrostatic forces in an exchange resin (Ahalya, Ramachandra and Kanamadi 2003). The ion exchange resin may be synthetic or a natural solid resin that can exchange its cations with heavy metals in wastewater (Fu and Wang 2011; Budak 2013). The most commonly used cation exchangers are strong acidic resins with sulfonic acid groups ($-SO_3H$) and weak acid resins with carboxylic acid groups (-COOH), where hydrogen, H^+, ions (in the sulfonic or carboxylic group) are exchanged with the metal ions in wastewater. Natural zeolites are also used as cation exchangers for removing heavy metals in water. The ability to achieve high treatment capacity, high removal efficiency and fast kinetics gives ion exchange resins an advantage over many other wastewater treatment processes (Fu and Wang 2011). However, their disadvantage is their high operational costs and partial removal of certain metal ions (Ahalya, Ramachandra and Kanamadi 2003; Fu and Wang 2011).

Ultrafiltration: This is a membrane filtration technique that is driven by pressure. The process works at low transmembrane pressures for the removal of dissolved and colloidal materials such as heavy metals by passing wastewater through a porous membrane (Ahalya, Ramachandra and Kanamadi 2003; Fu and Wang 2011). Due to the membrane pore size being larger than the dissolved metal ions in the form of hydrated ions or as low molecular weight complex ions, metal ions can pass easily through UF membranes, resulting in low metal ion removal efficiencies (Fu and Wang 2011).

Therefore, enhanced ultrafiltration techniques for improving removal efficiencies were developed and introduced such as the micellar enhanced ultrafiltration (MEUF) and polymer enhanced ultrafiltration (PEUF) methods. The disadvantage of the PEUF method is finding suitable polymers to achieve complexation with metal ions, some of which may be costly for specific metals (Fu and Wang 2011). The MEUF technique involves the addition of surfactants in wastewater to form agglomerates with metal ions present in water also known as micelles. The disadvantage of this method is the high ratio of surfactant to metal ion concentration, which may account for a large portion of operational costs, making it essential to recover and reuse for economic feasibility (Fu and Wang 2011).

Coagulation and Flocculation: Coagulation and flocculation are wastewater treatment methods used for removing heavy metals in water by introducing coagulants such as aluminium, ferrous sulfate and ferric chloride in wastewater. These coagulants assist by destabilizing colloidal matter by neutralizing the forces that keep them apart. The formed neutralized particles then carry on to form amorphous metallic hydroxide precipitates where heavy metals are then removed from wastewater through filtration (Fu and Wang 2011). Coagulation in water treatment is very important for treating waste and raw water, however, it is mainly directed at removing hydrophobic colloids and suspended particles and is not focused on removing soluble metals in water (Fu and Wang 2011). The process is greatly dependent on water pH whereby if pH is low substances with negative charges can then be coagulated; however, if pH is higher, then turbidity decreases and metal uptake increases. Therefore, additional chemicals such as sodium xanthogenate are added to wastewater to aid in the removal of soluble heavy metals to increase efficiency in metal uptake (Fu and Wang 2011). Flocculation is a process by which added polymeric flocculants form bridges between the flocs and particles together to form larger agglomerates or clumps. The formed suspended particles are then separated through filtration or floatation (Fu and Wang 2011). In general, the coagulation-flocculation technique is not efficient enough to remove or treat wastewater from heavy metals completely as this process is

mainly for reducing colloidal particles such as dissolved solids and is, therefore, not widely used for the removal of heavy metals (Fu and Wang 2011).

Adsorption: Adsorption is a separation process where fluid containing contaminants is passed through an adsorbent. Solute or species present in the liquid or gaseous stream is then diffused to the surface of the adsorbent (Ahalya, Ramachandra and Kanamadi 2003). The adsorption process can be distinguished between two types, namely physical adsorption and chemical adsorption (chemisorption). Physical adsorption, also known as van der Waals adsorption, involves only relatively weak intermolecular forces, where molecular interactions are fully reversible (Sincero and Sincero 2002; Faust and Aly 2013). During physical adsorption, adsorbed molecules are free to cover an entire surface of the adsorbent, making it non-site specific. However, chemisorption involves the formation of chemical bonds (ionic or covalent bonds) between the sorbate molecules and the surface of the adsorbent, making the process irreversible (Wang, Hung and Shammas 2007; Faust and Aly 2013). The performance of the adsorption process is dependent on the adsorbent and the process is driven by a species being readily adsorbed onto the surface of the adsorbent (Richardson, Harker and Backhurst 2002). Activated carbon is a microcrystalline material that is most widely used as an adsorbent in the adsorption process and it requires intensive energy to be produced by thermally decomposing coal and other agricultural wastes (Reimerink and Kleut 1999; Geankoplis, Hersel and Lepek 2018). Surface areas range from 300 to 1200 m^2/g with an average pore diameter of 10 to 60 Å (Geldenhuis and Bell 1998; Richardson, Harker and Backhurst 2002). Silica gel is mostly used for drying gases and removing unsaturated hydrocarbons in gas streams. Silica gel is produced from the acid treatment of sodium silicate which is dried to gel particles. The surface of the gel is hydrophilic and is not suitable for liquid adsorption with a surface area ranging from 200 to 500 m^2/g and a pore diameter of 20 to 50 Å (Geldenhuis and Bell 1998; Richardson, Harker and Backhurst 2002). Activated alumina is used for drying gases and liquids and can be used in moving-bed applications due to its superior mechanical strength. It has an affinity for water and hydroxyl groups. The

adsorbent has a well-defined pore structure with open crystal lattices with a surface area of approximately 350'000 m^2/kg and a pore diameter ranging from 20 to 140 Å (Richardson, Harker and Backhurst 2002; Geankoplis, Hersel and Lepek 2018). Zeolites are also porous crystalline aluminosilicates with uniform pore sizes, which are used in the separation of hydrocarbons, mixtures and other separation applications. Their pore size ranges from 3 to 10 Å (Geankoplis, Hersel and Lepek 2018). Synthetic polymers and resins are made from polymerizing two major types of monomers for two applications: (1) those that are made from aromatics are usually used for absorbing nonpolar organics from aqueous solutions and (2) those that are made from acrylic esters used for more polar solutes in aqueous solutions (Geankoplis, Hersel and Lepek 2018).

Many of these adsorbents are used for different applications specifically for waste gas streams and only some adsorbents are suitable for the removal of heavy metals present in wastewater. For example, activated carbon is derived from a coal-based commercial feed which requires high-intensive energy to produce the adsorbent and of which its source is depleting. As a result, prices of activated carbon have been increasing over time which will lead to its decline as costs continue to rise (Fu and Wang 2011; Ushakumary and Madhu 2013; Masukume, Onyango and Maree 2014). Other adsorbents as mentioned above are not suited for liquid or water applications and cannot perform well in removing heavy metals effectively for a wide range of metals. Therefore, research has turned to look at biological materials in particular agricultural waste as biomass adsorbents (biosorbents) for the removal of heavy metals in the adsorption process due to its ease of operation, inexpensive cost of biosorbent material as agricultural waste is free, biosorbent regeneration and reduced sludge discard of the adsorbent after use (Masukume, Onyango and Maree 2014; Bhatnagar, Sillanpää and Witek-Krowiak 2015; Deshmukh *et al.* 2017).

1.2 Problem Statement

Heavy metals in water are not biodegradable and so water is treated by removing these metals through biological, physical or chemical means (Hossain *et al.* 2012; Sedibe *et al.* 2017). Treatment

methods have been developed to remove heavy metals from water streams and rivers, however, these methods have been reported to be inefficient, expensive and environmentally unfriendly (Masukume, Onyango and Maree 2014). The adsorption process is also applied in the remediation of water treatment and its efficiency is mainly based on the performance of the adsorbent. Common adsorbents used in adsorption are energy-intensive, high in cost, limited in removing certain heavy metals in water and some are designed for removing specific pollutants in water such as activated carbon, silica gel, activated alumina, zeolites and synthetic polymers or resins (Masukume, Onyango and Maree 2014; Geankoplis, Hersel and Lepek 2018). Many research studies have shown great interest in using biomass materials such as seashells, natural clays, fruit and vegetable peels as adsorbents and have found good removal percentages in removing many heavy metals in water (Anwar *et al.* 2010; Bhatnagar, Sillanpää and Witek-Krowiak 2015; Ali, Saeed and Mabood 2016).

Banana peels are one of the agricultural wastes that have been experimented with in removing several heavy metals in water. In this project banana peels were used for removing Cr^{6+} (hexavalent chromium) and Cu^{2+} (copper) from contaminated potable water to below the guideline thresholds set by WHO and DWAF. Many studies have been done on batch experiments, however, more needs to be done in continuous flowing systems to understand the biosorption process between the biosorbent and the heavy metals, and this study included such studies between banana peels and Cr^{6+} in a fixed-bed column.

1.3 Aims and Objectives

1.3.1 Aims of the Project

The project had three aims:

1. The first aim was to evaluate the peels for removing Cr^{6+} and Cu^{2+} from contaminated wastewater in a batch process using jar tests.
2. The second aim was to characterize the banana peels by using analytical tools.

3. The third aim was to evaluate the banana peels for its dynamic behavior in a continuous fixed-bed column. In this experiment Cr^{6+} which is highly toxic and poisonous to humans was used for evaluation in a fixed-bed column.

1.3.2 Objectives of the Project

The objectives of this project were to:

- Conduct batch experiments for Cr^{6+} and Cu^{2+} in a single metal uptake application.
- Characterize banana peels to determine their physical and chemical properties before and after biosorption using the Fourier-Transform Infrared Spectroscopy (FTIR), Scanning Electron Microscopy (SEM), Energy Dispersive X-ray Spectroscopy (EDS), the X-ray Diffraction spectrometry (XRD), and the Brunauer-Emmett-Teller (BET).
- Identify applicable isotherms and kinetic models obtained from results during batch experiments such as the Langmuir, Freundlich and Elovich isotherms as well as the pseudo-first-order kinetic, pseudo-second-order kinetic and intra-particle diffusion models.
- Evaluate the performance of banana peels in a continuous flow fixed-bed column for Cr^{6+} at different bed heights through breakthrough curves, with constant influent flowrate, solution pH and metal concentration.
- Study the behaviour of the process by applying mathematical models such as the Thomas, Yoon-Nelson and Adams-Bohart models.

1.4 Structure of Dissertation

Chapter 1	The chapter introduces the reader to the background of the project and the problem statement which the project addresses. The aims and objectives are included for addressing the issues stated in the problem statement.
Chapter 2	The literature review looks at all the studies done by other researchers within the same or similar field and may also identify gaps within research. This chapter also includes all kinetic and dynamic models used for aiding in the interpretation of process behaviours in the biosorption of heavy metals using agro-waste and other biological material waste.
Chapter 3	The chapter contains the materials and methods used for executing the project from the aims and objectives of the project. This includes the instruments and equipment used.
Chapter 4	This section contains the results and the discussion. The section is separated into five parts and after each section, there is a conclusion. Part 1 consists of the study of batch experiments with a conclusion, part 2 consists of the isotherm and kinetic models applied with a conclusion, part 3 consists of the characterization of the banana peels with a conclusion, part 4 consists of the study of breakthrough curves in a fixed bed column and lastly, part 5 consists of the mathematical models applied with a conclusion.
Chapter 5	This section is the conclusion of the overall project collected from the experiments conducted in chapter 4. This chapter also includes recommendations that were observed during this study for further research.
Appendix	This section includes tables, graphs and calculations that formed part of the methods and discussions in Chapter 3 and 4.

CHAPTER 2: LITERATURE REVIEW

2.1 Introduction

The literature reviewed in this chapter looks at several research works done in using agricultural and other biological material in removing several of heavy metals from synthetic water and actual contaminated water and their findings. This chapter also looks at equilibrium, kinetic and mathematical models that have been used during research in batch studies and column studies to help determine behaviors occurring during the adsorbate-adsorbent interaction.

2.2 Biosorption of Heavy Metals Using Biomass Adsorbents

Adsorption is a separation process where fluid containing contaminants is passed through an adsorbent. Solute or species present in the liquid or gaseous stream is then diffused to the surface of the adsorbent (Ahalya, Ramachandra and Kanamadi 2003). Adsorption is widely known for its use in industries in removing organic and inorganic compounds from waste gas streams using adsorbents such as activated carbon, carbon molecular sieves, polymers, silica alumina, and zeolites (Reimerink and Kleut 1999), however, adsorption from liquid streams is less well understood as the application of adsorption in liquid streams has only been done in the laboratory and pilot-plant scale (Richardson, Harker and Backhurst 2002). Unlike physical adsorption, chemisorbed molecules are fixed at specific sites and may occur at high temperatures with specific activation energies (Faust and Aly 2013).

Over recent years attention has been directed to the process of biosorption as a means of treating water. Similarly to adsorption, biosorption uses biological material or biosorbents to remove heavy metals in water by accumulating metallic ions onto themselves through different mechanisms (Ahalya, Ramachandra and Kanamadi 2003). From several research works done on different biosorbent materials in removing heavy metals from water, biosorption is proving to be a promising

water treatment technique because of its ability to remove a wide range of heavy metals from wastewater. A study done by (Masukume, Onyango and Maree 2014) showed the removal of different heavy metals in AMD water from the Rand Uranium Mine, Randfontein, South Africa. The study used sea shells as a biosorbent to remove aluminium (Al), iron (Fe), and manganese (Mn) from the wastewater at varied biosorbent doses ranging from 0.1g/50mL to 1g/50mL. The removal efficiency for Al ranged from 91.4% to 100%, with Fe ranging from 54.7 to 100% and Mn ranging from 12.1 to 54.4% (Masukume, Onyango and Maree 2014). Another study done by (Schwantes *et al.* 2016) used cassava peels that were modified with hydrogen peroxide (H_2O_2), sulphuric acid (H_2S0_4) and sodium hydroxide (NaOH) for removing cadmium, Cd(II), lead, Pb(II) and chromium, Cr(III), from contaminated water. The adsorption capacities obtained from the Langmuir model were 19.54 mg Cd(II) per gram of modified NaOH, 42.46 mg Pb(II) per gram of modified NaOH and 43.97 mg of Cr(III) per gram of modified H_2O_2 (Schwantes *et al.* 2016). (Mahlangu, Simate and de Beer 2018) used banana peels to treat Mg(II) from actual AMD water and found that the peels' optimal removal was 59.49%. (Afolabi, Musonge and Bakare 2021c) evaluated the removal of Pb(II) using banana peels and found the optimal removal to be at 98.146% at an initial concentration of 100 mg/L, pH of 5, adsorbent dose of 0.55 grams and particle size of 75µm. (Isa *et al.* 2020) used eggshells and sugarcane bagasse as adsorbents to remove Cd (II) and Pb (II) from water and found a maximum adsorption capacity of 277.78 and 13.62 mg/g of Pb (II) and Cd (II), respectively; and 31.45 and 19.49 mg/g using sugarcane bagasse.

Biosorption is the ability of biological materials to accumulate heavy metals onto themselves from contaminated water. Similarly to the adsorption process where molecules present in a gaseous fluid diffuse to the surface of an adsorbent, species present in water or in an aqueous solution diffuse to the surface of a biosorbent through metabolic mediation or physic-chemical means (Ahalya, Ramachandra and Kanamadi 2003). As with adsorption, biosorption can be distinguished between two types, namely physical adsorption and chemical adsorption (chemisorption). Physical

adsorption, also known as van der Waals adsorption, involves only relatively weak intermolecular forces, where molecular interactions are fully reversible (Sincero and Sincero 2002; Faust and Aly 2013). During physical adsorption, adsorbed molecules are free to cover an entire surface of the adsorbent, making it non-site specific. However, chemisorption involves the formation of chemical bonds (ionic or covalent bonds) between the sorbate molecules and the surface of the adsorbent, making the process irreversible. Unlike physical adsorption, chemisorbed metal ions are fixed at specific sites and may occur at high temperatures with specific activation energies (Wang, Hung and Shammas 2007; Faust and Aly 2013). The efficiency of sorption of any species is affected by five factors, namely, temperature, pH of water/aqueous solution, biosorbent, metal concentration and biosorbent dosage.

2.2.1 Factors Affecting Biosorption

2.2.1.1 Temperature

The temperature during the biosorption process affects the performance of the adsorptive uptake of metal in the solution. An increase in temperature may result in more active sites being available for biosorption onto the biosorbent and a decrease in boundary layer thickness surrounding the biosorbent (Ahalya, Ramachandra and Kanamadi 2003). This may have a positive effect on the mass resistance of certain metals in the boundary layer. However, at certain temperatures, the biosorption capacity of a biosorbent may decrease due to the deactivation of biosorbent surfaces or the destruction of some active sites on the biosorbent surface, making the biosorbent sensitive to high temperatures. This phenomenon was noted by (Alpat *et al.* 2010) during the biosorption of nickel by *Circinella sp*, where at temperatures of 20°C and 30°C there was an increase in biosorption; however, at temperatures over 40°C, biosorption decreased. Generally, temperatures in the range of 20 to 25°C do not influence biosorption.

2.2.1.2 pH of Water

The pH of the solution is one of the most important factors during biosorption. The pH of the solution can change the solubility of metal ions and the ionization state of the functional groups in the biomass (Ahalya, Ramachandra and Kanamadi 2003; Alpat *et al.* 2010). There is also a competition of metallic ion uptake that is led by the solution pH, such that pH solutions in acidic regions create repulsive forces between the H^+ ions and the metal ions resulting in low metal uptake in the solution (Alpat *et al.* 2010).

2.2.1.3 Nature of Biosorbent

The nature of the biosorbent affects the uptake of the metal. The function of the chemical makeup of the microbial cells of a biosorbent is determined by the strong biosorbent behaviour of certain functional groups towards metallic ions. Some biological sorbents are broad range with the ability of binding and collect the bulk of heavy metals in an aqueous stream with no specific activity, while other biosorbents are specific for certain metals (Ahalya, Ramachandra and Kanamadi 2003). The degree of biosorbent affinity for a specific metal ion determines the distribution between the solid and liquid phase (Ahalya, Ramachandra and Kanamadi 2003). To increase the biosorption capacity of a biosorbent, alterations can be done to the surface through physical means such as autoclaving, drying and boiling, or through chemical remediation such as using acids and/or alkalis as pre-treatments (Shamim 2018).

2.2.1.4 Biosorbent Dosage

For specific biosorption processes, lower biomass concentrations in an aqueous solution increases specific metal uptake in water due to the availability of binding sites on the biosorbent, because the increase in biomass concentration may lead to possible interferences between the binding sites of the biomass and the uptake of metal ions (Alpat *et al.* 2010). However, for other biosorption processes, there is a direct proportionality between the biomass concentration and metal uptake efficiency,

where an increase in biomass dose increases metallic uptake as there are available adsorption sites (Shamim 2018).

2.2.1.5 Metal Concentration

Initial metal concentration is the driving force for overcoming mass transfer resistance between the liquid and solid phase during biosorption (Kanamarlapudi, Chintalpudi and Muddada 2018; Shamim 2018). It is an important factor in determining the saturation point at which the biosorption capacity of a biosorbent will have reached its limit in absorbing heavy metals by increasing the initial metal concentration in the liquid phase (Kanamarlapudi, Chintalpudi and Muddada 2018). At low metal concentrations biosorption is highly efficient due to complete ion interaction with the biosorbents binding sites, but at increasingly high metal concentrations the number of ions remaining in the liquid phase increases due to the saturation of available binding sites on the biosorbent; therefore, decreasing the removal efficiency during biosorption (Kanamarlapudi, Chintalpudi and Muddada 2018).

2.2.2 Biosorption Mechanisms in Water Using Biosorbents

The biosorption mechanism may be described as the course in which metal ions are taken up by the microbial cell during biosorption (Ahalya, Ramachandra and Kanamadi 2003). There are several ways in which a metal ion can be taken up, however, its mechanism is complex and has not been fully understood by most researchers (Ahalya, Ramachandra and Kanamadi 2003; Ushakumary and Madhu 2013). During biosorption, several process mechanisms may occur which include chemisorption, complexation, adsorption-complexation on surface and pores, ion exchange, chelation, micro-precipitation, heavy metal hydroxide condensation onto the biomass surface, as well as adsorption by physical forces (Ahalya, Ramachandra and Kanamadi 2003; Ushakumary and Madhu 2013). It is, however, theorized that the transport of heavy metals across microbial cell membranes may be aided by the same mechanism used for conveying metabolically essential ions

found in the soil such as potassium, sodium and magnesium (Ahalya, Ramachandra and Kanamadi 2003; Ushakumary and Madhu 2013).

2.2.3 The Use of Agricultural Waste Material as Biosorbents

Biosorbents have been classified as either living organic material which includes bacteria, fungi and algae or non-living organic material such as agricultural wastes (Shamim 2018). Living organic materials have some limitations as biosorbents such as pH where they may not be able to function in acid regions, or have to interact with toxic levels of heavy metals which may affect their metabolism; whereas non-living materials are physically and chemically more robust and can be modified for better adsorption capacity (Pejic *et al.* 2009).

Agricultural wastes such as vegetable and fruit peels have been seen as an ecological burden to society due to their accumulation as waste (Bhatnagar, Sillanpää and Witek-Krowiak 2015). Most agricultural wastes are discarded causing solid waste problems (Anwar *et al.* 2010). However, these discarded wastes have been studied to have great potential, particularly those that are rich in a lignocellulosic matter such as mango peels, orange peels, banana peels, Brazilian nuts, sugarcane bagasse and other such wastes to remove heavy metals from wastewater (Ushakumary and Madhu 2013; Bhatnagar, Sillanpää and Witek-Krowiak 2015; Schwantes *et al.* 2016; Deshmukh *et al.* 2017). Common functional groups such as hydroxyl, carboxyl, phosphate, thiol and amine groups that are found on the walls of waste materials, play important roles in removing metals from aqueous water solutions and can determine the adsorption mechanism of metal uptake in the adsorption process (Ahalya, Ramachandra and Kanamadi 2003; Deshmukh *et al.* 2017).

Orange peels studied by (Ajmal *et al.* 2000) showed the peel's ability to remove nickel, Ni^{2+}, from an aqueous solution containing Zn^{2+}, Cu^{2+}, Pb^{2+} and Cr^{3+}. It was found that the adsorption process followed a first-order kinetic order with monolayer adsorption of 96% at 50°C at an initial concentration of 50 mg L^{-1} and pH of 6. (Li *et al.* 2007) used orange peels that were chemically modified through different processes that included washing, alkali saponification, cross-linking

temperature and concentration of cross-linking reagent on the biosorbent for removing Cd (II) in wastewater. Crude orange peels were collected and characterized for their pore size and surface area and it was determined that the pore diameter was 30.5 Å and the specific surface area was 128.7 m^2 g^{-1}. The adsorption capacity for the orange peels after modification was found to be 0.90 mol kg^{-1}.

The adsorption of Pb(II) onto sugarcane bagasse was studied by (Hamza *et al.* 2013) and they found that the adsorption capacity for Pb(II) to the bagasse was 23.8 mg g^{-1} at 28°C. The adsorption process was found to be spontaneous and enthalpy-driven over a temperature range of 20-45°C. Another study was done using sugarcane bagasse by (Tejada-Tovar *et al.* 2020) for removing Pb(II) characterized their sugarcane bagasse and found that the cell walls of the bagasse contained hydroxyl, carboxyl and carbonyl functional groups. The structure of the bagasse was also determined to be a porous surface in a form of a fibrous cylinder which is typical for lignocellulosic materials. Mango peels were investigated by (Ushakumary and Madhu 2013) to remove several metals namely Cd(II), Pb(II), Zn(II), Cr(III) and Cu(II). The maximum adsorption capacities found for the heavy metals absorbed at equilibrium were 17.3, 31.05, 25.25, 16.4 and 24.8 mg g-1 for Cd (II), Pb (II), Zn (II), Cu (II) and Cr (III), respectively. The adsorption process was found to go well with the Langmuir model along with the pseudo-second kinetic order model.

2.2.4 Banana peels as a Biosorbent

Banana peels are one of the agricultural waste peels that are a burden to the ecology as they are discarded after the peel is removed from the fruit and accumulates in environmental spaces with no definite use. Bananas are tropical fruits that grow in tropical and subtropical areas. They are from the family *Musaceae* and they are cultivated primarily for their fruit (Anwar *et al.* 2010). The most common species cultivated in the Southern African regions is *Musa acuminata* under the Cavendish subgroup. Bananas grow in hanging clusters with approximately 20 fruits to a tier and 3 to 20 hands attached to a cluster (Anwar *et al.* 2010). Areas that grow and cultivate bananas in South Africa are

in the Kwa-Zulu Natal south coast, between Port Shepstone and Port Edward as well as in the northern regions of Kwa-Zulu Natal, north of Mtubatuba and St. Lucia (Lagerwall 2005).

Studies have shown that banana fruits are one of the most widely consumed fruits and they are the fourth most important food crop in the world. In 2016 it was estimated that South Africa produced 402 053 tons of bananas with 114 913 tons imported from other Southern African countries including Nigeria, Ecuador and the Philippines (Department of Agriculture 2017). Due to their abundance in nature and cultivation, several tons of banana waste peels are produced from marketplaces and households as garbage and it accumulates as environmental solid waste (Anwar *et al.* 2010; Bhatnagar, Sillanpää and Witek-Krowiak 2015). Some waste peels have been collected from juice stores and food industries and used for the production of composting, animal feed, as well as in the production of proteins, ethanol, methane, pectin and enzymes (Bhatnagar, Sillanpää and Witek-Krowiak 2015).

However, banana peels, like other agricultural waste peels, have been identified to have lignocellulosic characteristics which contain polymeric groups such as cellulose, hemicellulose and lignin within its structure, making it a potential to be used in removing heavy metals from wastewater (Anwar *et al.* 2010; Branca and Di Blasi 2015; Khawas and Deka 2016). Lignocellulosic materials tend to be hygroscopic (absorbs moisture from the air) and have an affinity to water. Water can permeate into the non-crystalline portion of the cellulose as well as all of the hemicellulose and lignin region (Pejic *et al.* 2009). Therefore, during biosorption water coming into contact with a very large area of different cell wall components is important for the removal of heavy metal ions (Pejic *et al.* 2009). With a very high moisture content of between 60 to 80%, a waste peel on average contains 7.5% of cellulose, 6-8% hemicellulose and 7-12% lignin with a total dietary fibre of around 40-50%; while the significant part of the water-soluble dietary fibers constitutes 10 – 13% of pectin (Branca and Di Blasi 2015). Cellulose is a homo-polymer of glucose of which the peels are richly sourced with it. It has been determined that cellulose-based material is a good biosorbent potential due to the

presence of hydroxyl functional groups within the cell walls of the material (Pejic *et al.* 2009; Jamshaid *et al.* 2017; Daochalermwong *et al.* 2020).

Lignin is the second most abundant polymer group that provides mechanical support to the cell walls of the peels (Branca and Di Blasi 2015; Naseer *et al.* 2019). It is termed as the aromatic subunits polymer and it is a class of macromolecules that can be obtained from phenyl amine, which is found in the secondary cell walls of plants. Lignin makes specific amorphous structures within the solid phase and it consists mainly of carboxylic, phenolic, hydroxyl and carbonyl groups within its structure (Pejic *et al.* 2009; Naseer *et al.* 2019).

Hemicellulose and pectin classify the matrix of polysaccharides where cellulose is embedded in (Khawas and Deka 2016). Both hemicellulose and pectin are hetero-polymers of polysaccharides, where they both play important biological roles in strengthening the cell walls by interacting with the cellulose and lignin. Pectin is a soluble dietary fiber that is widely used in the food, pharmaceutical and cosmetic industries (Khawas and Deka 2016). Both hemicellulose and pectin contain mainly carboxylic and hydroxyl function groups within their structures that aid in the removal of heavy metal ions in water (Pejic *et al.* 2009).

Banana peels also contain minerals that make the fruit a source of micronutrients such as potassium, K, which is the most abundant (Khawas and Deka 2016). Depending on the type of soil the fruit is grown in, the banana fruit may contain several different minerals within its cell walls. Table 2.1 below presents a number of studies done by different authors in removing single or several metals in water using banana peels.

2.2.4.1 Works Cited by Other Research Using Banana Waste Peels as Biosorbents

Below is a table of works done by several research using banana peels as biosorbents in removing one or more heavy metals in water.

Table 2.1 Works done using banana peels for removing heavy metals in water

Adsorbent Used	Metal Removed	% Removal	Adsorp. Capacity (mg/g)	Isotherm	Kinetic	Functional groups	Reference
Banana Peels	Pb^{2+}	98.146		Langmuir	Pseudo-second	OH stretching, CH stretching, C=O, C=C stretching	(Afolabi, Musonge and Bakare 2021c)
Banana Peels	Mg^{2+}	62.61	6.92	Langmuir	Pseudo-second	C-H; C-O; COO^-; N-H; O-H	(Mahlangu, Simate and de Beer 2018)
Banana Peels	Cr^{6+}	92		Langmuir			(Hernández and Romero 2019)
Banana Peels	Cu^{2+}	96	20.37	Langmuir	Pseudo-second		(Hossain et al. 2012)
Banana Peels	Cd^{2+} /Pb^{2+}		5.71/2.18	Freundlich/ Langmuir			(Anwar et al. 2010)
Banana Peels	Cu^{2+} & Pb^{2+}	37.7 & 66.72					(Leong 2018)
Moringa Seed & Banana Peels	Cr^{6+}					O-H stretching, C=O group	(Badessa, Wakuma and Yimer 2020)
Banana Peels	Cd^{2+}		5.91	Langmuir		Hydroxyl, carboxylic, amine groups	(Ali, Saeed and Mabood 2016; Deshmukh et al. 2017)

Mod. Banana Peels	Cr^{6+}	96		Freundlich/ Langmuir	Pseudo-second		(Ali, Saeed and Mabood 2016)
Banana Peels	Pb^{2+}		7.97	Freundlich			(Annadurai, Juang and Lee 2003)
Banana Peels	Cu^{2+}, Pb^{2+}		12.85, 10.9	Koble-Corrigan			(Vilardi, Di Palma and Verdone 2018)
Banana Peels	Co^{2+}, Ni^{2+}	81, 74	9.02, 8.91	Langmuir			(Abbasi et al. 2013)
Unripe Banana Peels	Cd^{2+}, Pb^{2+}		1.9051 , 1.630				(Sirilert and Maikrang 2018)
Ripe Banana Peels	Cd^{2+}, Pb^{2+}		2.6185 , 2.881				(Sirilert and Maikrang 2018)
Banana Peels	Metribuzin		167	Langmuir	Pseudo-second		(ul Haq et al. 2015)
Banana peels	Zn^{2+}	>90%		Langmuir			(Damal and Khanapure 2017)

2.3 Mathematical Models for Biosorption of Heavy Metals

2.3.1 Adsorption Equilibrium Isotherm Models

Adsorption isotherms generally describe the phenomenon governing the retention, release and/or mobility of a species from a fluid phase to a solid phase at constant temperature and pH (Foo and Hameed 2010). It is described by a curve expressing the quantity of adsorbed species in the solid phase against the concentration present in the liquid phase. Adsorption is highly governed by the adsorption equilibrium, which is the ratio between the adsorbed species in the solid phase to that in the liquid phase after a sufficient time of contact where the adsorbate in the bulk solution and in the solid phase are in equilibrium, i.e. there is no more transfer of species between the solid and liquid phase (Foo and Hameed 2010). A number of equilibrium models have been developed to describe the adsorption pathway of different species adsorbed such as the most commonly used Langmuir and Freundlich models amongst others. Research in biosorption have also used these models to help describe the relationship between the adsorbate and the biosorbent. A study done by (Issaoui *et al.* 2021) found that the biosorption of Zn^{2+} followed the Sips isotherm and for Cu^{2+}, Cd^{2+} and Pb^{2+} followed the Redlich-Peterson isotherm using solid free-formaldehyde phenolic foams based on tannins and lignin alkaline liquor. (Damal and Khanapure 2017) found that the biosorption of Zn^{2+} with banana peels favored the Langmuir isotherm model with a coefficient of determination, R^2, of 0.951. Another study done by (Buasri *et al.* 2012) found that the biosorption of Cu^{2+} and Zn^{2+} using hyacinth followed the Langmuir, Freundlich, Temkin and Dubinin-Radushkevich, while (Boulaiche, Hamdi and Trari 2019) found that the Freundlich and Temkin model favored their sorption process for the biosorption of Zn^{2+}, Cd^{2+} and Ni^{2+} with chitin.

2.3.1.1 Langmuir Isotherm

The Langmuir isotherm model was proposed by Irvin Langmuir during an experiment he did on gas-solid phase adsorption to describe a gradual increase of adsorbate molecules onto the surface of a

gas or liquid (Langmuir 1918). The model assumes that the adsorbate behaves as an ideal gas at isothermal conditions and that the surface of the solid is homogenous such that the sites on the surface have equal active sites. The binding of the adsorbate molecules onto the surface of the adsorbent undergoes a chemical adsorption reaction process, called chemisorption, due to active forces acting on the binding process (Langmuir 1918). The model also assumes monolayer or single layer binding of molecules onto the surface of the adsorbent with even distribution sites leading to the surface being chemically saturated (Langmuir 1918). The Langmuir isotherm looks at adsorption and desorption as being reversible where adsorption is proportional to the fraction of the surface of the adsorbent that is open, whereas desorption is proportional to the fraction of the adsorbent surface that is closed (Langmuir 1918). The disadvantage of this model is that it is well suited for low concentrations adsorbate-adsorbent interaction and does not fit well with high concentrations (Langmuir 1918).

The Langmuir isotherm model can be mathematically described by the following equation as described by,

$$\frac{q_e}{q_L} = \frac{K_L C_e}{1+K_L C_e} \qquad (2\text{-}1)$$

Equation 2-1 can also be linearized as,

$$\frac{C_e}{q_e} = \frac{1}{K_L q_L} + \frac{C_e}{q_L} \qquad (2\text{-}2)$$

Where q_e is the adsorption capacity of an adsorbent (mg/g), C_e is the equilibrium concentration (mg/L), K_L is the Langmuir constant (L/mg) and q_L is the Langmuir monolayer adsorption capacity (mg/g) (Hall *et al.* 1966).

The Langmuir isotherm has a separation factor that is used for describing the favorability of the adsorption system for systems favoring the Langmuir isotherm. The essential characteristics of the Langmuir equation can be expressed as a separation factor, R_L, given as,

$$R_L = \frac{1}{1+K_L C_O} \quad (2\text{-}3)$$

The R_L factor is bound between 0 and 1, where if R_L =0 then the system is irreversible, if 0< R_L <1 then the system is favorable, if R_L =1 then the system is linear and R_L > 1 means that the system is unfavorable and may not be of a Langmuir-type (Hall *et al.* 1966).

Although the Langmuir adsorption isotherm was developed primarily for gas-solid phases, the isotherm is an industry used standard for many adsorption applications and it has been used in a number of biosorption cases to describe the mechanism of experiments done by researches with various biosorbents (Memon *et al.* 2009; Imran Din *et al.* 2013; Ali *et al.* 2016; Ahad, Goswami and Syiem 2017).

2.3.1.2 Freundlich Isotherm

The Freundlich model is the earliest model used to describe gas phase and solute adsorption (Sparks 2003). The Freundlich isotherm is an empirical expression developed by Herbert Freundlich to give an empirical relation between the concentration of the solute on the surface of an adsorbent to the concentration of the solute in the gas/liquid phase (Freundlich 1922). The isotherm gives an expression representing the isothermal variation of adsorption of a quantity of gas adsorbed by unit mass of a solid adsorbent with pressure (Freundlich 1922).

The isotherm was developed based on the assumption that adsorption can occur on a heterogeneous surface of an adsorbent with non-uniform distribution of energy levels (Adamson and Gast 1967). It is assumed that an adsorbent with a homogeneous surface (single sites) has constant heat energy levels, however an adsorbent with a heterogeneous surface (multi sites) exhibits variable heat energy levels of adsorption which is dependent on the number of opened sites (Adamson and Gast 1967).

The Freundlich equation is expressed in the following linearized equation below,

$$q_e = K_f C_e^{\frac{1}{n}} \quad (2\text{-}4)$$

The Freundlich expression is an exponential equation, therefore, assuming that as the adsorbate concentration increases, the concentration of adsorbate on the adsorbent surface also increases (Hamdaoui and Naffrechoux 2007).

Equation 2-4 can also be linearized to,

$$\log q_e = \log K_f + \frac{1}{n} \log C_e \quad (2\text{-}5)$$

Where K_f is the Freundlich constant known as the sorption capacity (Batool *et al.* 2018). The slope, *1/n*, is the adsorption intensity or surface heterogeneity, where the slope ranges between 0 to 1 for a process that undergoes physical adsorption. If *1/n* is above 1 then the process would have gone chemisorption (Foo and Hameed 2010).

2.3.1.3 Elovich Isotherm

The Elovich isotherm model was developed based on the Elovich kinetic principle which assumes that adsorption sites increase exponentially with adsorption which is based on chemisorption of gas molecules onto the surface of solids (Ayawei, Ebelegi and Wankasi 2017). This model implies that the adsorption taking place is a multilayer adsorption (Ayawei, Ebelegi and Wankasi 2017). The Elovich isotherm equation can be expressed as follows,

$$\frac{q_e}{q_E} = K_E C_e e^{\frac{q_e}{q_E}} \quad (2\text{-}6)$$

Linearized, equation 2-6 is expressed as,

$$\ln \frac{q_e}{C_e} = \ln K_E q_E - \frac{q_e}{q_E} \quad (2\text{-}7)$$

Where K_E (L mg^{-1}) is the Elovich constant and q_E is the Elovich monolayer adsorption capacity (mg/g).

2.3.3 Adsorption Kinetic Models

The study of adsorption kinetics is used for investigating the mechanism of adsorption as well as the potential rate controlling or limiting steps such as mass transfer and chemical reaction processes (Ho and McKay 1998). There are several mathematical models that have been developed and used for describing a number of adsorption processes from process data and these models can generally be classified into two groups (Qiu *et al.* 2009). The first is adsorption diffusion models involving mainly three steps, consecutively; (1) diffusion across the liquid film surrounding the biosorbent particles, which is external or film diffusion; (2) diffusion in the liquid contained in pores and/or along the pore walls, which is internal or intra-particle diffusion; and, (3) biosorption and desorption between the adsorbate and active sites, which is mass transfer (Qiu *et al.* 2009). For processes governed by physical adsorption, mass transfer of solute to the adsorbent/biosorbent is very rapid, of which in some cases kinetic studies may be negligible. In such cases the kinetic process is controlled by liquid film or intraparticle diffusion. The second type of adsorption kinetic models are based on chemical reaction kinetics linked to the whole adsorption process without considering any diffusion mechanism (Qiu *et al.* 2009).

2.3.3.1 Pseudo-first Order Kinetic Equation Model (Lagergren's Kinetic Model)

The pseudo-first model was first represented by Lagergren to describe the kinetic relationship between the solid-liquid phase sorption of oxalic acid and malonic acid onto charcoal (Lagergren 1898). The model is based on the assumption that the rate of change of solute uptake with time is directly proportional to the difference in saturation concentration and the amount of solute uptake with time, usually applicable at the initial stages of adsorption (Sahoo and Prelot 2020). The model is based on the capacity of adsorption and it is described by the following equation (Ho 2006),

$$\frac{dq_t}{dt} = K_1(q_e - q_t) \qquad (2\text{-}8)$$

Where q_e and q_t (mg/g) are the adsorption capacities at equilibrium and time t (min) respectively, and K_1 (min-1) is the pseudo-first order rate constant. After integrating from $t = 0$ to $t = t$ and $q_e = 0$ to $q_e = q_t$ the above equation is shown below in a linearized form

$$\ln(q_e - q_t) = \ln q_e - \frac{K_1}{2.303} t \quad (2\text{-}9)$$

The above equation when applied to experimental data differs from a true first order equation in two ways (Ho and McKay 1998):

1. The parameter $k_1 (q_e - q_t)$ does not represent the number of available sites.
2. The parameter log (q_e) is an adjustable parameter and it is often found not equal to the intercept of a plot of log $(q_e - q_t)$ against t, whereas in a true first order log (q_e) should be equal to the intercept of a plot of log $(q_e - q_t)$ against t.

2.3.3.2 Pseudo-second Order Kinetic Equation Model

The pseudo-second order kinetic model was presented by Ho in 1995 in the adsorption of divalent Cu^{2+} ions from a gas phase onto peat. The model was described based on the peats solid adsorption capacity where peat contained polar functional groups of aldehydes, ketones, acids and phenols which were involved in the chemical bonding of divalent metal ions and where also responsible for the cation exchange on peat (Ho and McKay 1998; Ho 2006).

The assumptions for the pseudo-second model are that adsorption may be second-order and that the rate limiting step may be chemisorption involving valent forces through sharing or exchanging electrons between the biosorbent and divalent metal ions in an aqueous solution (Sahoo and Prelot 2020). The adsorption rate is dependent on the capacity of the adsorbent and not the concentration of the adsorbate (Sahoo and Prelot 2020). In addition, the adsorption/biosorption process follows the Langmuir equation (Ho and McKay 1998).

The pseudo-second order kinetic equation is expressed as,

$$\frac{dq_t}{dt} = K_2(q_e - q_t)^2 \quad (2\text{-}10)$$

Where K_2 is the pseudo-second order sorption constant (g/mg.min). When the equation is integrated and linearized, the following equation suffices,

$$\frac{t}{q_t} = \frac{1}{K_2 q_e^2} + \frac{1}{q_e} t \quad (2\text{-}11)$$

2.3.3.3 The Intraparticle Diffusion Model

The Weber-Morris diffusion model is based on the solute uptake which is almost proportional to the half time, $t^{\frac{1}{2}}$, rather than contact time (Qiu *et al.* 2009). When applied, the model involves a multi-step approach involving the transport of solute molecules from the aqueous solution phase to the surface of the biomass adsorbent particles, which is followed by diffusion of the solute molecules into the interior of the pores, which is likely to be a slow process (Agarwal *et al.* 2015). In theory for the model to be applicable, the plot of q_t must give a linear function where the line passes through the graph for intra-particle to be the rate-limiting step. However, on many occasions the plot does not pass through the origin indicating that there is more than one mechanism in the diffusion of solute to the adsorbent (Kajjumba *et al.* 2018). There are mainly four steps involved during adsorption and that is (Kajjumba *et al.* 2018),

1) mass transfer of solute onto the adsorbate of which is a rapid process and it is not considered for the design of kinetic systems,
2) film diffusion where there is a slow movement of the solute from the boundary layer to the adsorbents surface,
3) from the surface of the adsorbent, the solute moves to the pores of the adsorbent, and
4) adsorptive attachment of the solute onto the pores of the adsorbent, of which it is also rapid and not considered for design of kinetic systems.

The equation is described as follows,

$$q_t = K_{id} t^{1/2} \quad (2\text{-}12)$$

In general, biosorption kinetics may be controlled by film and intraparticle diffusion simultaneously, however for this model it is essential that the plot of the equation ($q_t \ vs. \ t^{1/2}$) goes through the origin if intraparticle diffusion is the sole rate-limiting step (Qiu et al. 2009). K_{id} is the intraparticle diffusion rate constant (mg. g^{-1} $min^{-1/2}$). However, if the plot does not pass through the origin then film diffusion is the rate-limiting step (Kajjumba *et al.* 2018).

2.3.4 Mathematical Models for Fixed-Bed Column Studies

Different mathematical models were developed to help determine the dynamic response of the column as the equations developed are dependent on the mechanism(s) responsible for metal uptake during adsorption. The mechanism by which adsorption takes place in a column may be through mass transfer of solute from liquid to the surface of the solid, diffusion and/or reaction on the solid surface (chemisorption) (Patel 2019; Mohanta *et al.* 2021). The most used adsorption models are the Thomas, Yoon-Nelson and Adams-Bohart models.

2.3.4.1 Thomas Model

The Thomas model is widely used in column performance studies for evaluating the capacity of the adsorbent in a fixed column (Masukume, Onyango and Maree 2014). The model is based on the assumption that the adsorption process is derived from the Langmuir isotherm model for adsorption-desorption and that the rate driving force follows the pseudo-second order reversible reaction kinetics with no dispersion and with a predominating film diffusion resistance (Saadi, Saadi and Fazaeli 2013; Patel 2019). The primary disadvantage of the Thomas model is that it is derived from the assumption that adsorption is only by second-order reaction kinetics, of which adsorption is not limited only to chemisorption but it is mostly controlled by interphase mass transfer (Aksu and Gönen 2004). The linearized form of the Thomas model can be expressed as,

$$\ln\left[\frac{C_O}{C_T}-1\right]=\frac{K_T q_T M}{Q}-K_T C_o t \quad (2\text{-}13)$$

Where, K_T is the Thomas model constant (L/ mg min), q_T is the adsorption capacity (mg/g), Q the volumetric flow rate (mL/min), M the mass of adsorbent (g), C_o initial metal concentration (mg/L), and C_T is the effluent concentration (mg/L).

2.3.4.2 Yoon-Nelson Model

The Yoon-Nelson model was developed as a relatively simple model to address adsorption and the breakthrough behavior of an adsorbate in a gas phase with respect to the adsorbent (Aksu and Gönen 2004). The model is based on the assumption that the rate of decrease in the probability of adsorption for each adsorbate molecule is proportional to the probability of adsorbate adsorption, as well as the probability of adsorbate breakthrough on the adsorbent (Aksu and Gönen 2004; Chowdhury *et al.* 2013). The Yoon-Nelson model does not take into details data concerning the characteristics of the adsorbate, the type of adsorbent and the physical properties of the adsorption bed (Aksu and Gönen 2004).

The following equation below is the linearized equation of the Yoon-Nelson model,

$$\ln\frac{C_t}{C_o-C_t}=k_{YN}t-\tau k_{YN} \quad (2\text{-}14)$$

Where k_{YN} and τ are the Yoon-Nelson rate constant (min^{-1}) and the time required for 50% adsorbate breakthrough (min).

2.3.4.3 Adams-Bohart Model

The Adams-Bohart model was developed with a basis on surface reaction theory where the relationship between the adsorption rate is proportional to the residual capacity of the adsorbent and the concentration of the species with an adsorption equilibrium that is not instantaneous (Masukume, Onyango and Maree 2014). This model describes the initial part of the breakthrough curve, as well

as the relationship between C_t/C_o and *t* during continuous operation (Ntimbani, Simate and Ndlovu 2016; Radhika *et al.* 2018).

$$\ln\left(\frac{C_t}{C_o}\right) = K_{AB}C_o t - K_{AB}N_o\left(\frac{Z}{U_o}\right) \quad (2\text{-}15)$$

Where K_{AB} is the Adams-Bohart kinetic constant (L/mg min), N_o is the saturation concentration (mg/L), Z is the adsorbent bed depth (cm), and U_o is the linear velocity defined as the ration of volumetric flowrate in (mL/min) to the cross-sectional area in (m^2) of the bed (cm/min).

CHAPTER 3

3.1 Introduction

Banana peels were used for evaluating its performance as a biomass adsorbent for removing Cr^{6+} and Cu^{2+} from water by performing batch and column experiments. This chapter describes in detail the materials, instruments and analytical tools used for evaluating the performance of banana peels as a biomass material for removing Cr^{6+} and Cu^{2+} from water. All experimental work was conducted from the Mangosuthu University of Technology and analysis of samples were done at the Mangosuthu University of Technology as well as the University of Kwa-Zulu Natal Pietermaritzburg. Other institutions were also involved in analyzing the characteristics of banana peels as will be mentioned further.

3.2 Methodology of Experiments and Materials

3.2.1 Materials

3.2.1.1 Banana Peels

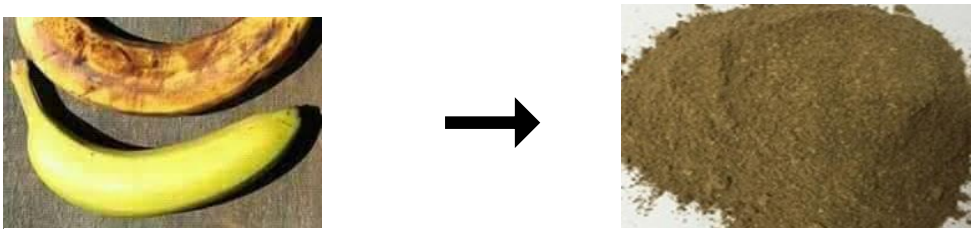

Figure 3.1: Banana peels collected and crushed to powder

Banana peels were collected from a local fruit and vegetable stores around Durban, Kwa-Zulu Natal, South Africa. The collected peels were washed twice with tap water followed twice by deionized water to remove dirt and impurities. The washed peels were then placed on a tray and dried in a convection dryer at a constant air speed of 1.6 m/s and temperature of 60°C for 48 hours. The dried peels were then crushed in a blender and reduced to powder of different particle sizes and then

washed again to remove impurities obtained while crushing. The resultant cake was then dried in an oven at constant temperature of 120℃ for 48 hours until the cake was dried back to powder. The powder was then sieved in a balance shaker for 10 minutes and collected a particle size distribution of 710µm (8%), 500 µm (16%), 355 µm (24%), 250 µm (32%) and 180 µm (20%). The powder was then stored in a sealing glass jar and used for studies.

3.2.1.2 Chemicals

Water was synthesized in the lab to represent drinkable water that has high metal content for human intake. This water represents water that can be found mostly in rural areas and villages where humans and animals are dependent on these waters for sustenance, but do not have the necessary means for treating such waters. The chemicals used for the experiment to produce synthetic contaminated potable water was of analytical grades. Both metals were prepared by adding precalculated quantities of analytical grade $CuSO_4.5H_2O$ (copper sulfate heptahydrate) and $Na_2CrO_4.4H_2O$ (sodium chromate tetrahydrate) to deionized water during experiments. Chemical assay of each metal salt is found in the Appendices, under Appendix A. During synthesizing of water for all experiments, all water solutions were mixed for 10 minutes and were left to rest for 30 minutes to ensure that the salts were fully dissolved in water. The pH values were adjusted by using 0.1*N* of HCl (hydrochloric acid) and 0.1*N* of NaOH (sodium hydroxide). Molecular weights of the salts were 249.69 g/mol for $CuSO_4.5H_2O$ and 234.04 g/mol for $Na_2CrO_4.4H_2O$. Batch studies of pH studies, agitation speed, biosorbent dosage, metal concentration and contact time only used single metal component in the water solutions synthesized of Cr^{6+} and Cu^{2+}. Calculations of synthetic water preparations can also be seen under Appendix B, in the Appendices.

3.2.2 Characterization of Banana Peels

The characterization of banana peels was done to determine the properties of the peels contain. The analytical instruments used for analyzing the properties in banana peels were the Fourier-Transform

Infrared Spectroscopy (FTIR) to determine the functional groups present in the peels, Scanning Electron Microscopy (SEM) and Energy Dispersive X-ray Spectroscopy (EDS) to determine the surface morphology and composition of the peels, the X-ray Diffraction spectrometry (XRD) to determine the phase of the peels, and the Brunauer-Emmett-Teller (BET) for analyzing pore size and volume on the surface of the banana peels.

3.2.2.1 Fourier-Transform Infrared Analysis (FTIR)

The FTIR Frontier model was used to determine the banana peel's molecular composition and structure. The FTIR analysis measures the range of wavelengths in the infrared region that are absorbed by a material. This is accomplished through the application of infrared radiation (IR) to samples of a material. The sample's absorbance of the infrared light's energy at various wavelengths is measured to determine the material's molecular composition and structure (Skoog *et al.* 2013). The basic theory at work is that the bonds between different elements absorb light at different frequencies. The light is measured using an infrared spectrometer which produces the output of an infrared spectrum. The IR spectrum is a graph of infrared light absorbance by the substance on the vertical axis and the frequency (wavelength) on the horizontal axis (Skoog *et al.* 2013).

Samples of banana peels were sent for FTIR analysis at the Mangosuthu University of Technology before and after adsorption of Cr^{6+} and Cu^{2+}. Results were displayed in a graph showing different peaks and bands indicating the functional groups contained in the banana peels and which groups have been active during adsorption of both metals.

3.2.2.2 Scanning Electron Microscope (SEM)/Energy Dispersive X-ray Spectroscopy (EDS)

The scanning electron microscope (SEM) is applied for the examination and analysis of the microstructure morphology and chemical composition characterizations of a given material (Zhou *et al.* 2006). SEM is a method for high-resolution imaging of surfaces. The SEM uses electrons for

imaging, whereas the light microscope uses visible light. The SEM generates a beam of incident electrons in an electron column above the sample chamber (Materials Evaluation and Engineering 2014b). The electrons are produced by a thermal emission source, such as a heated tungsten filament, or by a field emission cathode. The electrons are focused into a small beam by a series of electromagnetic lenses in the SEM column. Scanning coils near the end of the column direct and position the focused beam onto the sample surface. The electron beam is then scanned in a raster pattern over the surface for imaging. The beam can also be focused at a single point or scanned along a line for x-ray analysis (Materials Evaluation and Engineering 2014b).

Energy Dispersive X-Ray Spectroscopy (EDS or EDX) is a chemical microanalysis technique used in conjunction with SEM and the technique detects x-rays emitted from the sample during bombardment by an electron beam to characterize the elemental composition of the analyzed volume (Materials Evaluation and Engineering 2014a). When the sample is bombarded by the SEM's electron beam, electrons are ejected from the atoms comprising the sample's surface. The resulting electron vacancies are filled by electrons from a higher state, and an x-ray is emitted to balance the energy difference between the two electrons' states. The x-ray energy is characteristic of the element from which it was emitted (Materials Evaluation and Engineering 2014a).

Samples of banana peels were sent to the University of Cape Town to be analyzed for its morphological structure and elemental composition, before and after adsorption for both metals. SEM results displayed images of the peels and the EDS results displayed the elements present in the peels before and after adsorption.

3.2.2.3 X-ray Diffraction spectrometry (XRD)

The XRD-Bruker (D8 Advance) was used for the analysis. The XRD analysis is used for the identification of materials based on their diffraction pattern as well as for phase identification. X-ray diffraction is based on constructive interference of monochromatic X-rays and a crystalline sample (Dutrow 2020). These X-rays are generated by a cathode ray tube, filtered to produce monochromatic

radiation, collimated to concentrate, and directed toward the sample. The interaction of the incident rays with the sample produces constructive interference (and a diffracted ray) when conditions satisfy Bragg's Law. This law relates the wavelength of electromagnetic radiation to the diffraction angle and the lattice spacing in a crystalline sample (Dutrow 2020). These diffracted X-rays are then detected, processed and counted. By scanning the sample through a range of 2θangles, all possible diffraction directions of the lattice should be attained due to the random orientation of the powdered material. Conversion of the diffraction peaks to d-spacings allows identification of the mineral because each mineral has a set of unique d-spacings. Typically, this is achieved by comparison of d-spacings with standard reference patterns (Dutrow 2020).

The banana peel samples of before and after adsorption of both metals were sent for XRD analysis at the iThemba Labs, Western Cape Province. The results obtained are displayed in graphs as well as the data obtained was used for determining the crystallinity of the samples.

3.2.2.4 Brunauer-Emmett-Teller (BET)

The BET results were analyzed using the TriStar 3000 V6.08 A model. The BET analysis is a measurement used for determining the specific area of a certain material. This analysis is based on the BET theory explaining the physical adsorption oof gas molecules on a solid surface. The surface area of an adsorbent plays an important role in adsorption where the larger the surface area the greater the adsorption capacity (ODIYO and EDOKPAYI 2018). A sample is determined at an atomic level by adsorption of an unreactive gas such as nitrogen. During adsorption, the material is cooled and kept constant at isothermal conditions while increasing the pressure/concentration of the adsorbing gas. As pressure increases so does the gas molecules increase on the surface of the material. The number of gas molecules in the monolayer is recordable from the volume adsorbed. The cross-sectional area and pore size are then calculated from the volume recorded. A sample is determined at an atomic level by adsorption of an unreactive gas such as nitrogen. A sample is determined at an atomic level by adsorption of an unreactive gas such as nitrogen. A sample is determined at an atomic

level by adsorption of an unreactive gas such as nitrogen. A sample is determined at an atomic level by adsorption of an unreactive gas such as nitrogen.

Banana peel samples was sent for analysis to the Witwatersrand University, Johannesburg, to determine the surface area, pore volume and pore size of the peels. The particle size of the sample sent was $250 < d_s < 355$ µm.

3.2.3 Equipment used for Experiments

Jar tests were used for batch experiments as seen in figure 3.2. The jar test mixer contained 6 stations where one-liter beakers were used for the experiments. The paddles were pre-installed into the mixer and they were controlled by the speed gauge in RPM and the timer for controlling the time for experimental runs.

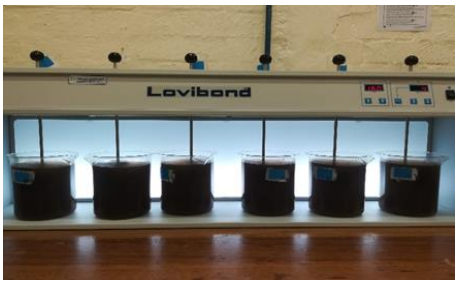

Figure 3.2: Jar Test Mixer

For the fixed-bed continuous column experiment, a glass column was used with a total height of 50 cm, outer and internal diameter of 3 cm and 2.3 cm, as seen in figure 3.3. A peristaltic pump was also used to inject influent stream into the column and to pass it through a fixed bed of crushed banana peels at a controlled volumetric flowrate.

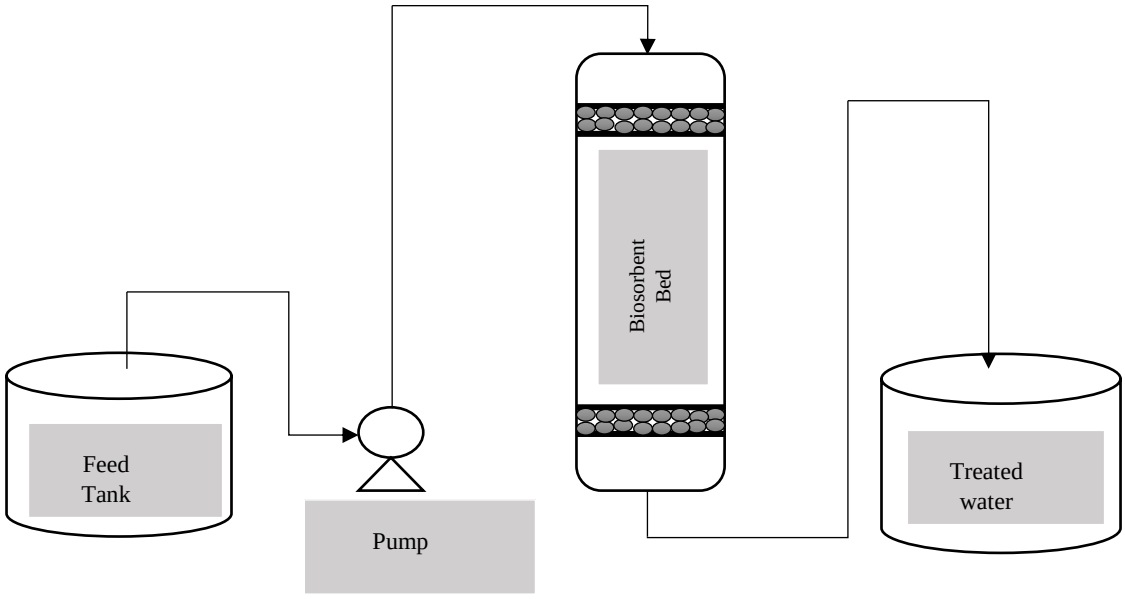

Figure 3.3: Continuous fixed-bed column

3.2.4 Equipment used for Sample Analysis

The Atomic Absorption Spectroscopic (AAS) and Inductively Coupled Plasma Mass Spectrometry (ICP-MS) were used for analyzing the filtrate after adsorption for all samples. The AAS was used for analyzing Cu^{2+} samples at the Mangosuthu University of Technology, whereas the Cr^{6+} samples were analyzed using the ICP-MS at the University of Kwa-Zulu Natal Pietermaritzburg.

3.2.5 *Study of Batch Experiments for Cr^{6+} and Cu^{2+}*

For batch experiments, the removal efficiency was calculated using eq 3.1

$$\%removal = \frac{C_o - C}{C_o} \times 100\% \qquad (3\text{-}1)$$

Where, C_o and C are the initial and final metal concentrations in mg/L.

3.2.5.1 Study of pH

The pH of water was prepared by adding 0.1*N* HCl and 0.1*N* NaOH. The pH range for the experiment was done at 2, 3, 4, 5, 6 and 7 with the intention of determining the solution pH at which banana peels performed best during biosorption. Parameters that were kept constant during the process were contact time of 120 min, biosorbent dosage of 4 g and agitation speed of 180 rpm.

3.2.5.2 Study of Agitation Speed

Agitation speed was evaluated by preparing water solutions at 5 and 10 mg/L of Cr^{6+} and Cu^{2+}, respectively. The following parameters kept constant were contact time of 120 min, adsorbent dosage of 4 g and pH of 4. Agitation speed was varied from 100 to 200 rpm at incremental intervals of 20 rpm, i.e., 100, 120, 140, 160, 180 and 200 rpm.

3.2.5.3 Study of Adsorbent Dosage

Adsorbent dosage was studied for its impact on metal uptake for metals. Water solutions were prepared in beakers at different adsorbent doses of 1, 2, 3, 4, 5 and 6 grams for Cr^{6+} and Cu^{2+}. The following parameters were kept constant: contact time of 120 min, pH of 4 and agitation speed of 180 rpm at 5 and 10 mg/L of Cr^{6+} and Cu^{2+}, respectively.

3.2.5.4 Study of Metal Concentration

This study was done to determine the biosorbent capacity of banana peels. The concentrations used for each metal separately were 5, 10, 15, 20, 30, 40 50, 60 and 80 mg/L. The experiments ran for a total of 120 minutes and parameters kept constant were adsorbent dose of 5 g, agitation of 180 rpm and pH of 4.

3.2.5.5 Study of Contact Time

Contact time was studied for establishing adsorption equilibrium. Total time measured for both metals was 140 minutes where samples were taken at time intervals of 5, 10, 15, 30, 40, 50, 80, 100,

120, and 140 minutes. Parameters kept constant were adsorbent dose, metal concentration, agitation speed and pH of 5 g, 10 mg/L, 180 rpm and pH of 4.

3.2.6 Study of Adsorption Isotherms

Adsorption isotherms were conducted for this study to determine the behavior of metal uptake by which adsorption takes place during the biosorption of Cr^{6+} and Cu^{2+} using banana peels. Isotherm studies were carried out by running batch experiments of different metal concentrations of 10, 15, 20, 30, 40, 50 and 60 mg/L of metal ion for 120 minutes at constant pH, biosorbent dose and agitation speed of 4, 3 grams and 180 rpm, respectively. The Langmuir, Freundlich and Elovich isotherm models were used for equilibrium studies, and the equations are stated in the Literature Review, Chapter 2.

3.2.7 Study of Adsorption Kinetics

Adsorption kinetics were also conducted to determine the mechanism, rate of biosorption and rate-limiting step for metal uptake of both Cr^{6+} and Cu^{2+} using banana peels. The study was carried out by varying contact time at 5, 10, 20, 30, 50, 80, 100 and 120 minutes. Parameters kept constant were pH of 4, agitation speed of 180 rpm, biosorbent dose of 5 g and metal concentration of 10 mg/L. The pseudo-first kinetic model, pseudo-second kinetic model and intra-particle diffusion kinetic model were used for kinetic studies and the equations are taken from the Literature Review section in Chapter 2.

3.2.8 Study of Breakthrough Curves in a Fixed-Bed Column

3.2.8.1 Study of Bed Height

Removal of Cr^{6+} was studied in a continuous fixed-bed column. The column performance in the fixed-bed column was determined by breakthrough curves which is a plot of the concentration ratio C_t/C_o against time t. Water was synthesized in a 10L container for continuous flow through the column. Studies were based on varying bed-height of banana peels at 5, 10, 15 and 30 cm. The

biosorbent particle size distribution was between $180 \leq d_s \leq 710$ µm. Banana peels were collected and dried for weighing to obtain the bulk density of the peels. The Cr^{6+} concentration of 5 mg/L, volumetric flowrate 4 mL/min and solution pH of 4 were kept constant. Calculations for bed height studies can be found in the Appendices, Appendix 4.

From literature, the breakthrough point should be within 0.01 and 0.05 of C_t/C_o (Geankoplis, Hersel and Lepek 2018), however, the threshold guideline of Cr^{6+} in drinking water from DWAF and WHO, water must not have a concentration exceeding 0.05 mg/L (50 µg/L). Therefore, the breakthrough time from the experiments conducted was determined at $C_t/C_o \leq 0.01$.

3.2.9 Study of Mathematical Adsorption Models for Fixed-Bed Columns

Mathematical models were applied from the results obtained in the study of bed heights. The equations used were the Thomas model, Yoon-Nelson model and Adams Bohart model equations for the evaluation of the dynamic behavior of the removal of Cr^{6+} ions in a fixed-bed column using banana peels.

CHAPTER 4

4.1 Introduction

The core of this chapter is to show the results obtained from all the experimental work done and to discuss on the findings and compare them with similar studies. The chapter is separated into mainly four sections, the first section is the batch experimental work, the second is the isotherm studies followed by the kinetic studies, the third section is the characterization of the banana peels before and after biosorption and the final section is the column experimental work. A conclusion is drawn after each section.

4.2 Preliminary Studies for the Biosorption of Cr^{6+} and Cu^{2+}

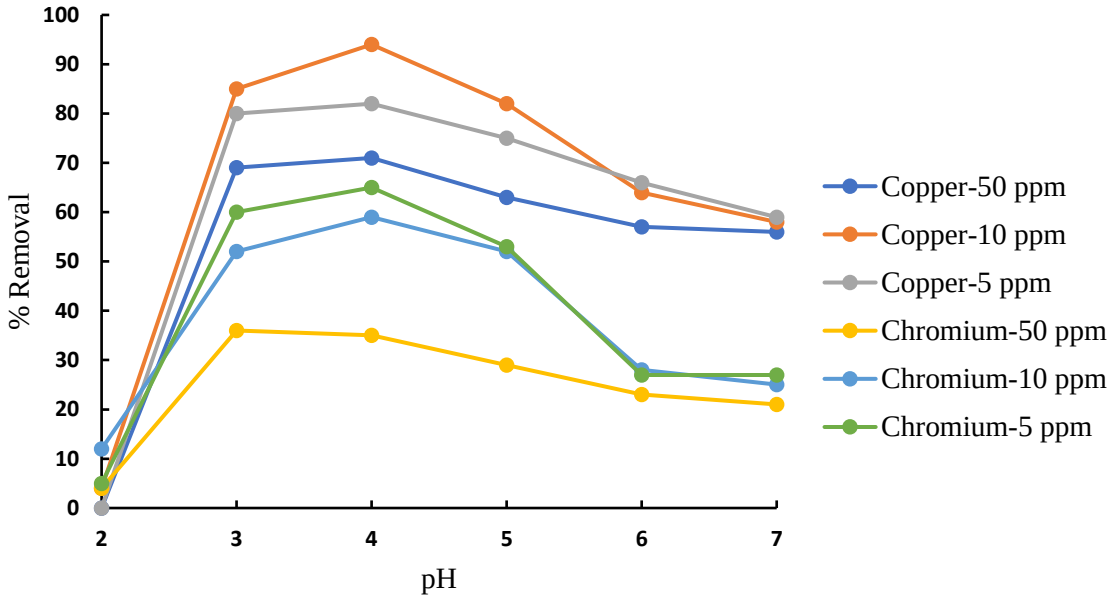

Figure 4.1: Preliminary studies of pH for the biosorption of Cr^{6+} and Cu^{2+}

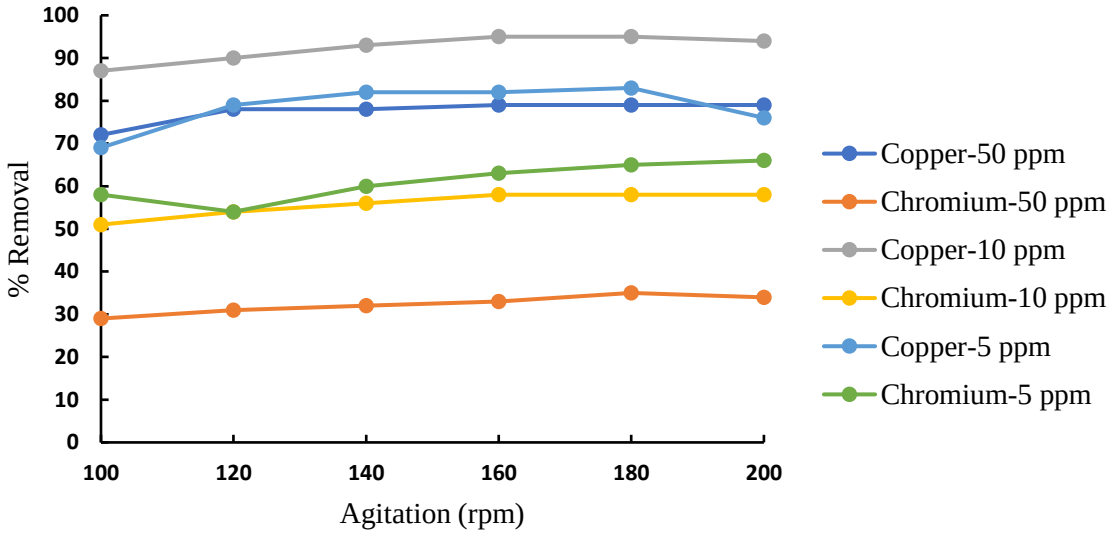

Figure 4.2: Preliminary studies of agitation speed for the biosorption of Cr^{6+} and Cu^{2+}

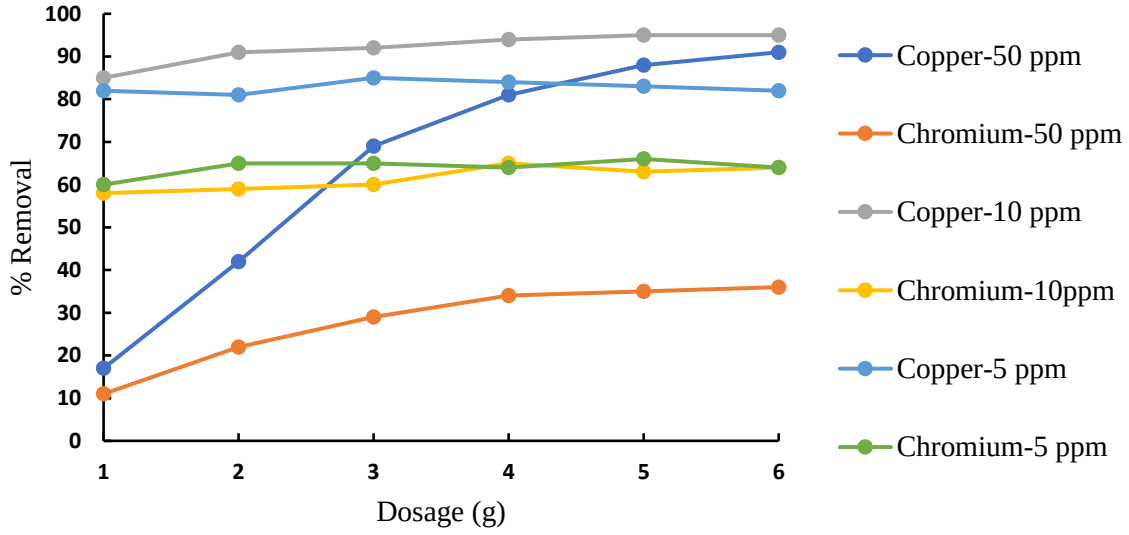

Figure 4.3: Preliminary study of biosorbent dosage

Preliminary studies were performed for pH, agitation speed and dosage to determine the removal performance of banana peels in removing Cr^{6+} and Cu^{2+} from water, as well as to determine which parameters had the most effect on the process. Preliminary studies of pH were conducted and found that solution pH of between 3 and 4 across the concentration range had better removal efficiency for both Cr^{6+} and Cu^{2+} as seen in figure 4.1. Therefore, the solution pH for all experiments, batch and

continuous, were conducted at pH of 4. Preliminary studies of agitation speed were also performed to determine batch study experiments going forward. From figure 4.2, the highest removal efficiency was found between 140 and 180 rpm for both metals and, therefore, 180 rpm was chosen for batch experiments. Preliminary studies for adsorbent dosage were performed to evaluate the effect of dosage against the concentration range and found that the highest removal was at 5 mg/L for Cr^{6+} and 10 mg/L for Cu^{2+}.

4.3 Batch Studies for the Biosorption of Cr^{6+} and Cu^{2+} in Water

4.3.1 The Study of pH

In this study a pH range of 2 to 7 in synthesized water was analyzed for its effect on biosorption with banana peels and the results are displayed in figure 4.4. The best removal efficiency was found at pH value of 3 and 4 for both Cu^{2+} and Cr^{6+}. At higher pH values of 5 for Cr^{6+} and 6 for Cu^{2+}, metal ions started to precipitate forming metal hydroxide ions of which biosorption may not only have been the only process taking place. The best removal efficiency at pH values of 3 and 4 was in line with works done by authors who used banana peels as a biosorbent for removing heavy metals in water (Hossain *et al.* 2012; Tasaso 2014; Mahlangu, Simate and de Beer 2018; Hernández and Romero 2019; Badessa, Wakuma and Yimer 2020). This showed that pH has a significant impact in biosorption and that the peels can remove metals in the acidic region due to the surface of the peels being acidic and making it possible for proton metal ion competition (Afolabi, Musonge and Bakare 2021b).

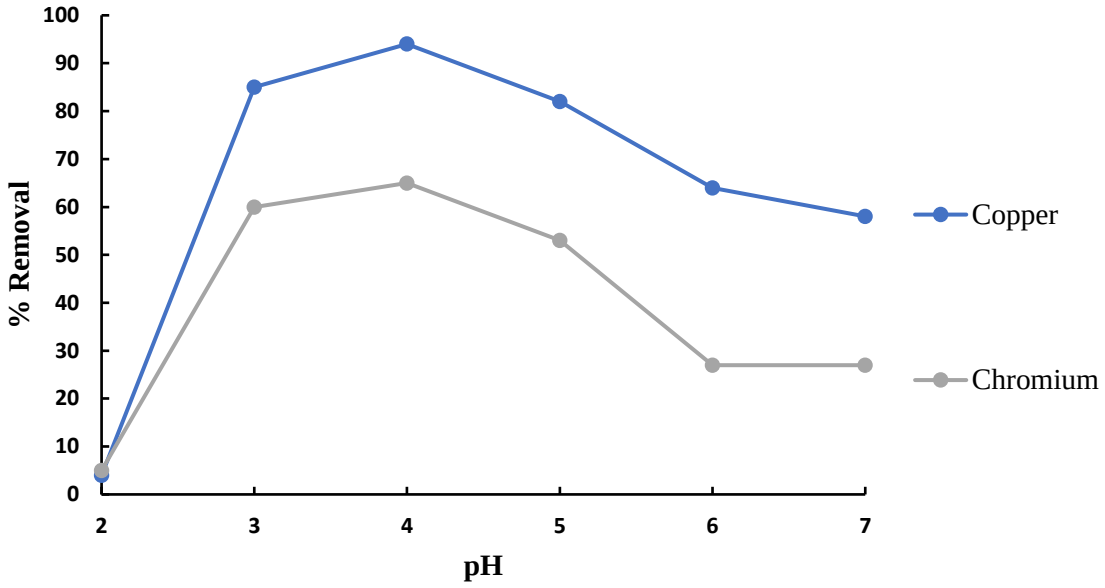

Figure 4.4: Results of pH variation for the biosorption of Cr^{6+} and Cu^{2+}

4.3.2 The Study of Agitation Speed

Agitation speed was varied between 100 to 200 rpm. In general, the variation in agitation speed did not have a significant impact in the removal of both metals during biosorption, between the given ranges as seen in figure 4.5. For Cu^{2+} the maximum removal was found between 160 to 180 rpm at 95% and for Cr^{6+} at 180 rpm at 67%. Agitation speeds above 200 rpm for a number of biosorbents have shown a decrease in metal uptake due to high turbulence caused by high agitation speeds, leading to desorption after equilibrium time was reached (Geethakarthi and Phanikumar 2011; Javaid *et al.* 2011; Zahoor 2011; Kanamarlapudi, Chintalpudi and Muddada 2018).

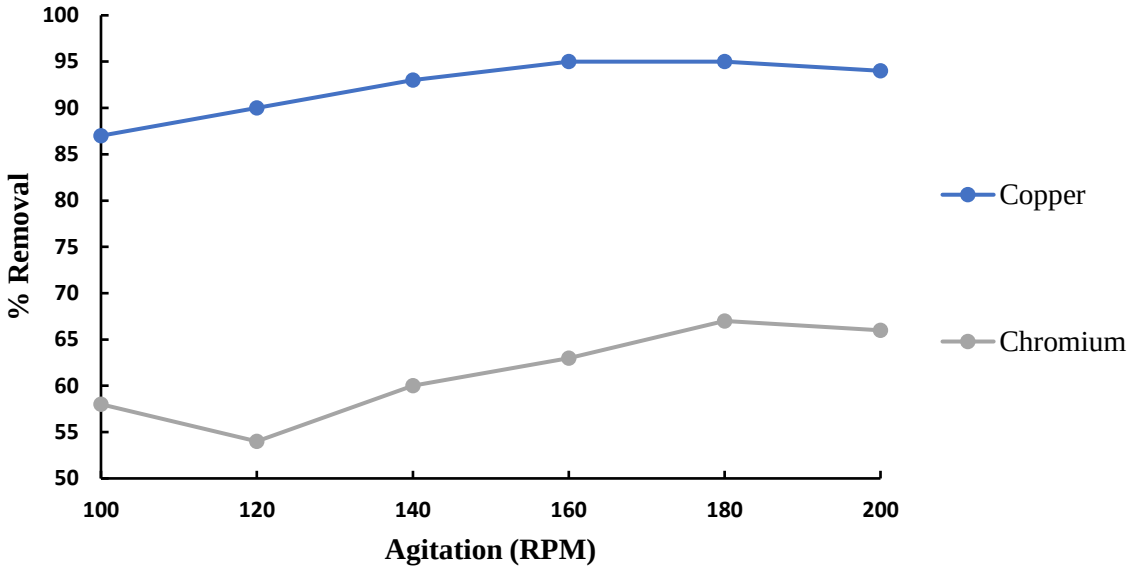

Figure 4.5: Results of the effects of agitation speed for the biosorption of Cr^{6+} and Cu^{2+}

4.3.3 The Study of Biosorbent Dosage

From figure 4.6, the increase of biomass dose for Cu^{2+} showed that there is an increase in removal efficiency from 1 g up to 6 g. The highest removal efficiency was obtained at 91% for a dose of 6 grams. These results are comparable with those reported by (Hossain *et al.* 2012; Mahlangu, Simate and de Beer 2018) on the biosorption of metal uptake onto banana peels. The increase in removal efficiency may be attributed to the availability of biosorbent sites for the uptake of Cu^{2+} ions as more particles were present during the process.

However, the increase of biomass dose for the removal of Cr^{6+} did not show any significant impact on the removal efficiency as the removal efficiency was between 58% and 65% across the dosage range, with the maximum being at 4 and 5 grams. From other reports by (Ali, Saeed and Mabood 2016; Badessa, Wakuma and Yimer 2020) increase in dosage increased their removal efficiency significantly. In the case of (Ali, Saeed and Mabood 2016), treated and modified their banana peels by grafting the peels with acrylonitrile to remove lignin and pectin which made their biosorbent more

porous and rougher with the cellulose being more exposed for biosorption. Therefore, as more biosorbent was increased during biosorption, so did their removal efficiency. A study done by (Kariuki, Kiptoo and Onyancha 2017) also expressed similar findings during their experiments in the biosorption of found Pb^{2+} and Cu^{2+} using mushrooms, where they found that there was no significance changes in removal efficiency when increasing biomass dose. This may be attributed to the overcrowding of the biomass in water which hindered the active sites for sorption of metal onto the adsorbent (Kariuki, Kiptoo and Onyancha 2017; Singh, Kumar and Panghal 2021). Other studies found that the removal efficiency of heavy metals was highest at lower biomass dose and decreased as biomass dose increased due to electrostatic interactions that occur at high biomass concentration inhibited metal biosorption (Fadel *et al.* 2017).

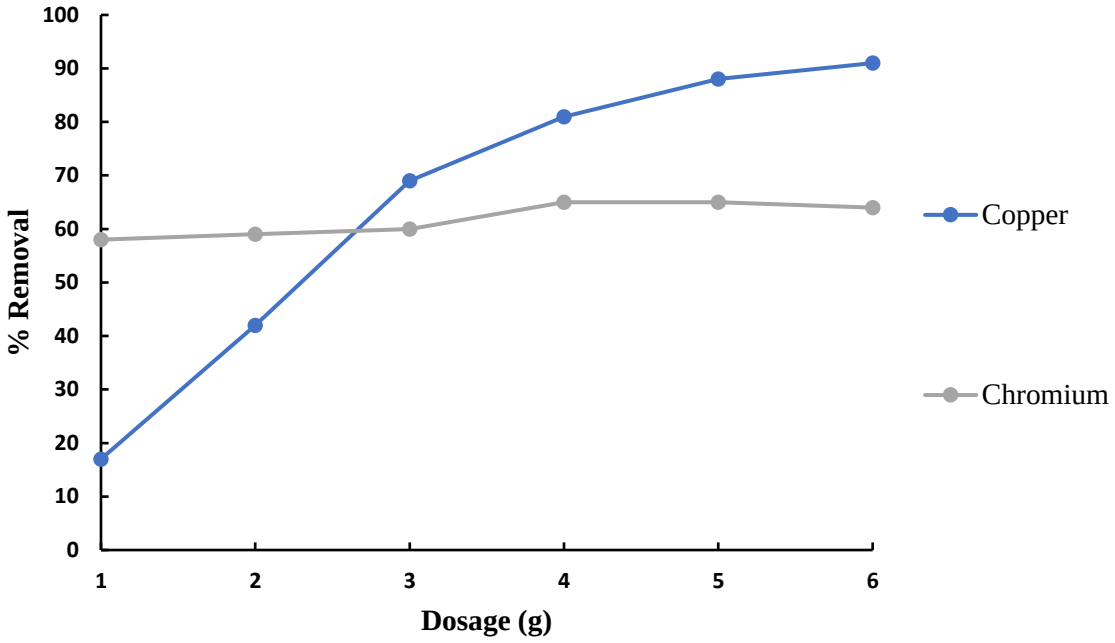

Figure 4.6: Results of the effects of biosorption dosage for the biosorption of Cr^{6+} and Cu^{2+}

4.3.5 The Study of Metal Concentration

Metal concentration was varied between 5 and 100 mg/L and it was found that the performance of the banana peels was more efficient at lower concentrations as seen in figure 4.7. Cu^{2+} reached a maximum removal of 95% at 10, 15 and 20 mg/L while the removal efficiency decreased to 27% as the concentration increased to 100mg/L. The maximum removal of Cr^{6+} was 65% at 5 mg/L and then decreased gradually to 21% at 100 mg/L. The decrease in removal efficiency with increase in initial concentration may be due to the saturation of available sites within the adsorbent. At low concentrations, adsorption increases as adsorption sites are readily available for fast adsorbate binding of which the process is faster. However at higher concentrations, the adsorbate must spread over the sorbent surface by intraparticle diffusion making the process slower (Singh, Kumar and Panghal 2021). Similar trends were noted by (Afolabi, Musonge and Bakare 2021a; Singh, Kumar and Panghal 2021) in the removal of Cr^{6+} and Cu^{2+} from water.

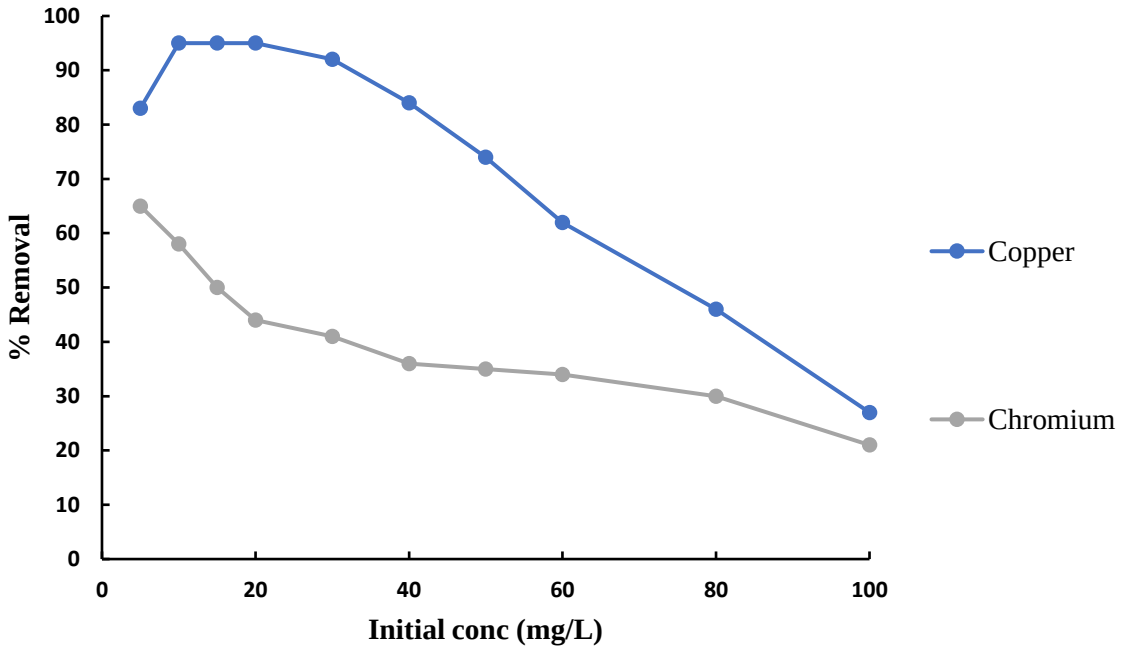

Figure 4.7: Results for the study of metal concentration of the biosorption of Cr^{6+} and Cu^{2+}

4.3.6 The Study of Contact Time

Contact time was varied from 5 to 140 minutes. Biosorption for both metals was rapid, where biosorption took place within 5 minutes with a removal efficiency of 75% and 40% for Cu^{2+} and Cr^{6+}, respectively. Although biosorption happened rapidly, the binding of metal ions onto the surface of the biosorbent may not have been permanent or strong. The removal efficiency at 10 minutes of biosorption dropped significantly, as seen in figure 4.8. The Cu^{2+} biosorption took place gradually from 10 minutes and equilibrium was reached within 50 minutes without any significant change beyond, and this is in alignment with the work done by (Hossain *et al.* 2012). For Cr^{6+}, biosorption was rapid again and equilibrium was reached within 30 minutes with no significant changes after that.

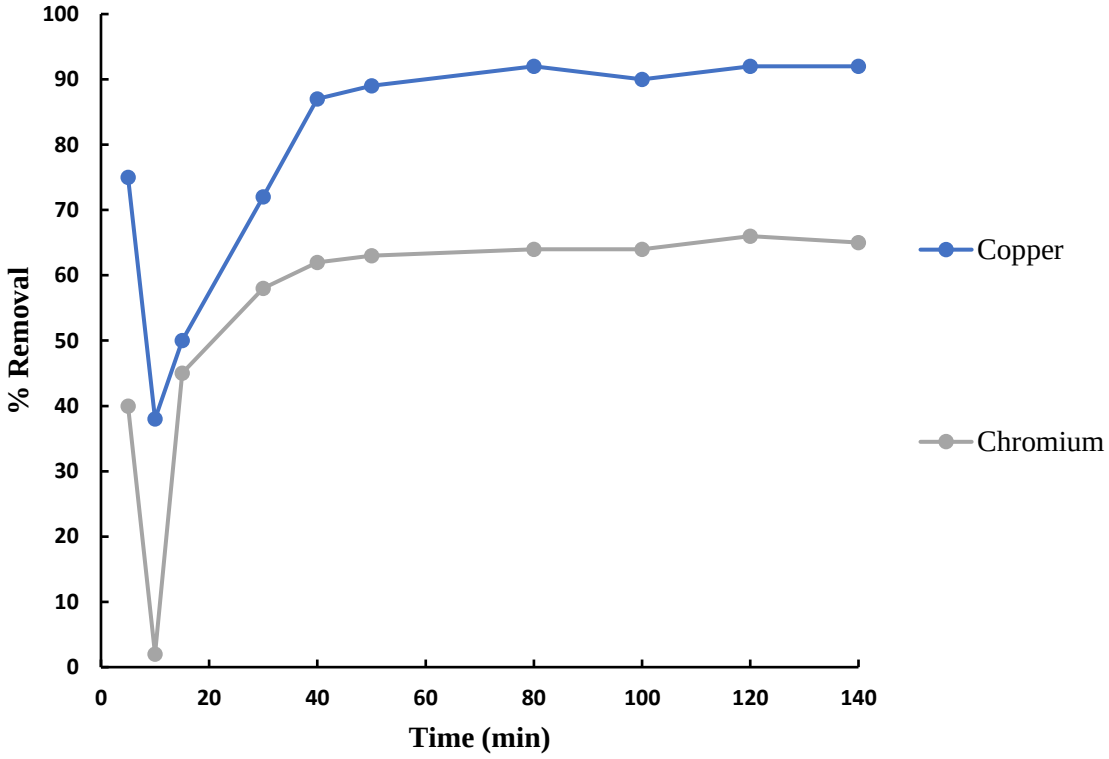

Figure 4.8: Results for the study of contact time for the biosorption of Cr^{6+} and Cu^{2+}

4.3.7 Conclusion on Batch Studies of Cr^{6+} and Cu^{2+}

Batch studies were conducted to evaluate the performance of banana peels for removing Cr^{6+} and Cu^{2+} from water by varying parameters such as the water pH, agitation speed, biosorbent dose, metal concentration and contact time.

Removal efficiency of 65% for Cr^{6+} was achieved at water pH "4" and agitation speed of 180 rpm. Increase in biomass dose did not seem to have much of an impact on the removal efficiency with the lowest removal efficiency at 58% at 1g and highest removal efficiency at 65% at 4 and 5g. A decrease in removal efficiency was seen as metal concentration increased and it was found that banana peels performed better at lower ion metal concentrations with the highest removal efficiency of 65% at 5 mg/L. Through contact time, biosorption was rapid where equilibrium was reached between 30 and 40 minutes.

The Cu^{2+} removal efficiency was found to be highest at a pH value of 4 with a removal efficiency of 94%. The lowest and highest removal efficiency of 87% and 95% was achieved at 100, 160 and 180 rpm, respectively. Biomass dose significantly increased from 17% at 1g to 91% at 6g. Like the biosorption of Cr^{6+}, banana peels performed better at lower Cu^{2+} concentrations with the highest removal at 95% for 10, 15 and 20 mg/L. Biosorption of Cu^{2+} was also rapid, where equilibrium was reached at 50 minutes.

For the overall conclusion, it was observed that banana peels had a higher affinity for Cu^{2+} ions than that of Cr^{6+}. According to (Torres 2020) the biosorption of Cr^{6+} requires a number of steps during biosorption where electrostatic attraction, surface complexation and heterogeneous redox reaction to form Cr^{3+} ions is involved. It is also noted that Cr^{6+} in water is anionic [i.e. chromate ($Cr_2O_4^{2-}$); hydrochromate ($HCrO^{4-}$); dichromate ($Cr_2O_7^{2-}$)] and changes form at different pH regions, unlike other metals which are mostly cationic. Therefore the behaviour towards the banana peels during biosorption may have been complex and requires more residence time as compared to Cu^{2+} (Torres 2020).

4.4 Study of Adsorption Equilibrium Isotherms and Kinetics

4.4.1 Study of Langmuir Isotherm Model

Parameters in table 4.1 were obtained by the plot of $^{1}/_{q_e}$ against $^{1}/_{C_e}$ given in figure 4.9. The coefficient of determination, R^2, was high for both metals and the adsorption capacities were comparable with the experimental values of 12.38 mg/g and 8.10 mg/g for Cu^{2+} and Cr^{6+}, respectively. The R_L values for Cr^{6+} and Cu^{2+} indicated that adsorption was favourable over the concentration range. Similar studies done by (Hossain *et al.* 2012; Hernández and Romero 2019; Afolabi, Musonge and Bakare 2021c) where banana peels were used for removing Cr^{6+} and Cu^{2+} in a single and/or binary system with other metals, found that the Langmuir model fitted well with their results. This indicated that the removal of both metals was of a homogeneous monolayer biosorption where the surface of the banana peels was active in binding the metals to itself and that the process for both metals may have undergone chemisorption.

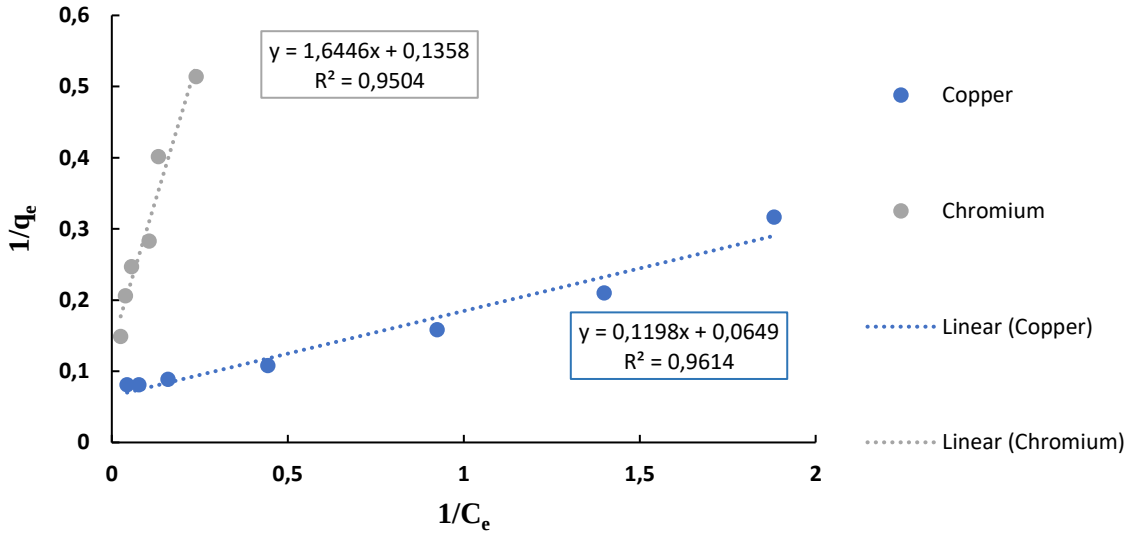

Figure 4.9: Langmuir isotherm graph for the biosorption of Cr^{6+} and Cu^{2+}

Table 4.1: Langmuir parameters for the biosorption of Cr^{6+} and Cu^{2+}

Langmuir					
Copper	q_m (mg/g)	15.41	Chromium	q_m (mg/g)	7.36
	K_L (mg/g)	0.503		K_L (mg/g)	0.083
	R_L	0.284 - 0.014		R_L	0.548-0.168
	R^2	0.96		R^2	0.95
	q_{exp} (mg/g)	12.38		q_{exp} (mg/g)	8.1

4.4.2 Study of Freundlich Isotherm Model

Parameters in table 4.2 were obtained by the plot of $\log q_e$ against $\log C_e$ given in figure 4.10. The adsorption favourability factor, *n*, was between 1 and 10 indicating that biosorption was favourable for both Cr^{6+} and Cu^{2+} ion uptake using banana peels.

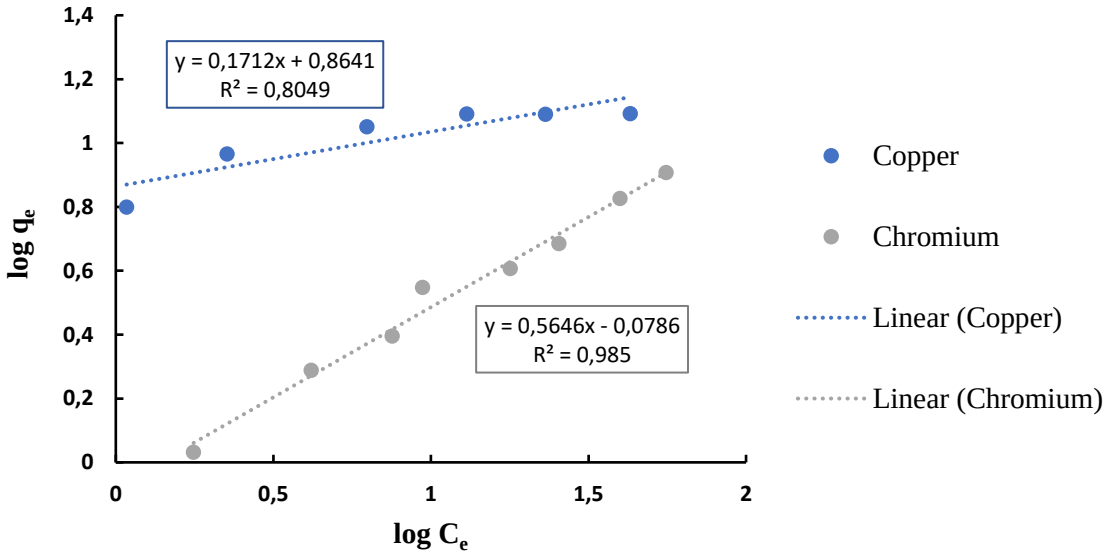

Figure 4.10: Freundlich isotherm graph for the biosorption of Cr^{6+} and Cu^{2+}

The biosorption intensity or surface heterogeneity, *1/n*, also indicated that biosorption had undergone a physical process as 1/*n* was < 1. R^2 for Cu^{2+} was 0.80 which was lower than the Langmuir model. The adsorption capacity K_f was also lower than q_e obtained from the experiments. Therefore, the Freundlich isotherm did not describe the adsorption of Cu^{2+} onto banana peels well. Cr^{6+} on the other

hand had a R^2 of 0.99 which showed that the experimental results fitted well with this model. (Ali, Saeed and Mabood 2016; Badessa, Wakuma and Yimer 2020) also found that the Freundlich model fitted well with the removal of Cr^{6+} using banana peels as a biosorbent. Therefore, the biosorption of Cr^{6+} may have also undergone physical adsorption with multiple sites active during the binding process.

Table 4.2: Freundlich isotherm parameters for the biosorption of Cr^{6+} and Cu^{2+}

	Freundlich				
Copper	K_f (mg/g)	7.313	Chromium	K_f (mg/g)	0.83
	1/n	0.17		1/n	0.56
	n	5.84		n	1.77
	R^2	0.80		R^2	0.99
	q_{exp} (mg/g)	12.38		q_{exp} (mg/g)	8.1

4.4.3 Study of Elovich Isotherm Model

Parameters for the Elovich isotherm model are found in table 4.3, where results were obtained by the plot of $\ln \frac{q_e}{C_e}$ against $\ln q_e$ given in figure 4.11.

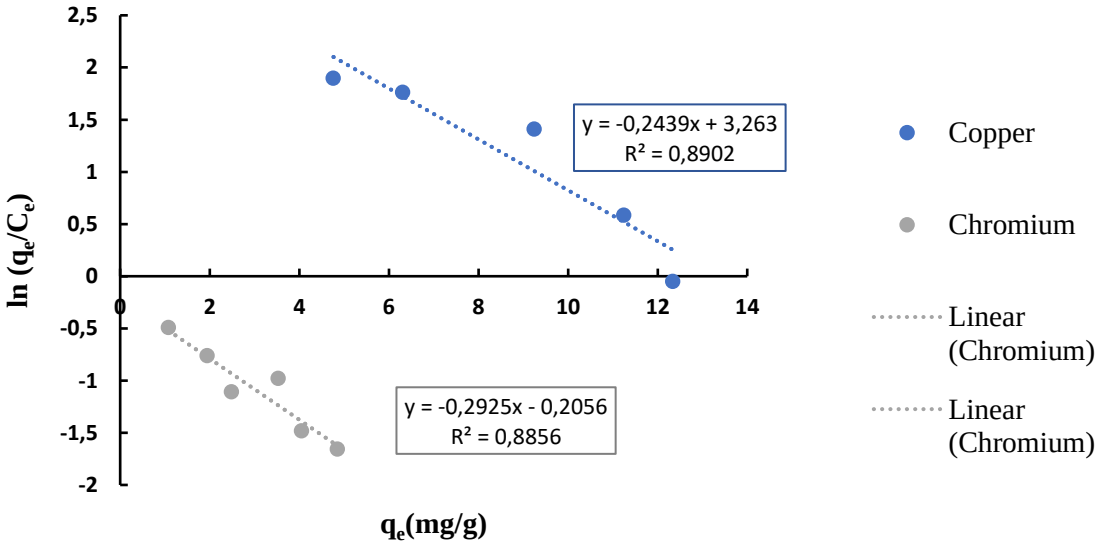

Figure 4.11: Elovich isotherm graph for the biosorption of Cr^{6+} and Cu^{2+}

The Elovich isotherm exhibited R^2 of 0.89 for both Cu^{2+} and Cr^{6+}, lower than that of the Langmuir and Freundlich isotherm coefficients. Therefore, the assumption of exponential coverage of adsorption sites implying multilayer adsorption did not adequately describe the biosorption processes for both metals with banana peels.

Table 4.3: Elovich isotherm parameters for the biosorption of Cr^{6+} and Cu^{2+}

Elovich					
Copper	ln ($K_E q_m$)	3.263	Chromium	ln ($K_E q_m$)	0.206
	$1/q_m$ (g/mg)	0.2439		$1/q_m$ (g/mg)	0.293
	q_m (mg/g)	4.10		q_m (mg/g)	3.42
	K_E (L/mg)	6.37		K_E (L/mg)	0.36
	R^2	0.89		R^2	0.89
	q_{exp} (mg/g)	12.38		q_{exp} (mg/g)	8.1

4.4.4 Study of Pseudo-First Order Kinetic Model

A graphical plot shown in figure 4.12 was done for the pseudo-first order, where $\ln(q_e - q_t)$ was plotted against *t*. The R^2 for Cu^{2+} was given at 0.98, showing that the model had a good fit for the process between 10 and 50 minutes. After 50 minutes, R^2 decreased as biosorption of Cu^{2+} slowed down due to saturation onto the banana peels. From the study of contact time, it was observed that equilibrium was reached within 50 minutes, therefore the model was able to describe the biosorption of Cu^{2+} onto banana peels well. (Hossain *et al.* 2012) also recorded similar R^2 values for their biosorption of Cu^{2+} with banana peels and found that the pseudo-first order kinetic model was the best suited model for their process. However, the R^2 for Cr^{6+} was very low at 0.61 showing a poor relation of the model to the process. This may be due to the rapid uptake of Cr^{6+} which required less time for the banana peels to be saturated with ions as compared to Cu^{2+}. Therefore, the assumption that rate of biosorption of Cr^{6+} onto banana peels is dependent upon time did not apply for this process.

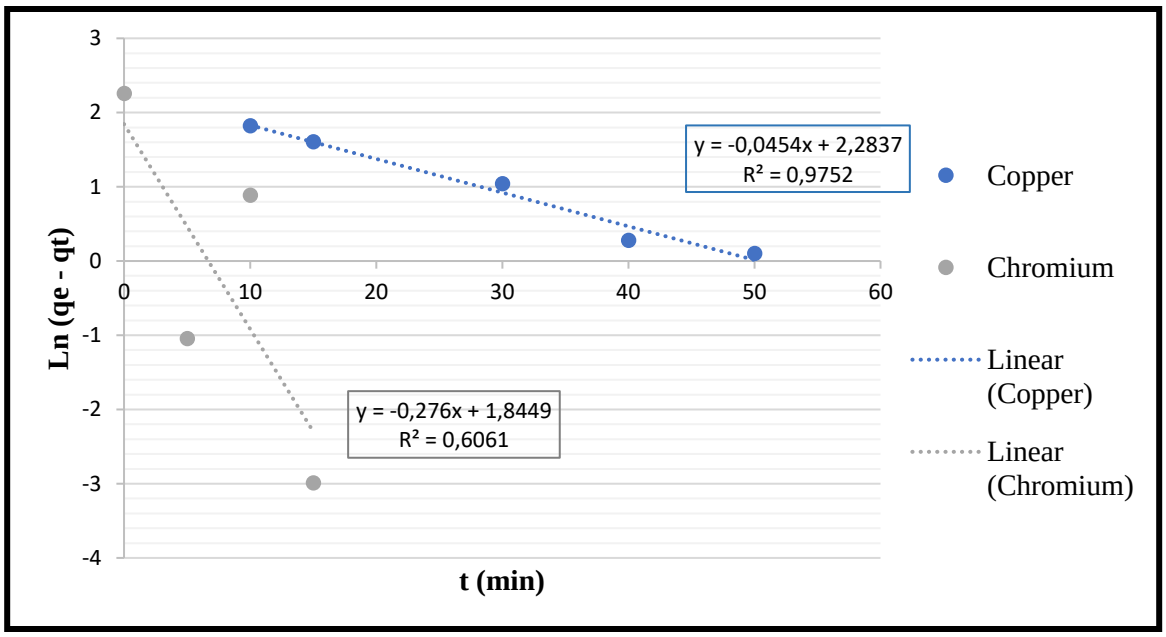

Figure 4.12: Pseudo-first order kinetic graph for the biosorption of Cr^{6+} and Cu^{2+}

Table 4.4: Pseudo-first order kinetic parameters for the biosorption of Cr^{6+} and Cu^{2+}

Pseudo-First Order Kinetic Parameters		
Parameters	Copper	Chromium
$q_{e\text{-}calc}$ (mg/g)	1.05	6.3
K_1 (min^{-1})	5.259	0.636
R^2	0.975	0.606
$q_{e\text{-}exp}$ (mg/g)	7.61	2.43

4.4.5 Study of Pseudo-Second Order Kinetic Model

Results in table 4.5 were obtained from the graphical plot of $\frac{1}{q_t}$ against $\frac{1}{t}$ shown in figure 4.13. The model fitted both processes well, especially for the uptake of Cr^{6+} with R^2 closer to 1. The R^2 for the

adsorption of Cu^{2+} was 0.97 which was slightly lower to the pseudo-first order model. However, the adsorption capacity calculated from the equation was closer to the experimental capacity obtained for both $Cr^{6+}$and Cu^{2+}. Therefore, the assumption that adsorption of $Cr^{6+}$and Cu^{2+} by banana peels was controlled by chemisorption through the entire range of the adsorption process may have been true for both metals and that this was due to the banana peels capacity to sorb the metals onto itself. The pseudo-second order may take precedence over the pseudo-first for Cu^{2+} because from the equilibrium studies, the process favored the Langmuir which supported chemisorption. (Khambhaty *et al.* 2009; Marandi 2011; Singh, Kumar and Panghal 2021) found that the removal of Cr^{6+} from water using different biosorbents was controlled by the pseudo-second order kinetic.

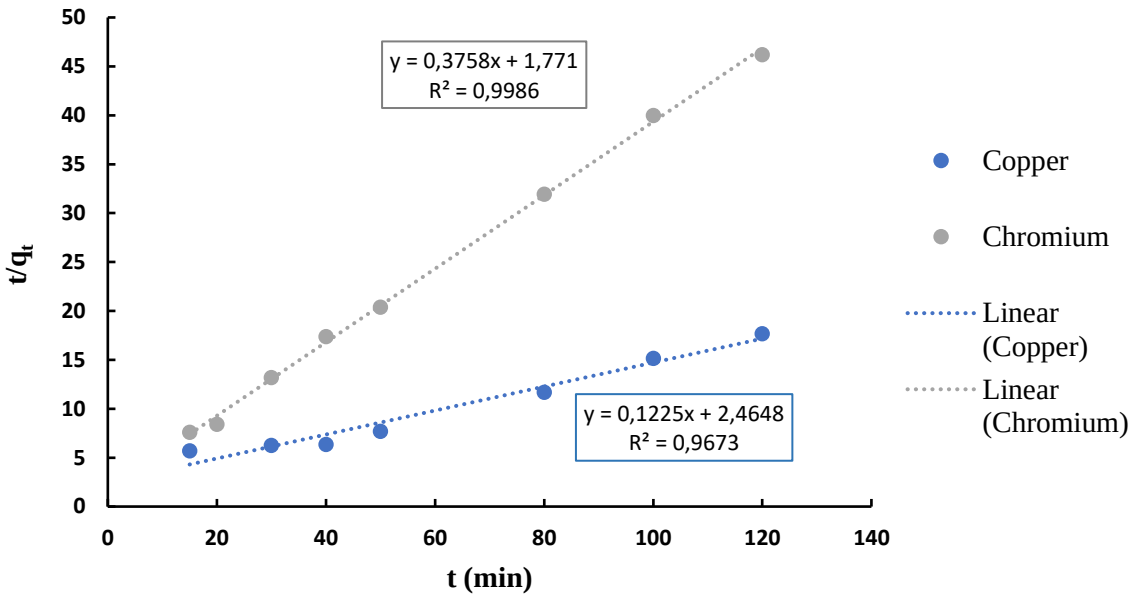

Figure 4.13: Pseudo-second order kinetic graph for the biosorption of Cr^{6+} and Cu^{2+}

Table 4.5: Pseudo-second order kinetic parameters for the biosorption of Cr^{6+} and Cu^{2+}

Pseudo-Second Order Kinetic Parameters		
Parameters	Copper	Chromium
$q_{e\text{-}calc}$ (mg/g)	8.16	2.66
K_2 (g/mg.min)	0.007	0.80
R^2	0.9673	0.9986
$q_{e\text{-}exp}$ (mg/g)	7.61	2.43

4.4.6 Study of Intra-particle Diffusion Model

Parameters in table 4.6 were obtained from the graphical plot of q_t against $t^{1/2}$ shown in figure 4.14. The model for the biosorption of Cu^{2+} also showed a good relation with an R^2 of 0.98.

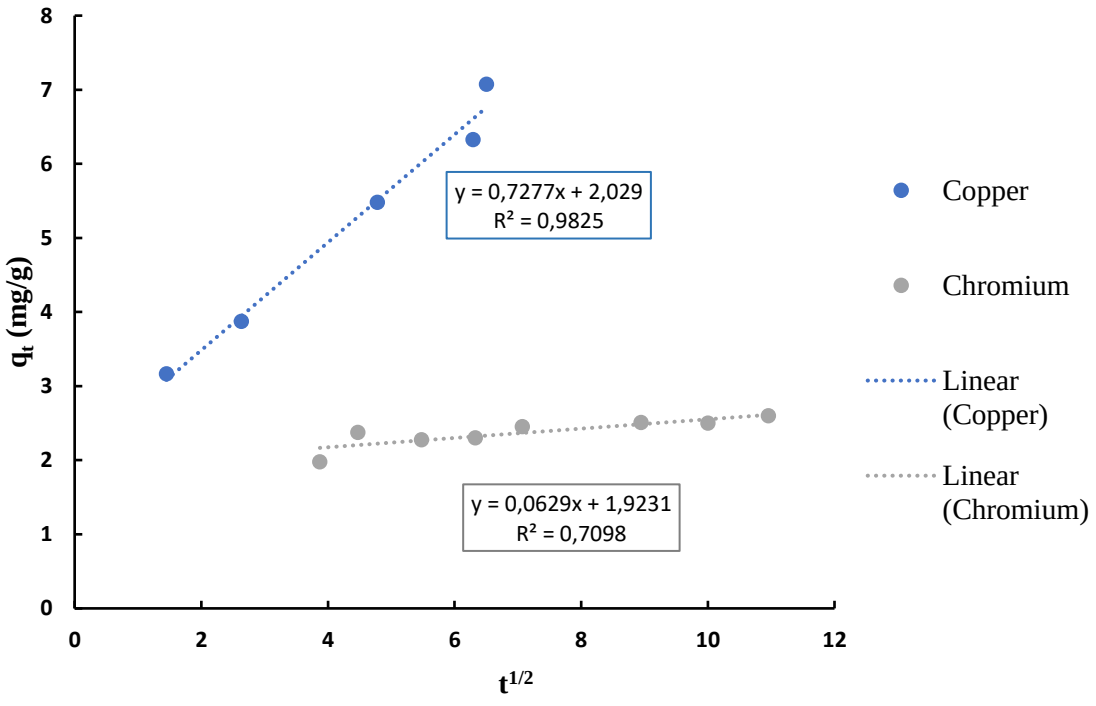

Figure 4.14: Intra-particle diffusion graph for the biosorption of Cr^{6+} and Cu^{2+}

The plot of the graph for Cu^{2+} in figure 4.14 leaned closer to the origin, however, it did not pass through the origin indicating that intra-particle diffusion was not the sole rate-limiting step for this process. As the case, the biosorption of Cu^{2+} may have been through film diffusion. R^2 of Cr^{6+} 0.71, indicating that the diffusion mechanism did not fit well for the biosorption of Cr^{6+} onto banana peels.

Table 4.6: Intra-particle diffusion model parameters for the biosorption of Cr^{6+} and Cu^{2+}

Intra-particle Diffusion Model Parameters		
Parameters	Copper	Chromium
$q_{e\text{-}calc}$ (mg/g)	2.03	1.92
K_{id} (mg/g.min$^{1/2}$)	0.728	0.063
R^2	0.98	0.71
$q_{e\text{-}exp}$ (mg/g)	7.61	2.43

4.4.7 Conclusion on Isotherm and Kinetic Studies for Cr^{6+} and Cu^{2+}

Isotherm and kinetic studies were conducted to determine the type of process taken place and biosorption mechanism for the removal of Cr^{6+} and Cu^{2+} by banana peels. The biosorption of Cr^{6+} favored both the Langmuir and Freundlich isotherms. The q_m (7.36 mg/g) from the Langmuir isotherm gave a value closer to the experimental capacity of 8.1 mg/g. The R^2 for Langmuir was 0.95 and for Freundlich was 0.99. The process also favored the pseudo-second order kinetic reaction model with an $R^2 \sim 1$. This showed that the rate-limiting step in the process was ion exchange as the Cr^{6+} ions exchanged with some elements within the cell walls of the peels. This is also indicated in analysis of banana peels after biosorption in its characterization. Both q_e (2.66 mg/g) from the kinetic model and q_e (2.43 mg/g) from experiments were similar in value.

The biosorption of Cu^{2+} by banana peels favored the Langmuir isotherm model with an R^2 of 0.96 and q_m of 15.41 mg/g. which was closer to the experimental value of 12.38 mg/g. The process favored the pseudo-first order, pseudo-second order and intra-particle diffusion with R^2 of 0.98, 0.97 and 0.98, respectively. The q_e (8.16 mg/g) from the pseudo-second order kinetic model had a closer value to the experimental value of 7.61 mg/g. Therefore, the biosorption of Cu^{2+} may have undergone more than one mechanism of which accounts for its high removal from the batch studies conducted.

Both Cr^{6+} and Cu^{2+} showed favorability through the separation factor R_L ($0 < R_L < 1$) and the favorability factor n ($1 < n < 10$). The Elovich isotherm model did not fit well for both processes.

4.5 Results and Discussion: Characterization of Banana Peels

4.5.1 Study of Fourier-Transform Infrared Analysis (FTIR) Results

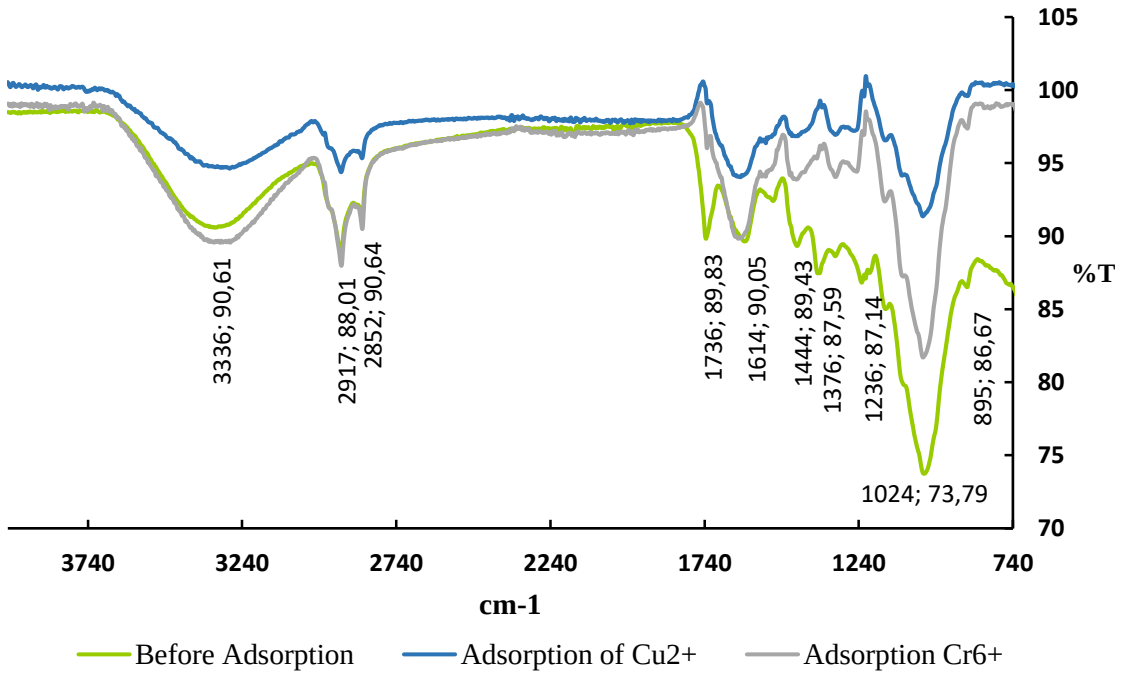

Figure 4.15: FTIR analysis of banana peels

According to literature, the functional groups most prevalent in many agricultural waste peels, including banana peels are groups of hydroxyls, aldehydes, ketones, carboxylic, phenolic and ether groups (Bhatnagar, Sillanpää and Witek-Krowiak 2015). From the FTIR analysis performed on banana peels, figure 4.15 illustrates graphs of functional groups present. Peaks that appeared at 3336 were groups of strong O-H stretching bonds as well as N-H stretching of amines of polymeric compounds such as pectin and lignin that contains groups of alcohols, phenols and carboxylic acids. Peaks at 2917 and 2852 were of C-H stretching of alkanes, at 1736 was of C=O stretching of carboxylic acids, at 1614 was of N-H bending vibrations of amines, at 1444 was of O-H bending of acids, at 1376 was of C-H bending of crystalline cellulose and hemicellulose or lignin, at 1236 and 1024 were of C-O stretching of carbonyls and at 895 was of aromatic hydrogen. Most of the

functional groups obtained in this study were very similar to the functional groups obtained by other authors (Yang *et al.* 2007; Hossain *et al.* 2012; Bhatnagar, Sillanpää and Witek-Krowiak 2015; Deshmukh *et al.* 2017; El-Din *et al.* 2018).

After biosorption of Cu^{2+} and Cr^{6+} there was a shift in graph for each metal, indicating that there were interactions between the metals and the functional groups on the banana peels. The peaks that showed the most changes were at 1236, 1376, 1614 and 1736 for Cu^{2+} and Cr^{6+} of which indicated that the carboxylic and amine groups were most active in the biosorption process. The peaks of Cu^{2+} were further affected by the alkane and hydroxyl groups at 2852, 2917 and 3336. From the FTIR results it was noted that a significant difference in the change illustrated in the graph for the removal of Cu^{2+} showed that more functional groups were interactive in removing the ion from water. Therefore, this confirms the high removal efficiency as seen in the previous section. For Cr^{6+}, it was noted that the carboxylic and amine groups were the most active during biosorption. Research done by (Wong *et al.* 2020) used coffee waste as a biosorbent in removing anionic textile dyes and found that an increase in positively charged amine groups in the coffee waste through treatment with polyethyleneimine increased biosorption significantly. Another study by (Ali, Saeed and Mabood 2016) used modified banana peels of which they treated the peels with acid and alkali, followed by grafting with an acrylonitrile monomer. This increased positively charged groups within the peels and their highest recorded removal efficiency after modification was 96%.

4.5.2 Study of SEM and EDS

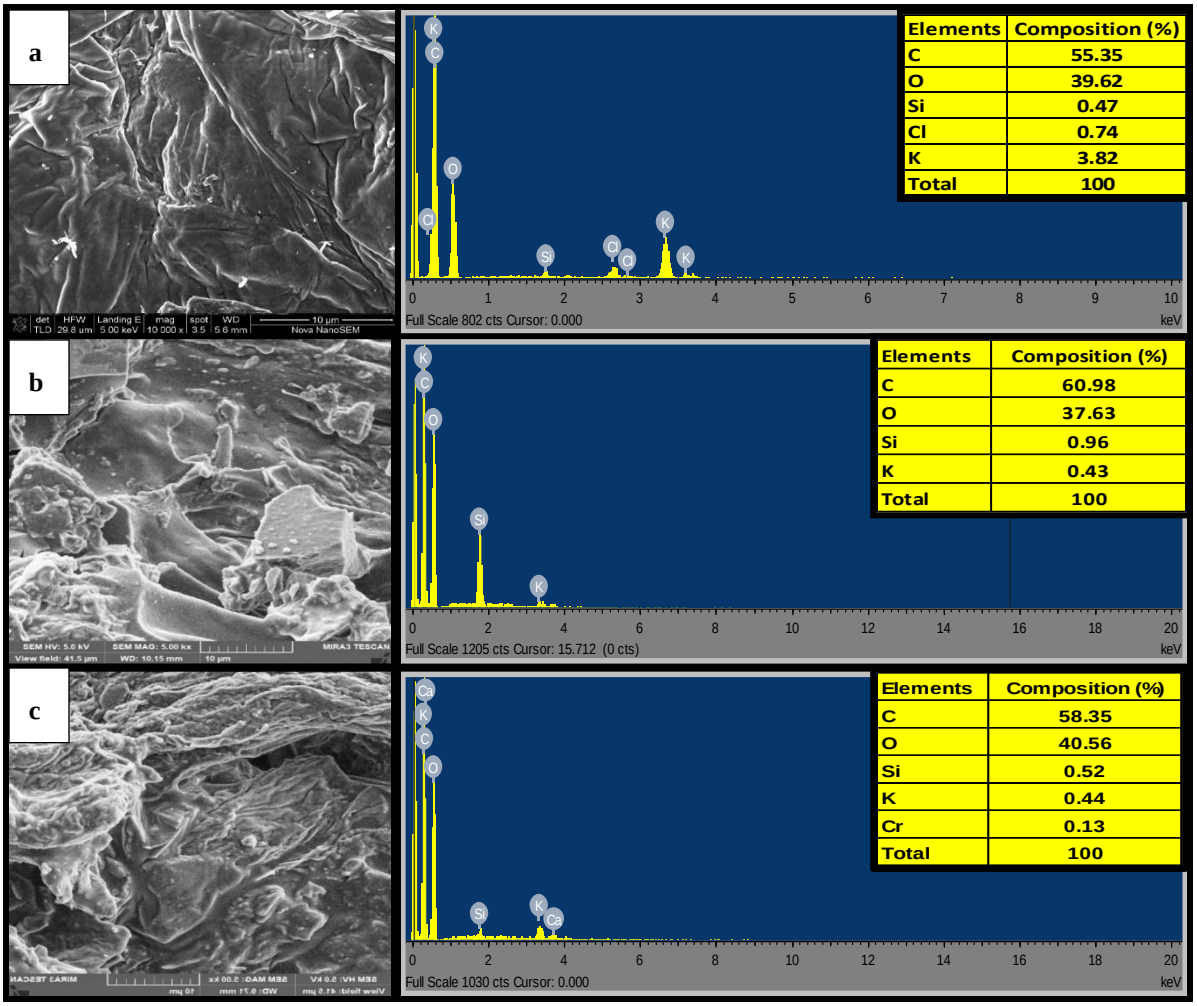

Figure 4.16: SEM/EDS analysis of banana peels for (a) before biosorption, (b) after biosorption of Cu^{2+}, and (c) after biosorption of Cr^{6+}

Studies on surface morphology of banana peels were done using the scanning electron microscopy to understand the surface structure of the peels before and after biosorption of Cu^{2+} and Cr^{6+}. Figure 4.16a showed a rough and uneven surface structure with no visible pores. After biosorption of Cu^{2+} in figure 4.16b, the surface of the peels became rougher with notable fractures. The biosorption of Cr^{6+} in figure 4.16c did not drastically change the surface of the peels as compared to that of Cu^{2+}, but the surface was noted to be more uneven with groves along the edges. From figure 4.16a, the energy dispersive x-ray spectroscopy showed a number of elements including potassium and chloride

as reported by other authors (Memon *et al.* 2008; Kamsonlian *et al.* 2011). After biosorption, it was noted in table 4.7 that the composition of K, Cl and Si changed significantly. Cr in figure 4.16c was present in the banana peels after biosorption, of which it showed that the metal was adsorbed within the cell walls of the peels. Ion exchange may also have taken place as K decreased during biosorption. Increase in C and decrease in O for the removal of Cu^{2+} may be attributed in cellulose being more exposed as hydroxyl groups present in lignin were active in the biosorption process.

Table 4.7: Composition of banana peels before and after biosorption

Elements	**Before Adsorption**	**After Adsorption Cu^{2+}**	**After Adsorption Cr^{6+}**
C	55.35	60.98	58.35
O	39.62	37.63	40.56
Si	0.47	0.96	0.52
Cl	0.74	0	0
K	3.82	0.43	0.44
Cr	0	0	0.13
Total	100	100	100

4.5.3 Study of X-ray Diffraction spectrometry (XRD)

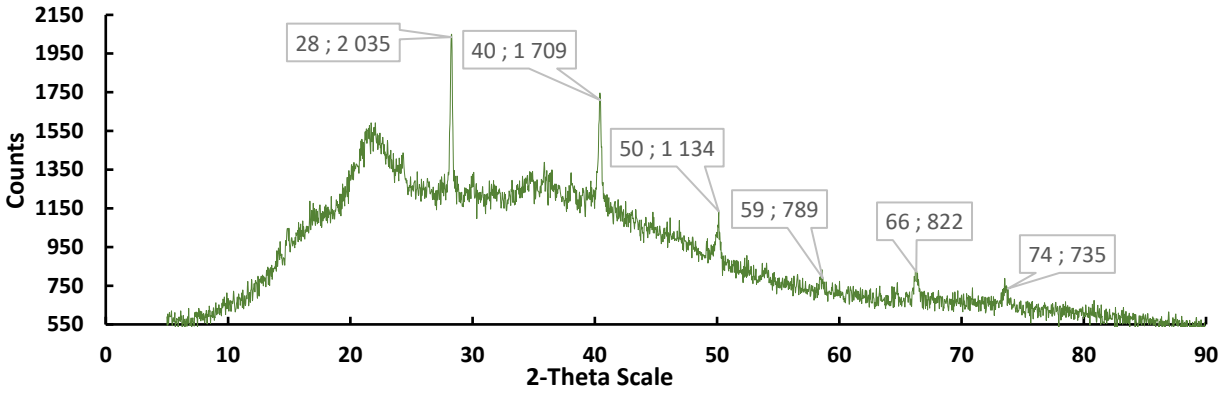

Figure 4.17: XRD analysis of banana peels before biosorption

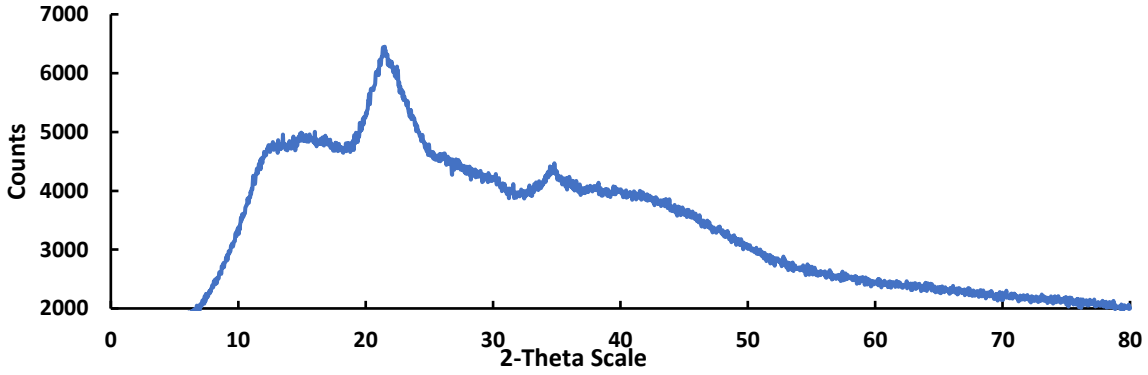

Figure 4.18: XRD analysis of banana peels after Cu^{2+} biosorption

Figure 4.19: XRD analysis of banana peels after Cr^{6+} biosorption

The x-ray diffraction analysis was done to determine the structural of the banana peels. The diffraction given in figure 4.17 showed that the structure of banana peels is mainly amorphous with a number of peaks indicating some crystallinity. The amorphous phase is due to the lignin content which is highly branched without a crystalline structure. Peaks that arose at 2θ values of 28°, 40°, 50°, 58°, 66° and 74° indicating a presence of a crystalline salt material called sylvite, KCl, which was also noted by (Oyewo, Onyango and Wolkersdorfer 2016). The peak at 2θ = 22° indicates crystallinity of native cellulose, which is the crystallographic plane for most cellulosic material (Isa *et al.* 2020; Khairiah *et al.* 2021). After biosorption of both Cr^{6+} and Cu^{2+}, the crystalline peaks decreased indicating a decrease of KCl salt after biosorption. The strongest peak exhibited at 22.3° in figure 4.18 representing native cellulose, followed by two low peaks at 14.8° and 34.5°. After biosorption of Cr^{6+} in figure 4.19, peaks were also exhibited at 15.8°, 21.26° and 34.82° and this was also agreed by (Sharma and Bhalerao 2018).

Study of Brunauer-Emmett-Teller (BET)

Table 4.8: BET analysis of banana peels

Physiochemical Characteristics	Banana Peels
BET Surface Area:	5.6909 m^2/g
BJH Adsorption cumulative volume of pores between 17.000 Å and 3000.000 Å diameter:	0.002605 cm^3/g
BJH Adsorption average pore diameter (4V/A):	28.894 Å

The BET analysis was done to determine the specific area of the banana peel sample. From table 4.8 the pores of the peels were found to be mesoporous with a pore size of 2.9 nm and the specific area calculated by the BET theory method was 5.6909 m^2/g, which was close to other specific areas of agricultural waste peels (Khiari *et al.* 2019; Tejada-Tovar, Gonzalez-Delgado and Villabona-Ortiz 2019). In general, lignocellulosic residues or wastes have low surface areas and pore volumes due to their biological structure, and, therefore, they are generally characterized as materials with reduced pores (Tejada-Tovar, Gonzalez-Delgado and Villabona-Ortiz 2019).

The BET theory was developed to explain physical adsorption of gases onto an adsorbent where multilayer adsorption takes place (Nasrollahzadeh *et al.* 2019). However, from the isotherm and kinetic studies performed for Cr^{6+} and Cu^{2+}, multilayered biosorption was not supported in the experiments as seen from the Elovich isotherm. Physical biosorption did not play a big role in the process, particularly in the biosorption of Cr^{6+} by which the rate-limiting step in the biosorption process was chemisorption through the pseudo-second order kinetic reaction model.

4.5.4 Conclusion on the Characterization of Banana Peels

Characterization of banana peels was studied to determine the physical and chemical properties of the peels. The FTIR analysis displayed several functional groups mainly hydroxyl, carbonyls, amines, and carboxylic groups. After biosorption of Cr^{6+} and Cu^{2+} from water, the functional groups that were active in removing Cr^{6+} from water were the carboxylic and amine groups. The functional groups that were active in removing Cu^{2+} were the hydroxyl, carboxylic, alkane and amine groups present in the peels.

The SEM analysis was done for before and after biosorption of the metals. Before biosorption the of surface the peels were rough and uneven. After biosorption the surface contained fractures and groves seen in some areas of the peels. The EDS analysis identified elements present in the peels such as C, O, K, Cl and Si. After biosorption, K and Cl decreased significantly indicating interaction during the process. In the removal of Cr^{6+} the metal Cr was noted to be present within the cell walls of the peels. A process of ion exchange may have taken place during biosorption.

The XRD analysis found that banana peels are amorphous in nature, with a few crystalline peaks of a crystal salt called sylvite. Sylvite is a crystal salt made of potassium and chloride (KCl), elements that were detected in the EDS analysis as well. After biosorption, the peaks in the amorphous region disappeared, however the overall structure was not altered significantly.

The BET analysis was used for measuring pore size and volume, and it was found that the peels of the banana were mesoporous with a surface area of 5.69 m^2/g and the pore volume was 0.002605 cm^3/g.

4.6 Biosorption of Cr^{6+} in a Fixed-Bed Column

4.6.1 The Study of Breakthrough Curves in the Adsorption Column

Bed height in adsorption is one of the most important factors considered when determining the performance and capacity of a column. Figure 4.20 shows the breakthrough curves obtained during experiments, and table 4.9 shows the data analyzed for the column to determine the performance of the column during operation. Figure 4.20 shows that bed height significantly influences breakthrough time. As bed height increased, so did the length of time of breakthrough increase as well.

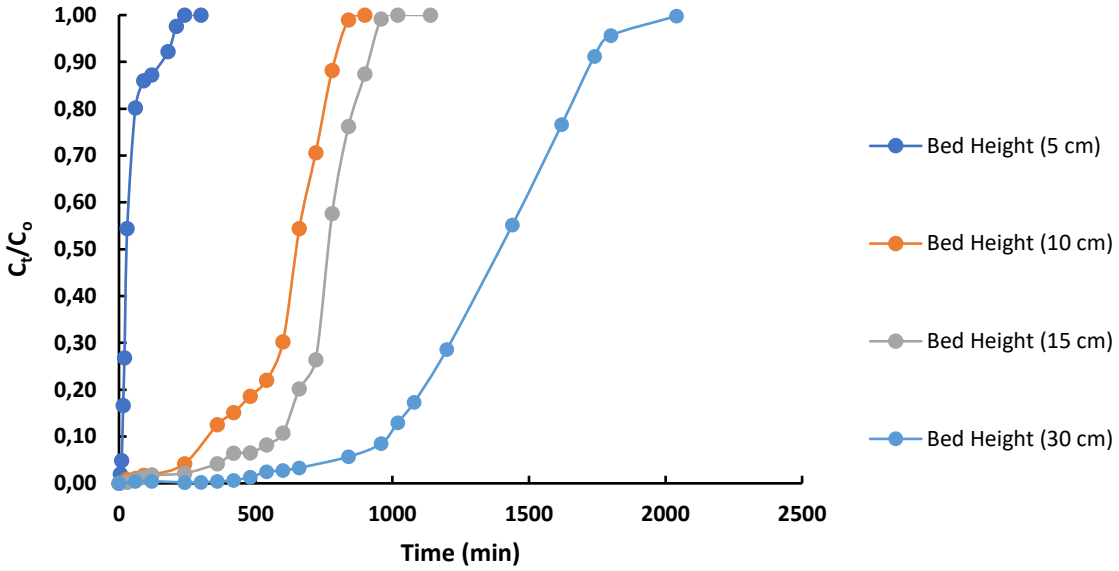

Figure 4.20: Breakthrough curves of Cr^{6+} at different bed heights

Table 4.9 displays the column performance during operation. The used bed H_B (also called the mass transfer zone) is where biosorption of Cr^{6+} took place. Table 4.9 shows that the unused bed height H_B, unused bed height H_{UNB}, the time of usable capacity up to breakthrough t_U, volumes processed at breakthrough V_B and at saturation V_T, all increased as bed height H_T increased. A study done by (Renu *et al*. 2020) also found that H_B increased during the adsorption of heavy metals containing Cr, Cu and Cd in a fixed-bed column from H_T of 15, 30 and 45 cm. The adsorption capacity at breakthrough q_B and at saturation q_t, as well as the amount of metal ions entering the column m_T also

increased as H_T increased, and this may be due to the increased surface area for more Cr^{6+} ions adsorbed onto the surface of the peels.

Table 4.9: Parameters of Column Performance

No.	C_o (mg/L)	C_t/C_o (mg/L)	m_{bio} (g)	ρ_{bio} (g/cm^3)	H_T (cm)	$V_{T\text{-}Bed}$ (mL)	H_B (cm)	H_{UNB} (cm)	t_T (min)
1	0.05	0.010	4.67	0.22	5	20.77	0.206	4.79	60
2	0.05	0.010	9.81	0.24	10	41.55	0.707	9.29	840
3	0.043	0.009	14.87	0.24	15	62.32	1.394	13.61	960
4	0.0495	0.010	30.76	0.25	30	124.64	7.426	22.57	1800

No.	t_B (min)	t_U (min)	V_B (mL)	q_B (mg/g)	q_T (mg/g)	m_T (mg)	V_T (mL)	NBV	AER (g/L)
1	2.5	2.48	10	0.011	0.5	4.2	840	1	5.56
2	60	59.40	240	0.121	6.2	16.8	3360	6	3.92
3	90	89.23	280	0.193	6.5	20.4	3840	9	3.87
4	450	445.55	1800	0.390	7.4	40.8	8160	14	3.77

Breakthrough time t_B and saturation time t_T also increased due to the residence time in the column for the effluent to pass through the column. This allowed more time for the banana peels to adsorb more of the ions on to its surface, which led to the increase of the mass transfer zone. After t_B, a steep trend was noted in figure 4.20 where the mass transfer zone moved quickly and reached the bottom of the column were saturation of the biosorbent occurred. H_{UNB} also increased as more biosorbent was present in the column, however, the ratio between H_{UNB} and H_B decreased as H_T increased. The increase in volumes (V_B and V_T) was also considered when H_T increased due to the time taken to process the constant amount of influent coming into the column. The behavior between H_T of the biosorbent and the Cr ions is in agreement with a number of authors in the biosorption of different biosorbents and metal ions (Mohamed *et al.* ; Srivastava, Agrawal and Mondal 2019; Yakout, Hassan and Omar 2019; Renu *et al.* 2020; Thirunavukkarasu, Nithya and Sivashankar 2021).

The adsorbent exhaustion rate (AER) is defined as the mass of adsorbent deactivated per unit volume of water treated at breakthrough point and it is used to determine the performance of the column (Bhaumik *et al.* 2013). An increase in the AER indicates that sorption is not efficient, whereas a decrease indicates that biosorption is efficient (Bhaumik *et al.* 2013; Vilardi *et al.* 2019). The general

drop in AER with increased bed height indicated an efficient process. The number of volumes processed (NBV) factor is also a performance indicator used for the up-scale of filter performance up to the breakthrough point (Chatterjee, Mondal and De 2018). From table 4.9, NBV increases as bed height increases, also showing that improvement in the performance of the column is dependent on bed height as observed by (Bhaumik *et al.* 2013; Chatterjee, Mondal and De 2018). (Chatterjee, Mondal and De 2018) used the NBV factor by multiplying NBV with the adsorbent volume in the scaled-up filter for a volume of treated water till breakthrough. However, factors such as the cross-sectional area of the column, influent flowrate and bed depth must be considered when upscaling.

Mathematical models were used for determining the dynamic behavior of the column experiments as well as to predict the breakthrough of the experimental data. Breakthrough curve modeling is crucial for describing and analyzing the lab-scale column studies for the purpose of industrial applications (Srivastava, Agrawal and Mondal 2019). The models used were the Thomas, Yoon-Nelson and Adams-Bohart models. The models were evaluated using the mean absolute error (MAE), root mean square error (RSME) and the coefficient of determination (R^2) for their performance measures in predicting results obtained from data. These error functions represent the error between the model predictions and the target values (Yaqub, Eren and Eyupoglu 2020). The values are measured between 0 and 1. The values closest to zero for MAE and RSME represent a good fit for the model, and the value closest to 1 for R^2 represents a good fit for the model.

4.6.2 Study of Adsorption Mathematical Models for Fixed-Bed Column

4.6.2.1 Thomas Model

The Thomas model was developed based on the assumption that adsorption is derived from the Langmuir isotherm model and that the driving force follows the pseudo-second order kinetic reaction with no axial dispersion (Patel 2019). The model is used for determining the adsorbent capacity in a fixed-bed column from plotting $\ln\left[\frac{C_o}{C_t}-1\right]$ against time *t*. Figure 4.21 below shows the experimental

breakthrough curves versus the predicted breakthrough curves by the Thomas model and table 4.10 shows the parameters obtained from the model.

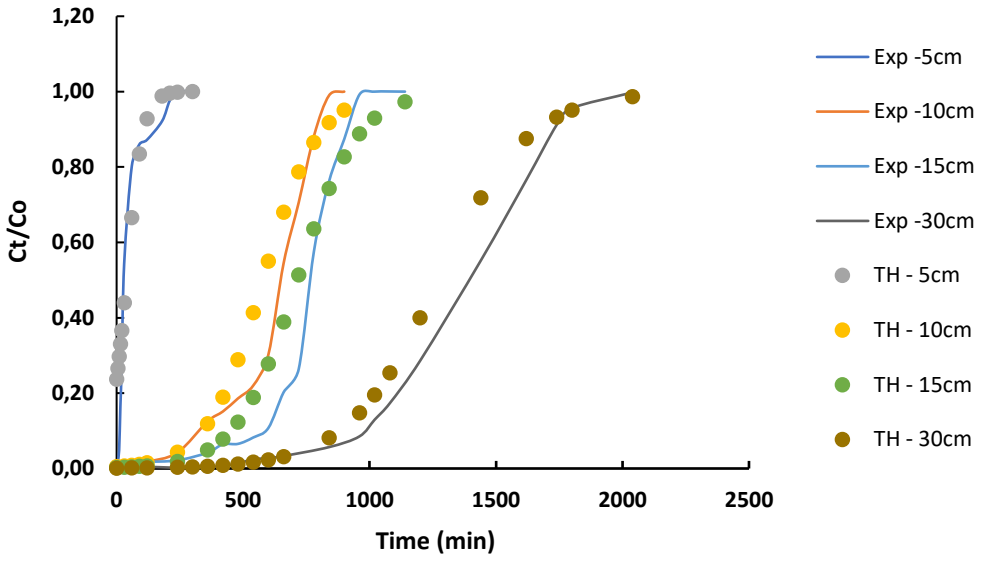

Figure 4.21: Breakthrough curves on the removal of Cr^{6+} predicted by the Thomas model

From table 4.10 it was noted that the adsorption capacity q_T increased from bed height of 5 cm, but the increase was random with no specific trend, whereas k_T decreased at increasing bed height. Both increase and decrease in q_T and k_T, respectively, are in line with other research works done on the adsorption of toxic substances from aqueous solution using biomass materials (Masukume, Onyango and Maree 2014; Ntimbani, Simate and Ndlovu 2015; Ansari, Harahap and Husin 2021; Mohanta *et al.* 2021). The coefficient of determination R^2 was low with a coefficient of 0.74 at 5 cm but increased as bed height increased up to 0.95. However, the Thomas model did not fit well with the experimental data as seen by the statistical errors of MAE and RSME, R^2, as well as q_T from the experimental data did not match closely with the capacity calculated from the model.

Table 4.10: Thomas model parameters

Height, Z (cm)	K_T (mL/ min mg)	q_T (mg/g)	R^2	MAE	RMSE
5	0.0052	242.28	0.80	0.07	0.25
10	0.0018	1178.83	0.91	0.04	0.16
15	0.0015	1044.02	0.93	0.03	0.13
30	0.0011	827.71	0.95	0.03	0.13

4.6.2.2 Yoon-Nelson Model

The Yoon-Nelson model assumes that the decrease in the rate of adsorption is directly proportional to the adsorbate adsorption and breakthrough on the adsorbate. The model does not take in to any account the properties of the adsorbate, type of adsorbent used and physical features of the adsorption bed (Patel 2019). $\ln\left[\frac{C_t}{C_o - C_t}\right]$ is plotted against t to obtain the time required for 50% adsorbate breakthrough τ and the Yoon-Nelson rate constant k_{YN}. Figure 4.22 shows the comparison of the experimental breakthrough curves against the breakthrough curves predicted by the model. From table 4.11, the parameters given by the model showed that k_{YN} decreased and τ increased as bed height increased. This trend was also noted by (Bhaumik *et al.* 2013) in the removal of Cr^{6+} using polypyrrole/Fe_3O_4 nanocomposite. The increase in τ can be attributed to the increased availability in the biosorbent where residence time of the passing influent stream is increased. For 10, 15 and 30 cm, the model fitted very well with the experimental data as given by the R^2, MAE and RSME values but not for 5 cm.

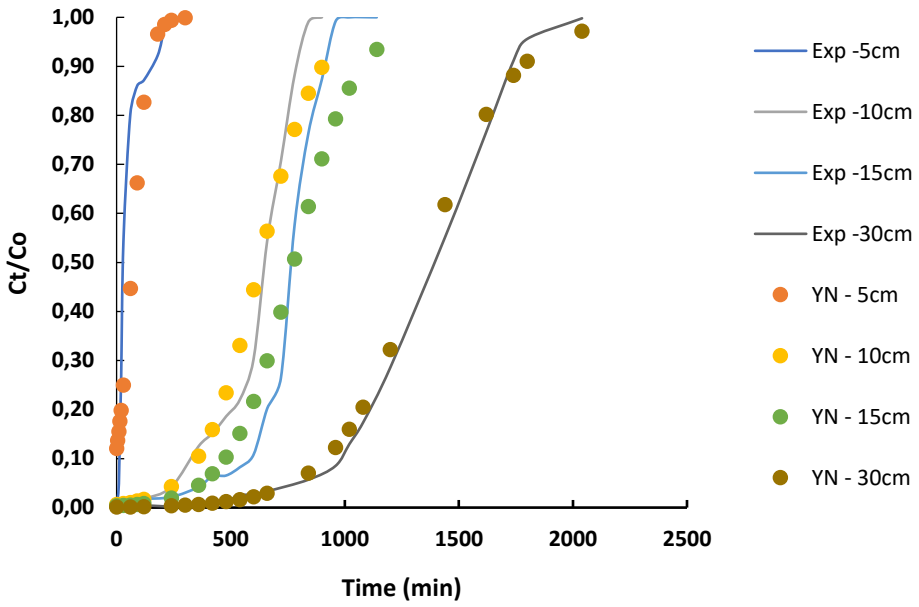

Figure 4.22: Breakthrough curves for the removal of Cr^{6+} predicted by the Yoon-Nelson model

Table 4.11: Yoon-Nelson parameters

Height, Z (cm)	K_T (min^{-1})	τ (min)	R^2	MAE	RMSE
5	0.0260	56.57	0.80	0.05	0.16
10	0.0080	627.94	0.97	0.00	0.02
15	0.0073	776.32	0.93	0.02	0.08
30	0.0051	1345.80	0.97	0.01	0.03

4.6.2.3 Adams-Bohart Model

The Adams-Bohart model is based on the surface reaction theory, and it describes the relationship between C_t/C_o in relation to time during continuous operation. The model assumes that equilibrium is not instantaneous and that it is used for describing the initial part of the breakthrough curve by plotting $\ln\frac{C_t}{C_o}$ against *t*. From the plot, the Adams-Bohart constant k_{AB} and saturation concentration

N_o can be obtained. Figure 4.23 below shows the comparison between experimental data and the data calculated by the model. Table 4.12 shows the parameters obtained from the model.

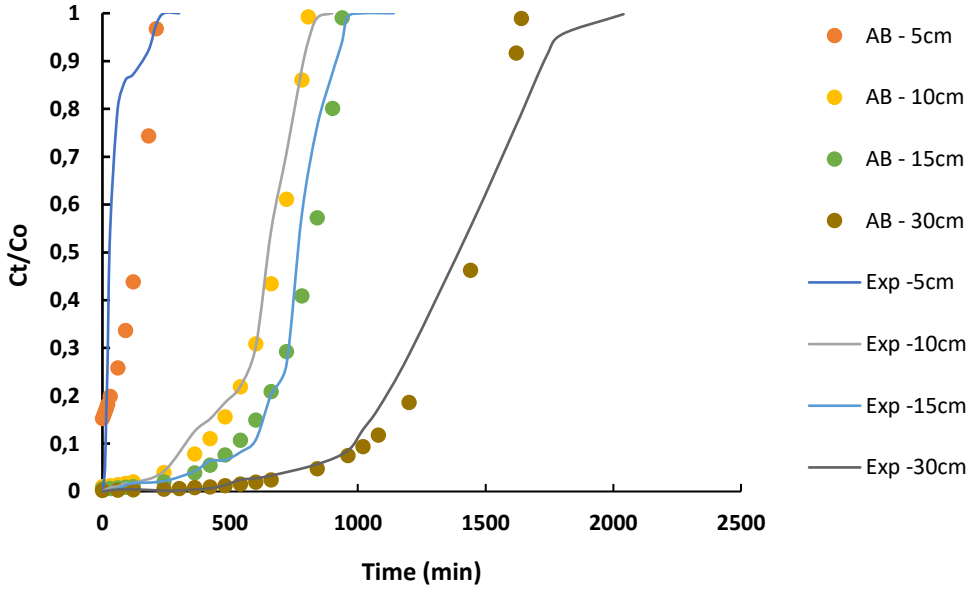

Figure 4.23: Breakthrough curves for the removal of Cr^{6+} predicted by the Adams-Bohart model

It was noted that the model described the initial part of the breakthrough curve well for 10 and 15 cm. The constant k_{AB} showed a decrease in value as height increased, while N_o increased randomly with no specific trend then decreased at 30 cm. This phenomenon was noted by (Sekhula *et al.* 2012; Radhika *et al.* 2018) where N_o increased as bed height increased but decreased as bed height continued to increase due to external mass transfer by axial dispersion of Cr ions onto the cell walls of the banana peels, particularly in the initial part of biosorption in the column while. The MAE, RSME and R^2 values showed a good fit at bed heights of 10 and 15 cm, therefore indicating that there was reaction between the surface of the banana peels with the Cr^{6+} ions during continuous operation. A study done by (García-Sánchez *et al.* 2016) on the removal of fluoride from well water found that the Adams-Bohart model fitted well with their experimental data with k_{AB} decreasing as bed height and this was due to an increase in mass transfer resistance as resistivity increases with increase in biomass material.

Table 4.12: Adams-Bohart parameters

Height, Z (cm)	k_{AB} (mL/ min mg)	N_o (mg/L)	R^2	MAE	RMSE
5	0.00262	154238.75	0.50	0.03	0.09
10	0.00114	388191.75	0.98	0.01	0.03
15	0.00112	301570.61	0.97	0.01	0.05
30	0.00076	263620.93	0.94	0.02	0.08

4.6.3 Conclusion on Removal of Cr^{6+} in Fixed-Bed Column: Dynamic Studies

Fixed-bed column studies were conducted on Cr^{6+}. According to literature, Cr exists in two states, Cr^{3+} which is required in the blood stream for blood mechanism maintenance in humans and animals, and Cr^{6+} which is the most poisonous form of Cr and can lead to very poor health and fatalities when ingested continuously. As a result, Cr^{6+} was used for further studies in the adsorption column.

Bed height was varied in a fixed bed column from 5, 10, 15 to 30 cm and parameters kept constant were volumetric flowrate, initial metal concentration and water pH during constant operations. The increase in bed height had a very significant impact in the performance of the column between the Cr ions and the banana peels. Increase in bed height generally improved the performance of the column where H_B, t_B, q_B, q_T and V_B increased. The longest breakthrough time reported was between 7 and 8 hours of continuous operation until saturation was reached (after 30 hours) at a bed height of 30 cm.

The Thomas, Yoon-Nelson and Adams-Bohart models were used for describing the biosorption process for fixed-bed columns. The overall process favored the Adams-Bohart and Yoon-Nelson models. The Thomas model did not fit well with experimental data for the removal of Cr^{6+} with banana peels.

CONCLUSION & RECOMMENDATIONS

The aim of this project was to evaluate the use of banana peels as a biomass adsorbent in removing heavy metals from water. The metals used for this project were Cr^{6+} and Cu^{2+} as these metals are some of the heavy metals that have been found to contaminate water bodies in South Africa through industrial activities as well as through acid mine drainage (AMD) from abandoned mines.

The first objective was to perform batch studies. Parameters such as pH, agitation speed, biosorbent dose, metal concentration and contact time were varied to look at their effect in the removal efficiency (%removal) for Cr^{6+} and Cu^{2+}. The pH of water was varied between 2 and 7, and the highest %removal was found at pH of 4 with 65% and 95% removal of Cr^{6+} and Cu^{2+}, respectively. Agitation speed was varied between 100 to 200 rpm, and the highest % removal for Cr^{6+} was at 67% at 180 rpm and for Cu^{2+} at 95% removal at 160 rpm and 180 rpm. Biomass dose of banana peels was varied between 1 to 6 grams and the highest % removal was achieved at 65% for Cr^{6+} at 5g and at 91% removal for Cu^{2+} at 6 g. Metal concentration was varied between 5 to 100 mg/L and found that banana peels performed better at low metal concentrations. The highest % removal for Cr^{6+} was 65% at 5 mg/L, and for Cu^{2+} was 95% at 10, 15 and 20 mg/L for all three concentrations. The last parameter studied was contact time of which it was studied from 5 to 140 minutes. Equilibrium was reached at 30 minutes for Cr^{6+} and at 50 minutes for Cu^{2+}.

The second objective was to use adsorption equilibrium isotherms and kinetic models to determine the type of biosorption taken place and their mechanism. For the biosorption of Cr^{6+}, the process favoured both the Freundlich and Langmuir isotherm model with R^2 of 0.99 and 0.95, respectively. The Langmuir adsorption capacity of 7.36 mg/g was close to the experimental value of 8.1 mg/g. The process mechanism favoured the pseudo-2^{nd} order kinetic reaction with an R^2 of ~1, where the rate-limiting step of the process was mainly by ion exchange. For the biosorption of Cu^{2+}, the process favored the Langmuir isotherm model with R^2 of 0.96 and the Langmuir capacity of 15.41 mg/g

which was closer to the experimental value of 12.38 mg/g. The process favored the pseudo-1st order kinetic, pseudo-2nd order kinetic reaction and intra-particle diffusion.

The third objective was to characterize banana peels by using analytical tools to determine their physical and chemical properties. The FTIR analysis detected peaks of hydroxyl groups, carboxylic acids, alkanes and amines which played significant roles in removing Cr^{6+} and Cu^{2+} from water. The SEM analysis showed a surface of the peels to be rough and uneven on the surface. After biosorption, there were changes on the surface where in some cases fractures and groves were formed on the surface of the peels. The EDS gave the elements present in the peels before and after biosorption of C, O, K, Si and Cl of which K and Cl were significantly reduced after biosorption with an addition of Cr. This indicated that there was some exchange of Cr ions with those that were on the surface of the banana peels. The XRD analysis found that the surface of the peels was amorphous in nature with a few crystalline peaks of KCl salt called sylvite. After biosorption, the structure of the peels did not change significantly, however the peaks recorded before biosorption disappeared from the material, which also was confirmed with the reduction in K and Cl. The BET analysis identified the pores of the banana peels to be mesoporous with a pore size of 2.9 nm, surface area of 5.691 m^2/g and pore volume of 0.002605 cm^3/g.

Lastly, the fourth objective was to evaluate the performance of banana peels in removing Cr^{6+} in water in a fixed-bed column at continuous operation. Bed height was varied at 5 different heights from 5, 10, 15, 20 to 30 cm at constant flowrate, pH and initial concentration of 4 mL/min, 4 and 5, respectively. The column studies breakthrough curves were developed, and the behavior of column showed that breakthrough time, saturation time and the mass transfer zone increased as bed height increased. Mathematical models for the column experiments were applied to determine the dynamic behavior in the column and the process was found to favor the Yoon-Nelson and Adams-Bohart models with R^2 ranging from 0.93 to 0.97 for the Yoon-Nelson and 0.94 to 0.98 for the Adams-Bohart model.

Banana peels have been evaluated for its performance in removing Cr^{6+} and Cu^{2+} from water and it can, therefore, be used for application in the adsorption process as a biomass adsorbent.

It is recommended that further column studies be done on the biosorption process, by looking at using real contaminated water from municipal water, surface water, groundwater or water from treatment facilities that are struggling with removing heavy metals from their facilities. This will confirm this study with regards to the banana peels' ability and performance in removing actual contaminated water as well as to determine upscale methods for its application for industrial use. It is recommended that improvements on the biosorbent be done such as modifying its properties to allow for a more robust material in removing more than one heavy metal and for increasing the removal efficiency. Lastly, it is also recommended to do a study in the recovery of heavy metals from banana peels, as well as the regeneration of banana peels as a means of influencing the reduction of operational costs for industrial application.

REFERENCES

Abbasi, Z., Alikarami, M., Nezhad, E. R., Moradi, F. and Moradi, V. 2013. Adsorptive removal of Co2+ and Ni2+ by peels of banana from aqueous solution. *Universal Journal of Chemistry*, 1 (3): 90-95.

Adamson, A. W. and Gast, A. P. 1967. *Physical chemistry of surfaces*. Interscience publishers New York.

Affairs, D. o. W. 2012. *2012 Resource Water Quality Objectives (RWQOs): Directorate Water Resource Planning Systems, Chief Directorate Integrated Water Resource Planning: Feasibility Study for a Long-Term solution to Address the Acid Mine Drainage*. Pretoria: Department of Water Affairs.

Afolabi, F. O., Musonge, P. and Bakare, B. F. 2021a. Application of the response surface methodology in the removal of Cu2+ and Pb2+ from aqueous solutions using orange peels. *Scientific African*, 13: e00931.

Afolabi, F. O., Musonge, P. and Bakare, B. F. 2021b. Bio-sorption of a bi-solute system of copper and lead ions onto banana peels: characterization and optimization. *Journal of Environmental Health Science and Engineering*, 19 (1): 613-624.

Afolabi, F. O., Musonge, P. and Bakare, B. F. 2021c. Evaluation of Lead (II) Removal from Wastewater Using Banana Peels: Optimization Study. *Polish Journal of Environmental Studies*, 30 (2)

Agarwal, A. K., Kadu, M. S., Pandhurnekar, C. P. and Muthreja, I. L. 2015. Kinetics study on the adsorption of Ni2+ ions onto fly ash. *Journal of Chemical Technology and Metallurgy*, 50 (5): 601-605.

Ahad, R. I. A., Goswami, S. and Syiem, M. B. 2017. Biosorption and equilibrium isotherms study of cadmium removal by Nostoc muscorum Meg 1: morphological, physiological and biochemical alterations. *3 Biotech*, 7 (2): 1-12.

Ahalya, N., Ramachandra, T. and Kanamadi, R. 2003. Biosorption of heavy metals. *Res. J. Chem. Environ*, 7 (4): 71-79.

Ajmal, M., Rao, R. A. K., Ahmad, R. and Ahmad, J. 2000. Adsorption studies on Citrus reticulata (fruit peel of orange): removal and recovery of Ni (II) from electroplating wastewater. *Journal of Hazardous Materials*, 79 (1-2): 117-131.

Akcil, A. and Koldas, S. 2006. Acid Mine Drainage (AMD): causes, treatment and case studies. *Journal of cleaner production*, 14 (12-13): 1139-1145.

Aksu, Z. and Gönen, F. 2004. Biosorption of phenol by immobilized activated sludge in a continuous packed bed: prediction of breakthrough curves. *Process biochemistry*, 39 (5): 599-613.

Ali, A., Saeed, K. and Mabood, F. 2016. Removal of chromium (VI) from aqueous medium using chemically modified banana peels as efficient low-cost adsorbent. *Alexandria Engineering Journal*, 55 (3): 2933-2942.

Ali, M. H., Hussian, A.-E. M., Abdel-Satar, A. M., Goher, M. E., Napiórkowska-Krzebietke, A. and Abd El-Monem, A. M. 2016. The isotherm and kinetic studies of the biosorption of heavy metals by non-living cells of Chlorella vulgaris. *Journal of elementology*, 21 (4): 1263-1276.

Alpat, S., Alpat, S. K., Çadirci, B. H., Özbayrak, Ö. and Yasa, İ. 2010. Effects of biosorption parameter: kinetics, isotherm and thermodynamics for Ni (II) biosorption from aqueous solution by Circinella sp. *Electronic Journal of Biotechnology*, 13 (5): 4-5.

Annadurai, G., Juang, R.-S. and Lee, D. 2003. Adsorption of heavy metals from water using banana and orange peels. *Water science and technology*, 47 (1): 185-190.

Ansari, W., Harahap, H. and Husin, A. 2021. Fixed-bed column adsorption performance for ammonia removal using adsorbent from zeolite. In: Proceedings of *IOP Conference Series: Materials Science and Engineering*. IOP Publishing, 012076.

Anwar, J., Shafique, U., Salman, M., Dar, A. and Anwar, S. 2010. Removal of Pb (II) and Cd (II) from water by adsorption on peels of banana. *Bioresource technology*, 101 (6): 1752-1755.

Ayawei, N., Ebelegi, A. N. and Wankasi, D. 2017. Modelling and interpretation of adsorption isotherms. *Journal of chemistry*, 2017

Ayres, D., Davis, A. and Gietka, P. 1994. Removing heavy metals from wastewater-engineering research center report. *University of Maryland, Maryland*,

Badessa, T. S., Wakuma, E. and Yimer, A. M. 2020. Bio-sorption for effective removal of chromium (VI) from wastewater using Moringa stenopetala seed powder (MSSP) and banana peel powder (BPP). *BMC chemistry*, 14 (1): 1-12.

Batool, F., Akbar, J., Iqbal, S., Noreen, S. and Bukhari, S. N. A. 2018. Study of isothermal, kinetic, and thermodynamic parameters for adsorption of cadmium: an overview of linear and nonlinear approach and error analysis. *Bioinorganic chemistry and applications*, 2018

Bell, F., Bullock, S., Hälbich, T. and Lindsay, P. 2001. Environmental impacts associated with an abandoned mine in the Witbank Coalfield, South Africa. *International journal of coal geology*, 45 (2-3): 195-216.

Bhatnagar, A., Sillanpää, M. and Witek-Krowiak, A. 2015. Agricultural waste peels as versatile biomass for water purification–A review. *Chemical Engineering Journal*, 270: 244-271.

Bhaumik, M., Setshedi, K., Maity, A. and Onyango, M. S. 2013. Chromium (VI) removal from water using fixed bed column of polypyrrole/Fe3O4 nanocomposite. *Separation and Purification Technology*, 110: 11-19.

Boulaiche, W., Hamdi, B. and Trari, M. 2019. Removal of heavy metals by chitin: equilibrium, kinetic and thermodynamic studies. *Applied Water Science*, 9 (2): 1-10.

Branca, C. and Di Blasi, C. 2015. A lumped kinetic model for banana peel combustion. *Thermochimica Acta*, 614: 68-75.

BrbootI, M. M., AbiD, B. A. and Al-ShuwaikI, N. M. 2011. Removal of heavy metals using chemicals precipitation. *Eng. Technol. J*, 29 (3): 595-612.

Buasri, A., Chaiyut, N., Tapang, K., Jaroensin, S. and Panphrom, S. 2012. Biosorption of heavy metals from aqueous solutions using water hyacinth as a low cost biosorbent. *Civ Environ Res*, 2 (2): 17-25.

Budak, T. B. 2013. Removal of heavy metals from wastewater using synthetic ion exchange resin. *Asian Journal of Chemistry*, 25 (8): 4207-4210.

Chatterjee, S., Mondal, S. and De, S. 2018. Design and scaling up of fixed bed adsorption columns for lead removal by treated laterite. *Journal of cleaner production*, 177: 760-774.

Chowdhury, Z., Zain, S., Rashid, A., Rafique, R. and Khalid, K. 2013. Breakthrough curve analysis for column dynamics sorption of Mn (II) ions from wastewater by using Mangostana garcinia peel-based granular-activated carbon. *Journal of chemistry*, 2013

Damal, M. V. S. and Khanapure, M. V. 2017. Removal of Zinc Metal Ions from Electroplating Industrial Waste Water by Using Bio-Sorbent. *International Journal of Advanced Engineering Research and Science*, 4 (7): 237218.

Daochalermwong, A., Chanka, N., Songsrirote, K., Dittanet, P., Niamnuy, C. and Seubsai, A. 2020. Removal of heavy metal ions using modified celluloses prepared from pineapple leaf fiber. *ACS omega*, 5 (10): 5285-5296.

Department of Agriculture, F. a. F. 2017. *A Profile of the South African Banana Market Value Chain*. Aracdia: Department of Agriculture, Forestry and Fisheries.

Deshmukh, P. D., Khadse, G. K., Shinde, V. M. and Labhasetwar, P. 2017. Cadmium removal from aqueous solutions using dried banana peels as an adsorbent: kinetics and equilibrium modeling. *Journal of Bioremediation & Biodegradation*, 8 (03): 395.

Dutrow, B. C., CM. 2020. *X-ray Powder Diffraction (XRD)*. Available: https://serc.carleton.edu/research_education/geochemsheets/techniques/XRD.html (Accessed

Edokpayi, J. N., Enitan, A. M., Mutileni, N. and Odiyo, J. O. 2018. Evaluation of water quality and human risk assessment due to heavy metals in groundwater around Muledane area of Vhembe District, Limpopo Province, South Africa. *Chemistry Central Journal*, 12 (1): 1-16.

El-Din, G. A., Amer, A., Malsh, G. and Hussein, M. 2018. Study on the use of banana peels for oil spill removal. *Alexandria Engineering Journal*, 57 (3): 2061-2068.

Fadel, M., Hassanein, N. M., Elshafei, M. M., Mostafa, A. H., Ahmed, M. A. and Khater, H. M. 2017. Biosorption of manganese from groundwater by biomass of Saccharomyces cerevisiae. *Hbrc Journal*, 13 (1): 106-113.

Fashola, M. O., Ngole-Jeme, V. M. and Babalola, O. O. 2016. Heavy metal pollution from gold mines: environmental effects and bacterial strategies for resistance. *International journal of environmental research and public health*, 13 (11): 1047.

Faust, S. D. and Aly, O. M. 2013. *Adsorption processes for water treatment*. Elsevier.

Foo, K. Y. and Hameed, B. H. 2010. Insights into the modeling of adsorption isotherm systems. *Chemical Engineering Journal*, 156 (1): 2-10.

Forestry, D. o. W. A. a. 1996. South African Water Quality Guidelines. Available: www.dwaf.gov.za/IWQS/wq_guide/domestic.pdf (Accessed June/25/2018).

Freundlich, H. 1922. *Kapillarchemie, eine Darstellung der Chemie der Kolloide und verwandter Gebiete*. akademische Verlagsgesellschaft.

Fu, F. and Wang, Q. 2011. Removal of heavy metal ions from wastewaters: a review. *Journal of environmental management*, 92 (3): 407-418.

García-Sánchez, J., Solache-Ríos, M., Alarcón-Herrera, M. and Martínez-Miranda, V. 2016. Removal of fluoride from well water by modified iron oxides in a column system. *Desalination and Water Treatment*, 57 (5): 2125-2133.

Geankoplis, C. J., Hersel, A. A. and Lepek, D. H. 2018. *Transport processes and separation process principles*. Prentice hall Boston, MA.

Geethakarthi, A. and Phanikumar, B. 2011. Adsorption of reactive dyes from aqueous solutions by tannery sludge developed activated carbon: Kinetic and equilibrium studies. *International journal of environmental science & technology*, 8 (3): 561-570.

Geldenhuis, S. and Bell, F. 1998. Acid mine drainage at a coal mine in the eastern Transvaal, South Africa. *Environmental Geology*, 34 (2-3): 234-242.

Gunatilake, S. 2015. Methods of removing heavy metals from industrial wastewater. *Methods*, 1 (1): 14.

Hall, K. R., Eagleton, L. C., Acrivos, A. and Vermeulen, T. 1966. Pore-and solid-diffusion kinetics in fixed-bed adsorption under constant-pattern conditions. *Industrial & engineering chemistry fundamentals*, 5 (2): 212-223.

Hamdaoui, O. and Naffrechoux, E. 2007. Modeling of adsorption isotherms of phenol and chlorophenols onto granular activated carbon: Part I. Two-parameter models and equations allowing determination of thermodynamic parameters. *Journal of Hazardous Materials*, 147 (1-2): 381-394.

Hamza, I. A., Martincigh, B. S., Ngila, J. C. and Nyamori, V. O. 2013. Adsorption studies of aqueous Pb (II) onto a sugarcane bagasse/multi-walled carbon nanotube composite. *Physics and Chemistry of the Earth, Parts A/B/C*, 66: 157-166.

Hernández, M. L. and Romero, M. L. 2019. Remoción de cromo hexavalente en aguas contaminadas utilizando cáscara de plátano (Musa paradisiaca) como adsorbente. *Revista Torreón Universitario*, 8 (23): 73-83.

Ho, Y.-S. 2006. Review of second-order models for adsorption systems. *Journal of Hazardous Materials*, 136 (3): 681-689.

Ho, Y. and McKay, G. 1998. A comparison of chemisorption kinetic models applied to pollutant removal on various sorbents. *Process safety and environmental protection*, 76 (4): 332-340.

Hossain, M., Ngo, H., Guo, W. and Nguyen, T. 2012. Biosorption of Cu (II) from water by banana peel based biosorbent: experiments and models of adsorption and desorption. *Journal of Water sustainability*, 2 (1): 87-104.

Imran Din, M., Mirza, M. L., Ata, S., Athar, M. and Mohsin, I. U. 2013. Thermodynamics of biosorption for removal of Co (II) ions by an efficient and ecofriendly biosorbent (Saccharum bengalense): kinetics and isotherm modeling. *Journal of chemistry*, 2013

Isa, Y. M., Harripersadth, C., Musonge, P., Sayago, A. and Morales, M. G. 2020. The application of eggshells and sugarcane bagasse as potential biomaterials in the removal of heavy metals from aqueous solutions. *South African Journal of Chemical Engineering*, 34 (1): 142-150.

Issaoui, H., Sallem, F., Lafaille, J., Grassl, B. and Bouhtoury, C. E. 2021. Biosorption of heavy metals from water onto phenolic foams based on tannins and lignin alkaline liquor. *International Journal of Environmental Research*, 15 (2): 369-381.

Jamshaid, A., Hamid, A., Muhammad, N., Naseer, A., Ghauri, M., Iqbal, J., Rafiq, S. and Shah, N. S. 2017. Cellulose-based Materials for the Removal of Heavy Metals from Wastewater–An Overview. *ChemBioEng Reviews*, 4 (4): 240-256.

Javaid, A., Bajwa, R., Shafique, U. and Anwar, J. 2011. Removal of heavy metals by adsorption on Pleurotus ostreatus. *Biomass and Bioenergy*, 35 (5): 1675-1682.

Kajjumba, G. W., Emik, S., Öngen, A., Özcan, H. K. and Aydın, S. 2018. Modelling of adsorption kinetic processes—errors, theory and application. *Advanced sorption process applications*: 187-206.

Kamsonlian, S., Suresh, S., Majumder, C. and Chand, S. 2011. Characterization of banana and orange peels: biosorption mechanism. *International Journal of Science Technology & Management*, 2 (4): 1-7.

Kanamarlapudi, S., Chintalpudi, V. K. and Muddada, S. 2018. Application of biosorption for removal of heavy metals from wastewater. *Biosorption*, 18: 69.

Kariuki, Z., Kiptoo, J. and Onyancha, D. 2017. Biosorption studies of lead and copper using rogers mushroom biomass 'Lepiota hystrix'. *South African Journal of Chemical Engineering*, 23 (1): 62-70.

Khairiah, K., Frida, E., Sebayang, K., Sinuhaji, P. and Humaidi, S. 2021. Data on characterization, model, and adsorption rate of banana peel activated carbon (Musa Acuminata) for adsorbents of various heavy metals (Mn, Pb, Zn, Fe). *Data in Brief*, 39: 107611.

Khambhaty, Y., Mody, K., Basha, S. and Jha, B. 2009. Kinetics, equilibrium and thermodynamic studies on biosorption of hexavalent chromium by dead fungal biomass of marine Aspergillus niger. *Chemical Engineering Journal*, 145 (3): 489-495.

Khawas, P. and Deka, S. C. 2016. Comparative nutritional, functional, morphological, and diffractogram study on culinary banana (Musa ABB) peel at various stages of development. *International Journal of Food Properties*, 19 (12): 2832-2853.

Khiari, B., Wakkel, M., Abdelmoumen, S. and Jeguirim, M. 2019. Dynamics and kinetics of cupric ion removal from wastewaters by Tunisian solid crude olive-oil waste. *Materials*, 12 (3): 365.

Lagergren, S. K. 1898. About the theory of so-called adsorption of soluble substances. *Sven. Vetenskapsakad. Handingarl*, 24: 1-39.

Lagerwall, G. 2005. *Bananas in KwaZulu-Natal*. Available: https://www.kzndard.gov.za/images/Documents/Research%20and%20Technology%20Development%20Services/Publications/RESEARCH%20REPORTS/BananasinKwaZulu-Natal.pdf (Accessed

Langmuir, I. 1918. The adsorption of gases on plane surfaces of glass, mica and platinum. *Journal of the American Chemical society*, 40 (9): 1361-1403.

Leong, K. 2018. Adsorption of heavy metals using banana peels in wastewater treatment. *The Eurasia Proceedings of Science Technology Engineering and Mathematics*, (2): 312-317.

Li, X., Tang, Y., Xuan, Z., Liu, Y. and Luo, F. 2007. Study on the preparation of orange peel cellulose adsorbents and biosorption of Cd2+ from aqueous solution. *Separation and Purification Technology*, 55 (1): 69-75.

Loock, M., Beukes, J. and Van Zyl, P. 2014. A survey of Cr (VI) contamination of surface water in the proximity of ferrochromium smelters in South Africa. *Water Sa*, 40 (4): 709-716.

Mahlangu, J., Simate, G. and de Beer, M. 2018. Adsorption of Mn2+ from the Acid Mine Drainage using banana peel. *International Journal of Water and Wastewater Treatment*, 4 (1): 153-159.

Manne, R., Kumaradoss, M. M. R. M., Iska, R. S. R., Devarajan, A. and Mekala, N. 2022. Water quality and risk assessment of copper content in drinking water stored in copper container. *Applied Water Science*, 12 (3): 1-8.

Marandi, R. 2011. Biosorption of hexavalent chromium from aqueous solution by dead fungal biomass of Phanerochaete crysosporium: batch and fixed bed studies. *Can. J. Chem. Eng. Technol*, 2 (2): 8-22.

Masukume, M., Onyango, M. S. and Maree, J. P. 2014. Sea shell derived adsorbent and its potential for treating acid mine drainage. *International Journal of Mineral Processing*, 133: 52-59.

Materials Evaluation and Engineering, I. 2014a. Handbook of Analytical Methods for Materials. In: *Energy Dispersive X-ray Spectroscopy*. Available: https://www.mee-inc.com/files/9314/2118/3293/HAMM_2014-EnergyDispersiveX-RaySpectroscopy.pdf (Accessed

Materials Evaluation and Engineering, I. 2014b. Scanning Electron Microscopy. In: *Handbook of Analytical Methods for Materials*. Available: https://www.mee-inc.com/files/1014/2118/3300/HAMM_2014-ScanningElectronMicroscopy.pdf (Accessed

Memon, J. R., Memon, S. Q., Bhanger, M., Memon, G. Z., El-Turki, A. and Allen, G. C. 2008. Characterization of banana peel by scanning electron microscopy and FT-IR spectroscopy and its use for cadmium removal. *Colloids and surfaces B: Biointerfaces*, 66 (2): 260-265.

Memon, J. R., Memon, S. Q., Bhanger, M. I., El-Turki, A., Hallam, K. R. and Allen, G. C. 2009. Banana peel: a green and economical sorbent for the selective removal of Cr (VI) from industrial wastewater. *Colloids and surfaces B: Biointerfaces*, 70 (2): 232-237.

Mohamed, M. H., Udoetok, I. A., Solgi, M., Steiger, B., Zhou, Z. and Wilson, L. D. Design of Sustainable Biomaterial Composite Adsorbents for Point-of-Use Removal of Lead Ions from Water. *Frontiers in Water*: 1.

Mohanta, S., Sahu, M. K., Mishra, P. C. and Giri, A. K. 2021. Removal of Cr (VI) from aqueous solution by activated charcoal derived from Sapindus trifoliate L fruit biomass using continuous fixed bed column studies. *Water science and technology*,

Mulopo, J. 2015. Making sense of our mining wastes: removal of heavy metals from AMD using sulphidation media derived from waste gypsum. *Journal of the Southern African Institute of Mining and Metallurgy*, 115 (12): 1193-1197.

Naseer, A., Jamshaid, A., Hamid, A., Muhammad, N., Ghauri, M., Iqbal, J., Rafiq, S. and Shah, N. S. 2019. Lignin and lignin based materials for the removal of heavy metals from waste water-an overview. *Zeitschrift für Physikalische Chemie*, 233 (3): 315-345.

Nasrollahzadeh, M., Atarod, M., Sajjadi, M., Sajadi, S. M. and Issaabadi, Z. 2019. Plant-mediated green synthesis of nanostructures: mechanisms, characterization, and applications. In: *Interface science and technology*. Elsevier, 199-322.

Ntimbani, R. N., Simate, G. S. and Ndlovu, S. 2015. Removal of copper ions from dilute synthetic solution using staple ion exchange fibres: Equilibrium and kinetic studies. *Journal of Environmental Chemical Engineering*, 3 (2): 1258-1266.

Ntimbani, R. N., Simate, G. S. and Ndlovu, S. 2016. Removal of copper ions from dilute synthetic solution using staple ion exchange fibres: dynamic studies. *Journal of Environmental Chemical Engineering*, 4 (3): 3143-3150.

ODIYO, J. O. and EDOKPAYI, J. N. 2018. Physico-chemical and surface characterisation of a renewable low-cost biosorbent for the uptake of heavy metal ions from aqueous solution. *WIT Transactions on Ecology and the Environment*, 228: 317-327.

Olalde, M. 2016. What's left in the wake of South Africa's abandoned gold mines. *Available in: https://www. greenbiz. com/article/whats-left-wake-south-africas-aba ndoned-gold-mines.(Accessed 7 July 2020),*

Olujimi, O., Fatoki, O., Odendaal, J. and Oputu, O. 2015. Variability in heavy metal levels in river water receiving effluents in Cape Town, South Africa. *Research and practices in water quality*: 193-211.

Organization, W. H. 1993. *Guidelines for drinking-water quality*. World Health Organization.

Organization, W. H. 2020. *Chromium in Drinking-water*. World Health Organization.

Oyewo, O. A., Onyango, M. S. and Wolkersdorfer, C. 2016. Application of banana peels nanosorbent for the removal of radioactive minerals from real mine water. *Journal of environmental radioactivity*, 164: 369-376.

Patel, H. 2019. Fixed-bed column adsorption study: a comprehensive review. *Applied Water Science*, 9 (3): 1-17.

Pejic, B., Vukcevic, M., Kostic, M. and Skundric, P. 2009. Biosorption of heavy metal ions from aqueous solutions by short hemp fibers: effect of chemical composition. *Journal of Hazardous Materials*, 164 (1): 146-153.

Qiu, H., Lv, L., Pan, B.-c., Zhang, Q.-j., Zhang, W.-m. and Zhang, Q.-x. 2009. Critical review in adsorption kinetic models. *Journal of Zhejiang University-Science A*, 10 (5): 716-724.

Radhika, R., Jayalatha, T., Jacob, S., Rajeev, R. and George, B. K. 2018. Adsorption performance of packed bed column for the removal of perchlorate using modified activated carbon. *Process safety and environmental protection*, 117: 350-362.

Reimerink, W. and Kleut, D. 1999. Air pollution control by adsorption. In: *Studies in Surface Science and Catalysis*. Elsevier, 807-819.

Renu, Agarwal, M., Singh, K., Gupta, R. and Dohare, R. 2020. Continuous fixed-bed adsorption of heavy metals using biodegradable adsorbent: Modeling and experimental study. *Journal of Environmental Engineering*, 146 (2): 04019110.

Richardson, J. F., Harker, J. H. and Backhurst, J. R. 2002. *Coulson and Richardson's chemical engineering: Particle technology and separation processes*. Butterworth-Heinemann.

Saadi, Z., Saadi, R. and Fazaeli, R. 2013. Fixed-bed adsorption dynamics of Pb (II) adsorption from aqueous solution using nanostructured γ-alumina. *Journal of Nanostructure in Chemistry*, 3 (1): 1-8.

Sahoo, T. R. and Prelot, B. 2020. Adsorption processes for the removal of contaminants from wastewater: the perspective role of nanomaterials and nanotechnology. In: *Nanomaterials for the Detection and Removal of Wastewater Pollutants*. Elsevier, 161-222.

Schwantes, D., Gonçalves, A. C., Coelho, G. F., Campagnolo, M. A., Dragunski, D. C., Tarley, C. R. T., Miola, A. J. and Leismann, E. A. V. 2016. Chemical modifications of cassava peel as adsorbent material for metals ions from wastewater. *Journal of chemistry*, 2016

Sedibe, M., Achilonu, M., Tikilili, P., Shale, K. and Ebenebe, P. 2017. South African mine effluents: Heavy metal pollution and impact on the ecosystem.

Sekhula, M. M., Okonkwo, J. O., Zvinowanda, C., Agyei, N. N. and Chaudhary, A. J. 2012. Fixed bed column adsorption of Cu (II) onto maize tassel-PVA beads.

Shamim, S. 2018. Biosorption of heavy metals. *Biosorption*, 2: 21-49.

Sharma, A. S. and Bhalerao, S. A. 2018. Batch removal of Chromium (VI) by biosorption on to banana peels (Musa Paradisiaca L.). *World Wide Jounral Of Multidisciplinary Research And Development*, 4

Sincero, A. P. and Sincero, G. A. 2002. *Physical-chemical treatment of water and wastewater*. CRC press.

Singh, A., Kumar, S. and Panghal, V. 2021. Adsorption of chromium (Cr6+) on dead biomass of Salvinia molesta (Kariba weed) and Typha latifolia (broadleaf cattail): isotherm, kinetic, and thermodynamic study. *Applied Water Science*, 11 (9): 1-16.

Sirilert, M. and Maikrang, K. 2018. Adsorption isotherm of some heavy metals in water on unripe and ripe peel of banana. *Naresuan University Journal: Science and Technology (NUJST)*, 26 (1): 128-141.

Skoog, D. A., West, D. M., Holler, F. J. and Crouch, S. R. 2013. *Fundamentals of analytical chemistry*. Cengage learning.

Sparks, D. L. 2003. *Environmental soil chemistry*. Elsevier.

Srivastava, S., Agrawal, S. and Mondal, M. 2019. Fixed bed column adsorption of Cr (VI) from aqueous solution using nanosorbents derived from magnetite impregnated Phaseolus vulgaris husk. *Environmental Progress & Sustainable Energy*, 38 (s1): S68-S76.

Tasaso, P. 2014. Adsorption of copper using pomelo peel and depectinated pomelo peel. *Journal of Clean Energy Technologies*, 2 (2): 154-157.

Tejada-Tovar, C., Gonzalez-Delgado, A. D. and Villabona-Ortiz, A. 2019. Characterization of residual biomasses and its application for the removal of lead ions from aqueous solution. *Applied Sciences*, 9 (21): 4486.

Tejada-Tovar, C., Mancilla, H. B., Moreyra, J. D. P. and Toro, R. O. 2020. Effect of the adsorbent dose in Pb (II) removal by using sugar cane bagasse: Kinetics and isotherms. *Revista Mexicana de Ingeniería Química*, 19 (3): 1413-1423.

Thirunavukkarasu, A., Nithya, R. and Sivashankar, R. 2021. Continuous fixed-bed biosorption process: a review. *Chemical Engineering Journal Advances*, 8: 100188.

Torres, E. 2020. Biosorption: A review of the latest advances. *Processes*, 8 (12): 1584.

Tutu, H., McCarthy, T. and Cukrowska, E. 2008. The chemical characteristics of acid mine drainage with particular reference to sources, distribution and remediation: the Witwatersrand Basin, South Africa as a case study. *Applied geochemistry*, 23 (12): 3666-3684.

ul Haq, A., Shah, J., Jan, M. R. and ud Din, S. 2015. Kinetic, equilibrium and thermodynamic studies for the sorption of metribuzin from aqueous solution using banana peels, an agro-based biomass. *Toxicological & Environmental Chemistry*, 97 (2): 124-134.

Ushakumary, E. and Madhu, G. 2013. Waste water treatment using low cost natural adsorbents. Cochin University Of Science And Technology.

Verlicchi, P. and Grillini, V. 2020. Surface water and groundwater quality in South Africa and mozambique—Analysis of the Most critical pollutants for drinking purposes and challenges in water treatment selection. *Water*, 12 (1): 305.

Vilardi, G., Di Palma, L. and Verdone, N. 2018. Heavy metals adsorption by banana peels micro-powder: Equilibrium modeling by non-linear models. *Chinese Journal of Chemical Engineering*, 26 (3): 455-464.

Vilardi, G., Rodriguez-Rodriguez, J., Ochando-Pulido, J. M., Di Palma, L. and Verdone, N. 2019. Fixed-bed reactor scale-up and modelling for Cr (VI) removal using nano iron-based coated biomass as packing material. *Chemical Engineering Journal*, 361: 990-998.

Wang, L. K., Hung, Y.-T. and Shammas, N. K. 2007. *Advanced physicochemical treatment technologies*. Springer.

Wilson, D. R. *Health benefits and risks of copper* (online). 2017. Available: https://www.medicalnewstoday.com/articles/288165.php (Accessed

Wong, S., Abd Ghafar, N., Ngadi, N., Razmi, F. A., Inuwa, I. M., Mat, R. and Amin, N. A. S. 2020. Effective removal of anionic textile dyes using adsorbent synthesized from coffee waste. *Scientific reports*, 10 (1): 1-13.

Yakout, S., Hassan, M. and Omar, H. 2019. Fixed-bed column study for the removal of hexavalent chromium ions from aqueous solutions via pyrolysis of the rice husk. *Desalination and Water Treatment*, 170: 128-137.

Yang, H., Yan, R., Chen, H., Lee, D. H. and Zheng, C. 2007. Characteristics of hemicellulose, cellulose and lignin pyrolysis. *Fuel*, 86 (12-13): 1781-1788.

Yaqub, M., Eren, B. and Eyupoglu, V. 2020. Soft computing techniques in prediction Cr (VI) removal efficiency of polymer inclusion membranes.

Zahoor, M. 2011. Effect of agitation speed on adsorption of imidacloprid on activated carbon. *Journal of the Chemical Society of Pakistan*, 33 (6): 305.

Zhou, W., Apkarian, R., Wang, Z. L. and Joy, D. 2006. Fundamentals of scanning electron microscopy (SEM). In: *Scanning microscopy for nanotechnology*. Springer, 1-40.

APPENDICES

6.1 Appendix A: Composition of Salt Metals Used During Experiments

Table 6.1.A: Typical metal composition of elements in metal salts used for experiments

Typical Composition of Elements of Metal Salts Used for Experiments		
Elements	**Copper Sulphate Pentahydrate**	**Sodium Chromate Tetrahydrate**
Cu	99-100%	0.0005%
Cl	0.002%	0.0050%
Fe	0.005%	0.0005%
Pb	1.000%	0%
Cr	0%	99.5%
Ca	0%	0.0005%
SO_4	0%	0.0050%

6.2 Appendix B: Batch Studies – Calculations

Salt conc in water calculations:

$$Salt\ conc. = \frac{MW_{salt}}{MW_{element}} \times Conc\ of\ metal$$

$$i.e.\ for\ Cr\ 5\ {}^{mg}/_{L}: Cr_{salt} = \frac{234.03}{51.996} \times 5\ {}^{mg}/_{L} = 22.5046\ {}^{mg}/_{L}$$

$$i.e.\ for\ Cu\ 5\ {}^{mg}/_{L}: Cu_{salt} = \frac{249.69}{63.546} \times 5\ {}^{mg}/_{L} = 22.5046\ {}^{mg}/_{L}$$

Table 6.2B: Calculated initial salt concentrations

Cu ($CuSO_4.5H_2O$)		**Cr ($Na_2CrO_4.4H_2O$)**	
Metal conc. (mg/L)	Salt Conc (mg/L)	Metal conc. (mg/L)	Salt Conc (mg/L)
5	19.65	5	22.51
10	39.29	10	45.01
15	58.94	15	67.52
20	78.59	20	90.02
30	117.88	30	135.03
40	157.17	40	180.04
50	196.46	50	225.06
60	235.76	60	270.07
80	314.34	80	360.09
100	392.93	100	450.11
120	471.51	120	540.13
140	550.10	140	630.16

6.2.1 Removal efficiency calculations:

$$\%removal = \frac{C_o - C}{C_o} \times 100\%$$

$$i.e. for\ Cu\ 10ppm\ \left(\frac{mg}{L}\right)\ \%rem = \frac{10 - 0.57}{10} \times 100\% = 94\%$$

Table 6.2B: Calculated final metal concentrations and removal efficiencies

pH Results					**Agitation Speed Results**				
	Cu-50 ppm		**Cr-50 ppm**			**Cu-50 ppm**		**Cr-50 ppm**	
pH	C_F (mg/L)	% Rem	C_F (mg/L)	% Rem	**RPM**	C_F (mg/L)	% Rem	C_F (mg/L)	% Rem
2	50.00	0%	48	4%	**100**	13.78	72%	35.3	29%
3	15.52	69%	32.1	36%	**120**	10.89	78%	34.7	31%
4	14.65	71%	32.36	35%	**140**	11.19	78%	34.2	32%
5	18.67	63%	35.6	29%	**160**	10.32	79%	33.65	33%
6	21.57	57%	38.5	23%	**180**	10.43	79%	32.45	35%
7	22.20	56%	39.4	21%	**200**	10.39	79%	33.1	34%
	Cu-10 ppm		**Cr-10ppm**			**Cu-10 ppm**		**Cr-10ppm**	
pH	C_F (mg/L)	% Rem	C_F (mg/L)	% Rem	**RPM**	C_F (mg/L)	% Rem	C_F (mg/L)	% Rem
2	9.65	4%	8.78	12%	**100**	1.30	87%	4.87	51%
3	1.47	85%	4.79	52%	**120**	0.98	90%	4.62	54%
4	0.57	94%	4.14	59%	**140**	0.67	93%	4.37	56%
5	1.79	82%	4.76	52%	**160**	0.54	95%	4.22	58%
6	3.57	64%	7.2	28%	**180**	0.53	95%	4.22	58%
7	4.21	58%	7.5	25%	**200**	0.61	94%	4.21	58%
	Cu-5 ppm		**Cr-5 ppm**			**Cu-5 ppm**		**Cr-5 ppm**	
pH	C_F (mg/L)	% Rem	C_F (mg/L)	% Rem	**RPM**	C_F (mg/L)	% Rem	C_F (mg/L)	% Rem
2	4.98	0%	4.74	5%	**100**	1.57	69%	2.1	58%
3	1.02	80%	1.98	60%	**120**	1.07	79%	2.3	54%
4	0.91	82%	1.77	65%	**140**	0.88	82%	1.98	60%
5	1.25	75%	2.35	53%	**160**	0.89	82%	1.87	63%
6	1.69	66%	3.65	27%	**180**	0.87	83%	1.67	67%
7	2.04	59%	3.67	27%	**200**	1.20	76%	1.72	66%
Biosorbent Dosage Results									
	Cu-50 ppm		**Cr-50 ppm**			**Cu-5 ppm**		**Cr-5 ppm**	
Gram (g)	C_F (mg/L)	% Rem	C_F (mg/L)	% Rem	**Gram (g)**	C_F (mg/L)	% Rem	C_F (mg/L)	% Rem
1	41.52	17%	44.7	11%	**1**	0.92	82%	2.01	60%
2	28.90	42%	39.1	22%	**2**	0.85	83%	1.76	65%
3	15.56	69%	35.6	29%	**3**	0.73	85%	1.77	65%
4	9.48	81%	33.1	34%	**4**	0.78	84%	1.8	64%
5	6.10	88%	32.3	35%	**5**	0.83	83%	1.7	66%
6	4.25	91%	32.1	36%	**6**	0.90	82%	1.79	64%
	Cu-10 ppm		**Cr-10ppm**						
Gram (g)	C_F (mg/L)	% Rem	C_F (mg/L)	% Rem					

1	2.53	75%	4.2	58%	
2	1.95	81%	4.1	59%	
3	1.10	89%	4	60%	
4	0.75	93%	3.5	65%	
5	0.54	95%	3.7	63%	
6	0.49	95%	3.6	64%	

6.3 Appendix C: Isotherm and kinetic studies calculations

6.3.1 Langmuir isotherm calculations

$$\frac{1}{q_e} = \frac{1}{K_L q_L C_e} + \frac{1}{q_L}$$

$$q_e = \frac{(C_o - C_e)V}{M}$$

$$i.e. for\ Cr: q_e = \frac{\left[5\left(\frac{mg}{L}\right) - 1.77\ \left(\frac{mg}{L}\right)\right] \times 1L}{3\ g} = 1.0783\ {}^{mg}/_{g}$$

From figure 4.9, the of $\frac{1}{q_e}$ against $\frac{1}{C_e}$ for the biosorption of Cr yielded the following equation

$$y = 1.6446x + 0.1358$$

$$Where, \frac{1}{q_L} = 0.1358$$

$$q_L = 7.364\ mg/g$$

$$\frac{1}{K_L q_L} = 1.6446$$

$$\therefore\ K_L = 0.083\ mg/g$$

$$i.e. for\ Cu: q_e = \frac{\left[5\left(\frac{mg}{L}\right) - 0.86\ \left(\frac{mg}{L}\right)\right] \times 1L}{3\ g} = 1.3786\ {}^{mg}/_{g}$$

From figure 4.9, the of $\frac{1}{q_e}$ against $\frac{1}{C_e}$ for the biosorption of Cu yielded the following equation

$y = 0.1198x + 0.0649$

$Where, \frac{1}{q_L} = 0.0649$

$q_L = 15.41\ mg/g$

$\frac{1}{K_L q_L} = 0.1198$

$\therefore\ K_L = 0.503\ mg/g$

6.3.2 Freundlich isotherm calculations

$\log q_e = \frac{1}{\mathrm{n}} \log C_e + \log K_f$

From figure 4.10, the of $\log q_e$ against $\log C_e$ for the biosorption of Cr yielded the following equation

$y = 0.5646x - 0.0786$

$Where, \log K_f = 0.0786\ mg/g$

$K_f = 0.83\ mg/g$

$\frac{1}{\mathrm{n}} = 0.5646$

$\therefore\ n = 1.77$

From figure 4.10, the of $\log q_e$ against $\log C_e$ for the biosorption of Cu yielded the following equation

$y = 0.1712x - 0.8641$

$Where, \log K_f = 0.8641\ mg/g$

$K_f = 7.313\ mg/g$

$\frac{1}{\mathrm{n}} = 0.1712$

$\therefore\ n = 5.84$

6.3.3 Elovich isotherm calculations

$\ln\frac{q_e}{C_e} = \ln K_e q_m - \frac{\mathrm{q}_e}{q_m}$

From figure 4.11, the of $\ln\frac{q_e}{C_e}$ against q_e for the biosorption of Cr yielded the following equation

$y = -0.2925x - 0.2056$

$Where, \frac{1}{q_m} = 0.2925$

$q_m = 3.42\ mg/g$

$K_e = 0.36\frac{L}{mg}$

From figure 4.11, the of $\ln\frac{q_e}{C_e}$ against q_e for the biosorption of Cu yielded the following equation

$y = -0.2439x + 3.263$

$Where, q_m = 0.244\ mg/g$

$K_e = 6.37\ L/mg$

6.3.4 Pseudo-first order kinetic calculations

$\log(q_e - q_t) = \log q_e - \frac{K_1}{2.303}t$

From figure 4.12, the of $\log(q_e - q_t)$ against $\log q_e$ for the biosorption of Cr yielded the following equation

$y = -0.276x + 1.8449$

$Where, \log q_e = 1.8449$

$q_e = 6.3\ mg/g$

$\frac{K_1}{2.303} = 0.276$

$K_1 = 0.636\ min^{-1}$

For Cu,

$y = -0.0454x + 2.2837$

$Where, q_e = 1.05\ mg/g$

$K_1 = 5.259\ min^{-1}$

6.3.5 Pseudo-second order kinetic calculations

$$\frac{t}{q_t} = \frac{1}{K_2 q_{e2}^2} + \frac{1}{q_{e2}} t$$

From figure 4.13, the of $\frac{t}{q_t}$ against t for the biosorption of Cr yielded the following equation

$y = 0.3758x + 1.771$

$Where, \frac{1}{q_{e2}} = 0.3758$

$q_{e2} = 2.66\ mg/g$

$K_2 = 0.80 \frac{g}{mg.min}$

For Cu,

$y = 0.1225x + 2.4648$

$q_{e2} = 8.16\ mg/g$

$$K_2 = 0.007 \frac{g}{mg.min}$$

6.3.6 Intra-particle diffusion kinetic calculations

$$q_t = K_{id}\sqrt{t} + C$$

From figure 4.14, the of q_t against$\sqrt{t}$ for the biosorption of Cr yielded the following equation

$$y = 0.0629x + 1.9231$$

$$Where, q_{e-int} = 1.92\ mg/g$$

$$K_{id} = 0.063 \frac{mg}{g.min^{1/2}}$$

For Cu,

$$y = 0.7277x + 2.029$$

$$Where, q_{e-int} = 2.029\ mg/g$$

$$K_{id} = 0.729 \frac{mg}{g.min^{1/2}}$$

6.4 Appendix D: Breakthrough Curves in a Fixed-Bed Column

6.4.1 Calculations for column performance parameters from breakthrough for the biosorption of Cr^{6+} by banana peels

In a fixed-bed continuous system the performance of the column is determined by the breakthrough curve as seen in figure 7.1D below. Figure 7.1D represents the adsorption profile during the process of adsorption across the length of the column with a total bed height H_T of adsorbent. At t_1 and t_2 the mass transfer zone is at the entrance of the bed height and it is assumed at the entrance the adsorbent is almost saturated with the adsorbate (Geankoplis, Hersel and Lepek 2018). At t_3 half of the bed height is saturated with the outlet still at approximately zero and this continues until t_4. The mass transfer zone rises from t_4 and a breakthrough point c_b (break point) is reached at t_5. From t_5 to t_6 a rapid increase in concentration ratio c/c_o is noted until the bed reaches the saturation point c_d where the entire bed is no longer effective, i.e. $c/c_o = 1$ (Geankoplis, Hersel and Lepek 2018).

Figure 7.2D is given below to help determine the column capacity from breakthrough curves. For this project a number of bed heights have been evaluated for its performance on the removal of Cr^{6+} and it is useful to determine the column capacity which includes total bed height H_T, height or length of used bed H_B and length of unused bed H_{UNB} in relation to time t (Geankoplis, Hersel and Lepek 2018).

6.4.1.1 Calculation of column capacity from breakthrough curves for determining the breakthrough point

The total shaded area in figure 7.2D is represented as

$$t_t = \int_0^\infty \left(1 - \frac{c}{c_o}\right) dt \qquad (6\text{-}1)$$

Where t_t is the time equivalent to the total or stoichiometric capacity. The unusable capacity of the bed to the break-point t_b is (Geankoplis, Hersel and Lepek 2018)

$$t_u = \int_0^{t_b} \left(1 - \frac{c}{c_o}\right) dt \quad (6\text{-}2)$$

$i.e. for\ H_T\ of\ 15\ cm\ for\ removal\ of\ Cr\ from\ table\ 4.9$

$$t_u = \int_0^{70min} \left(1 - \frac{0.043}{5}\right) dt$$

$$t_u = 69.4\ min$$

Where t_u is the time equivalent to unusable capacity or time at which the effluent concentration reaches its maximum permissible level (Geankoplis, Hersel and Lepek 2018).

Breakthrough time and adsorption capacity can also be calculated using the following equation

$$q_b = \left(\frac{x}{m}\right)_b = \frac{x_b}{m_{adsorbent}} = Q\left(C_o - \frac{C_B}{2}\right)\frac{t_b}{m_{adsorbent}} \quad (6\text{-}3)$$

$At\ H_T = 15\ cm\ from\ table\ 4.9,$

$$q_b = Q\left(C_o - \frac{C_B}{2}\right)\frac{t_b}{m_{adsorbent}} = 0.004\frac{L}{min}\left(5\frac{mg}{L} - \frac{0.032\frac{mg}{L}}{2}\right) \times \left(\frac{90\ min}{14.87\ g}\right) = 0.121\ mg/g$$

Where q_b is the adsorption capacity at breakthrough (mg/g), x_b is the mass of metal ions adsorbed (mg) and Q is the flowrate (mL/min) (Mohanta *et al.* 2021).

To determine the length of unused bed H_{UNB} in a column

$$H_{UNB} = \left(1 - \frac{t_u}{t_t}\right) H_T \quad (6\text{-}4)$$

$$Where, H_{UNB} = \left(1 - \frac{89.23}{960}\right) \times 15cm = 13.61\ cm$$

Where the length of bed used up to the break point H_B is

$$H_B = \left(\frac{t_u}{t_t}\right) H_T \qquad (6\text{-}5)$$

$$H_B = \left(\frac{89.23}{960}\right) \times 15\ cm = 1.394\ cm$$

Where the ratio t_u/t_b is the fraction of the total bed capacity or length utilized up to the break point (Geankoplis, Hersel and Lepek 2018). H_B represents the mass transfer zone and it is independent of total height of the column. The full-scale adsorber bed can be designed by first calculating the height of bed required to achieve capacity H_B at break point, then H_{UNB} is added to H_B to obtain total height H_T (Geankoplis, Hersel and Lepek 2018).

$$H_T = H_B + H_{UNB} \qquad (6\text{-}6)$$

$$H_T = 13.61 + 1.394 = 15\ cm$$

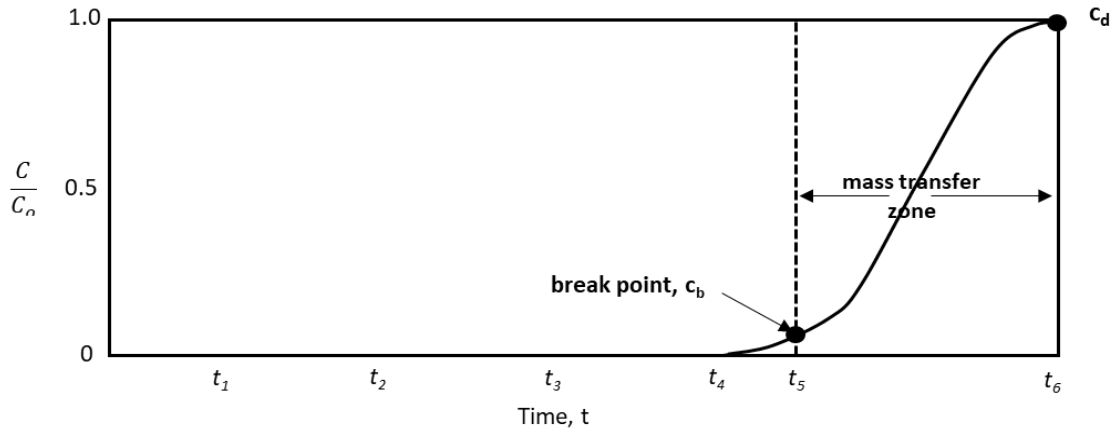

Figure 6.1D: Concentration profile for adsorption in a fixed bed column

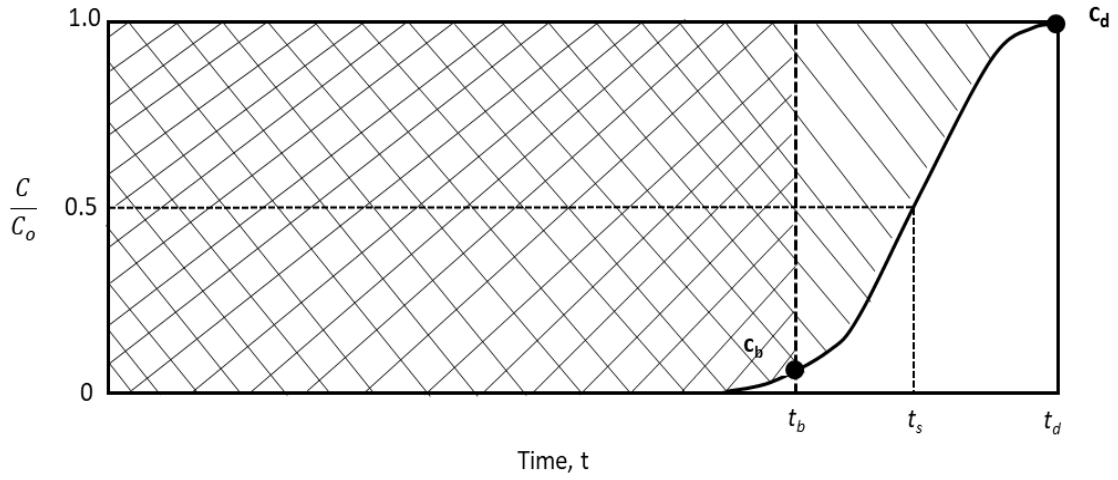

Figure 6.2D: Determination of capacity of column from breakthrough curve

6.4.1.2 Calculation of total amount of metal ions entering the column, m_T

$$\boldsymbol{m_T = \frac{C_o G t_t}{1000}} \quad (6\text{-}7)$$

$$m_T = \frac{5mg}{L} \times \frac{4mL}{min} \times 300\ min \times \frac{L}{1000mL} = 6\ mg\ of\ Cr\ entering\ the\ column\ at\ 5cm$$

6.4.1.3 Calculation of adsorption capacity for the column, q_T

$$q_T = \frac{QA}{m_{bio}} = Q \int_{t=0}^{t_t} (C_o - C_t)dt \quad (6\text{-}8)$$

$$q_T = \frac{Q}{m_{bio}} \times \sum_{i=1}^{t_t} (C_o - C_t)t = \frac{4\frac{mL}{min}}{4.67g} \times \sum 2.28328 \frac{mg\ min}{mL} = 0.5\ mg/g\ \ at\ 5cm$$

Where Q is the flowrate, m_{bio} is the mass of the adsorbent and A is the area under the breakthrough curve.

6.4.1.5 Calculation of number of bed volumes (NBV) and adsorption exhaustion rate (AER) as performance indicators in column studies

$$NBV = \frac{volume\ of\ water\ treated\ at\ breakthrough\ point}{volume\ of\ adsorbent\ bed} \quad (6\text{-}9)$$

$$AER = \frac{mass\ of\ adsorbent\ in\ column}{volume\ of\ water\ treated\ until\ exhaustion} \quad (6\text{-}10)$$

6.4.3 Thomas model calculations

$$\ln\left[\frac{C_o}{C_t} - 1\right] = \frac{K_T q_T M}{Q} - K_T C_o t$$

Plot of ln [C_o/C_t – 1] against t at 10 cm yielded the following graph,

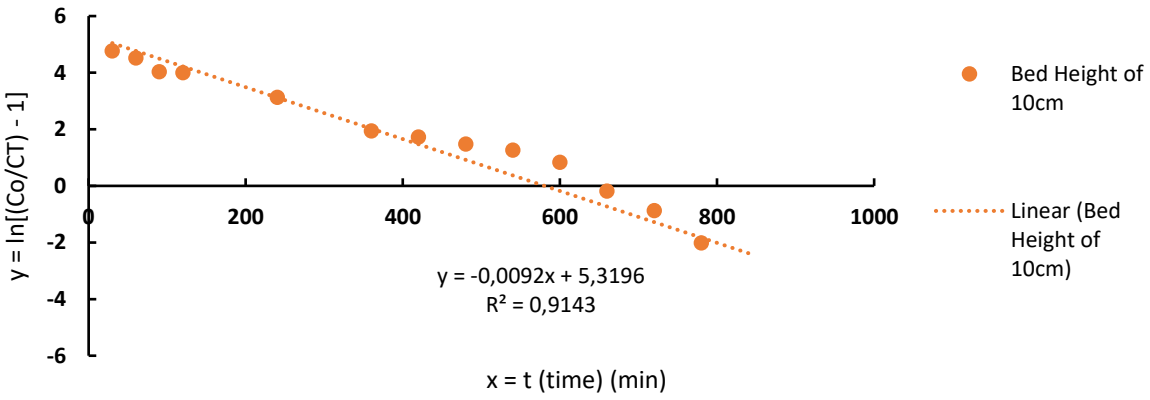

Figure 6.3D: Thomas model graphs at bed height of 10 cm

From the graph, parameters obtained were tabulated in table 4.10

$$i.e.\ for\ 10\ cm, \ln\left[\frac{C_o}{C_t} - 1\right] = -0.0092t + 5.3196$$

$$K_T C_o = 0.0092$$

$$Since\ C_o\ is\ 5\frac{mg}{L}, \therefore K_T = 0.00184\ mL/\min mg$$

$$\frac{K_T q_T M}{Q} = 5.3196$$

$$Q = 4ml/min\ ;\ M = 9.81\ g;\ \therefore q_T = 1178.83\ mg/g$$

Parameters obtained in table 4.10 were used to reproduce the same experimental data, where comparison between actual and calculated data are displayed in figure 4.21.

6.4.4 Yoon-Nelson model calculations

$$\ln\frac{C_t}{C_o - C_t} = k_{YN}t - \tau k_{YN}$$

Plot of ln [C_t/C_o – C_t] against t at 10 cm yielded the following graph,

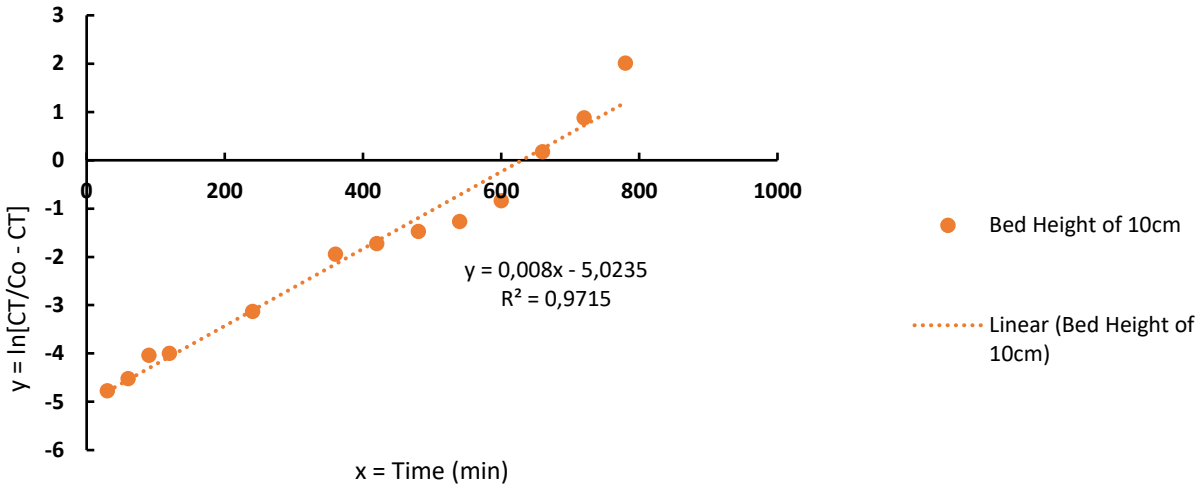

Figure 6.4D: Yoon-Nelson graphs at bed heights of 10 cm

From the graph, parameters obtained were tabulated in table 4.11

$$i.e.\ for\ 10\ cm, \ln\left[\frac{C_t}{C_o - C_t}\right] = -0.008x + 5.0235$$

$$K_{YN} = 0.008$$

$$\tau k_{YN} = 5.3196$$

$$\therefore, \tau = 627.94\ min$$

Parameters obtained in table 4.11 were used to reproduce the same experimental data, where comparison between actual and calculated was performed and displayed in figure 4.22.

6.4.5 Adams-Bohart Model Calculations

$$\ln\left(\frac{C_t}{C_o}\right) = k_{AB}C_o t - K_{AB}N_o\left(\frac{Z}{U_o}\right)$$

Plot of ln [C_t/C_o] against t at 10 cm yielded the following graph,

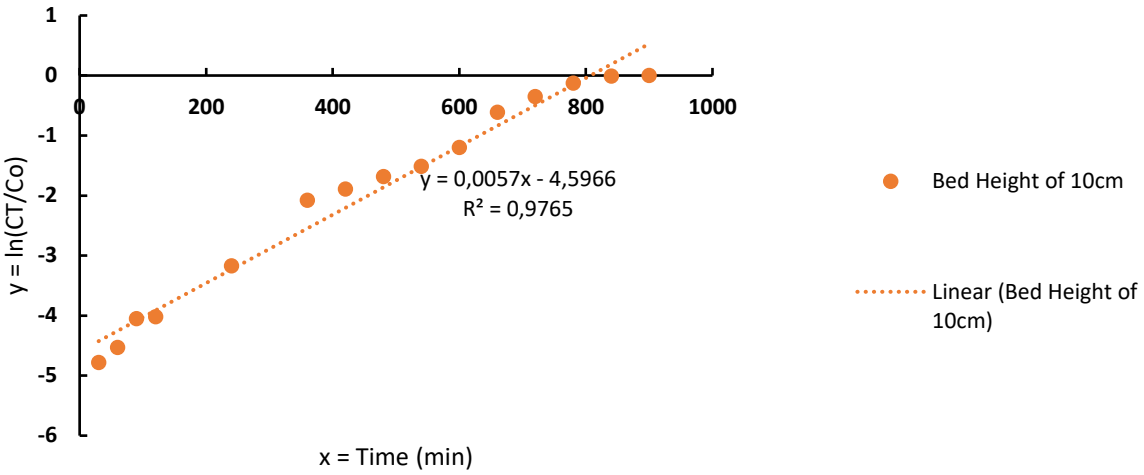

Figure 6.5D: Adams-Bohart graphs at bed heights of 10 cm

From the graph, parameters obtained were tabulated in table 4.12

$$i.e.\ for\ 10\ cm, \ln\left[\frac{C_t}{C_o}\right] = -0.0057x + 4.5966$$

$$K_{AB}C_o = 0.0057$$

$$K_{AB} = 0.00114\ {}^{mL}/_{\min mg}$$

$$K_{AB}N_o\left(\frac{Z}{U_o}\right) = 4.5966$$

$$U_o = \frac{Q}{A} = \frac{4\ {}^{cm^3}/_{min}}{4.155 cm^2} = 0.963\ cm/min$$

$$Z = 10\ cm, \therefore N_o = 388191.75\ mg/L$$

Parameters obtained in table 4.12 were used to reproduce the same experimental data, where comparison between actual and calculated was performed and displayed in figure 4.23.

6.4.7 Performance metrics index

Mean absolute error: $\boldsymbol{MAE = \frac{1}{n}\sum_{i=1}^{n}\left|\frac{C_t}{C_o} - \frac{\widehat{C_t}}{C_o}\right|_i}$ (6-11)

Root mean squared error: $\boldsymbol{RSME = \sqrt{\frac{1}{n}\sum_{i=1}^{n}\left(\frac{C_t}{C_o} - \frac{\widehat{C_t}}{C_o}\right)_i^2}}$ (6-12)

$$i.e.\ Thomas\ Model\ @\ 5cm: MAE = \frac{1}{n}\sum_{i=1}^{n}\left|\frac{C_t}{C_o} - \frac{\widehat{C_t}}{C_o}\right|_i = \frac{1}{12} \times 0.86 = 0.07207$$

$$i.e. RMSE = \sqrt{\frac{1}{n}\sum_{i=1}^{n}\left(\frac{C_t}{C_o} - \frac{\widehat{C_t}}{C_o}\right)_i^2} = \sqrt{\frac{1}{12} \times (0.86)^2} = 0.24967$$

Table 6.3D: Combination of the Thomas model, Y-N model, and A-B model used for Column Experiments at 5, 10, 15, 20, 30 cm

	Thomas Model Parameters					**Yoon-Nelson Parameters**				
Height, Z (cm)	**K_T (mL/ min mg)**	**q_T (mg/g)**	**R^2**	**MAE**	**RMSE**	**K_T (min^{-1})**	**τ (min)**	**R^2**	**MAE**	**RMSE**
5	0.0062	161.87	0.80	0.07	0.25	0.0296	67.20	0.77	-0.05	0.16
10	0.0018	1178.83	0.91	0.04	0.16	0.0080	627.94	0.97	0.00	0.02
15	0.0017	959.96	0.88	0.03	0.13	0.0073	776.32	0.93	-0.02	0.08
30	0.0011	827.71	0.95	0.03	0.13	0.0051	1345.80	0.97	0.01	0.03
	Adams-Bohart Parameters									
Height, Z (cm)	**K_{AB} (mL/ min mg)**	**N_o (mg/L)**	**R^2**	**MAE**	**RMSE**					
5	0.0018	205777.30	0.47	-0.025	0.09					
10	0.0011	388191.75	0.98	-0.006	0.03					
15	0.0011	301570.61	0.97	-0.011	0.05					
30	0.0008	263620.93	0.94	0.0175	0.08					

Table 6.4D: Data obtained from the Thomas, Y-N, and A-B models in figures 7.4.3D to 7.4.5D

		Exp -5cm		TH - 5cm		YN - 5cm	AB - 5cm
Bed Height (5 cm)	Time	C_t (mg/L)	C_t/C_o	C_o/C_t	C_t/C_o	C_t/C_o	C_t/C_o
	0	0	0.00	4.227475	0.236547839	0.120341524	0.152452836
	5	0.1	0.02	3.764058	0.265670699	0.136909432	0.159310524
	10	0.243	0.05	3.367181	0.296984289	0.155355472	0.166476687
	15	0.83	0.17	3.02729	0.330328429	0.175780619	0.1739652
	20	1.34	0.27	2.736202	0.365470086	0.198260805	0.181790564
	30	2.72	0.54	2.273412	0.439867455	0.249515118	0.198513137
	60	4.01	0.80	1.502429	0.665588647	0.446900979	0.258489553
	90	4.3	0.86	1.198235	0.834560546	0.662577125	0.336586535
	120	4.36	0.87	1.078215	0.927459224	0.826754768	0.438278818
	180	4.61	0.92	1.012176	0.987970608	0.965736157	0.74311832
	210	4.88	0.98	1.004804	0.995218938	0.985611032	0.967635318
	240	5	1.00	1.001895	0.998108138	0.994028692	1.259985232
	300	5	1.00	1.000295	0.999705018	0.998983934	2.136352638
		Exp -10cm		**TH - 10cm**		**YN - 10cm**	**AB - 10cm**
Bed Height (10 cm)	0	0	0.00	205.3021	0.00487087	0.006538419	0.01008607
	30	0.042	0.01	156.0271	0.006409143	0.008297244	0.011967029
	60	0.054	0.01	118.6366	0.008429104	0.010524179	0.014198769
	90	0.087	0.02	90.26415	0.011078595	0.013340769	0.016846708
	120	0.09	0.02	68.73479	0.014548672	0.016898292	0.019988463
	240	0.21	0.04	23.45695	0.042631294	0.042963114	0.039612918
	360	0.627	0.13	8.445427	0.118407277	0.104940188	0.078504447
	420	0.756	0.15	5.287055	0.189141216	0.159292723	0.110515444
	480	0.93	0.19	3.468474	0.288311258	0.234423471	0.155579255
	540	1.1	0.22	2.42134	0.412994479	0.33103669	0.219018298
	600	1.51	0.30	1.818403	0.549933002	0.444356434	0.308325264
	660	2.72	0.54	1.471234	0.679701422	0.56377572	0.434048066
	720	3.53	0.71	1.271335	0.786574564	0.676230029	0.611035634
	780	4.41	0.88	1.156234	0.864876787	0.771447028	0.860191707
	840	4.95	0.99	1.089959	0.917465607	0.845077062	1.210943733
	900	5	1.00	1.051798	0.950752726	0.898119264	1.704718509
		Exp -15cm		**TH - 15cm**		**YN - 15cm**	**AB - 15cm**
Bed Height (15 cm)	0	0.00	0.00	402.8183	0.002482509	0.003445963	0.005182851
	30	0.013	0.00	313.3112	0.003191715	0.004286026	0.006130984
	60	0.032	0.01	243.7422	0.004102695	0.005329787	0.007252566
	90	0.065	0.01	189.6701	0.005272312	0.006626039	0.008579325
	120	0.087	0.02	147.6428	0.006773102	0.008234941	0.010148798
	240	0.108	0.02	54.51703	0.018342891	0.01954878	0.019872866

	360	0.211	0.04	20.53094	0.04870697	0.045690397	0.038914047
	420	0.321	0.06	12.79883	0.078132169	0.06906766	0.054453944
	480	0.327	0.07	8.127781	0.123034807	0.103113407	0.076199529
	540	0.411	0.08	5.30596	0.188467325	0.151215417	0.106628974
	600	0.538	0.11	3.601271	0.277679776	0.21634407	0.149210085
	660	1.01	0.20	2.571452	0.388885353	0.299621687	0.208795495
	720	1.32	0.26	1.949329	0.512997071	0.398648391	0.292175684
	780	2.88	0.58	1.573498	0.635526513	0.506724595	0.408852837
	840	3.81	0.76	1.346456	0.742690545	0.614175947	0.57212373
	900	4.37	0.87	1.209297	0.826926578	0.711545089	0.800595062
	960	4.96	0.99	1.126438	0.887753822	0.792637907	1.120303914
	1020	5.00	1.00	1.076383	0.929037662	0.855560985	1.567684986
	1140	5.00	1.00	1.027876	0.972880283	0.934312358	3.069761895
		Exp -30cm		**TH - 30cm**		**YN - 30cm**	**AB - 30cm**
Bed Height (30 cm)	0	0	0.00	1248.504	0.000800959	0.001044053	0.00194382
	60	0.02	0.00	892.4952	0.001120454	0.001417276	0.002441604
	120	0.023	0.00	638.083	0.001567194	0.00192366	0.003066863
	240	0.009	0.00	326.3495	0.0030642	0.003541702	0.004838744
	300	0.011	0.00	233.5023	0.004282614	0.004803478	0.006077876
	360	0.021	0.00	167.1515	0.005982597	0.006511841	0.007634331
	420	0.032	0.01	119.7357	0.008351728	0.008822398	0.009589371
	480	0.067	0.01	85.85127	0.011648051	0.011942942	0.012045068
	540	0.123	0.02	61.63668	0.016224105	0.01614926	0.015129633
	600	0.137	0.03	44.33237	0.02255688	0.021804354	0.01900411
	660	0.166	0.03	31.96631	0.03128293	0.029380595	0.023870784
	840	0.284	0.06	12.3011	0.081293548	0.070462926	0.047306858
	960	0.426	0.09	6.771315	0.147681796	0.122646904	0.074638412
	1020	0.647	0.13	5.124315	0.195148026	0.159547333	0.093752214
	1080	0.866	0.17	3.947331	0.253335738	0.204956348	0.11776078
	1200	1.43	0.29	2.505161	0.39917591	0.322217425	0.185797111
	1440	2.76	0.55	1.392547	0.718108818	0.617842324	0.462504034
	1620	3.83	0.77	1.143259	0.874692316	0.80192987	0.916585433
	1740	4.56	0.91	1.07316	0.93182709	0.881884694	1.446142982
	1800	4.78	0.96	1.052282	0.950315452	0.910226203	1.816478978
	2040	4.99	1.00	1.013635	0.98654821	0.97181567	4.521754128